

RICE UNIVERSITY

**Controlled Growth Factor Delivery from Biodegradable
Hydrogel Scaffolds for Articular Cartilage Repair**


by

Theresa A. Holland

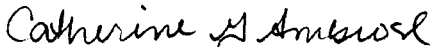
A THESIS SUBMITTED
IN PARTIAL FULFILLMENT OF THE
REQUIREMENTS FOR THE DEGREE

Doctor of Philosophy

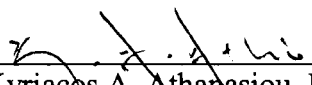
APPROVED, THESIS COMMITTEE:



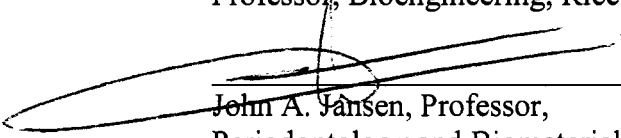
Antonios G. Mikos, John W. Cox Professor,
Bioengineering, Rice University



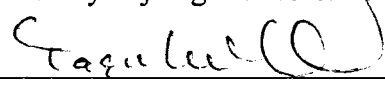
Catherine G. Ambrose, Associate Professor,
Orthopaedic Surgery, University of Texas-Houston



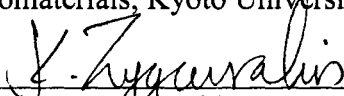
Kyriacos A. Athanasiou, Karl F. Hasselmann
Professor, Bioengineering, Rice University



John A. Jansen, Professor,
Periodontology and Biomaterials, Radboud
University Nijmegen Medical Center



Yasuhiko Tabata, Professor,
Biomaterials, Kyoto University



Kyriacos Zyggourakis, J. Hartsook Professor,
Chair, Chemical Engineering, Rice University

HOUSTON, TEXAS

MAY 2006

UMI Number: 3216720

INFORMATION TO USERS

The quality of this reproduction is dependent upon the quality of the copy submitted. Broken or indistinct print, colored or poor quality illustrations and photographs, print bleed-through, substandard margins, and improper alignment can adversely affect reproduction.

In the unlikely event that the author did not send a complete manuscript and there are missing pages, these will be noted. Also, if unauthorized copyright material had to be removed, a note will indicate the deletion.

UMI[®]

UMI Microform 3216720

Copyright 2006 by ProQuest Information and Learning Company.

All rights reserved. This microform edition is protected against unauthorized copying under Title 17, United States Code.

ProQuest Information and Learning Company
300 North Zeeb Road
P.O. Box 1346
Ann Arbor, MI 48106-1346

ABSTRACT

Controlled Growth Factor Delivery from Biodegradable Hydrogel Scaffolds for Articular Cartilage Repair

by

Theresa A. Holland

The use of oligo(poly(ethylene glycol) fumarate) (OPF) hydrogels as carriers of growth factors for articular cartilage repair has been investigated. *In vitro* release studies examined release of transforming growth factor- β 1 (TGF- β 1) directly from OPF hydrogels and also from gelatin microparticles encapsulated within these OPF networks. These studies showed that hydrogel mesh size and microparticle content can be altered to control growth factor release rates. In particular, sustained delivery of TGF- β 1 was achieved by utilizing microparticles as a secondary drug carrier within OPF hydrogels. An *in vitro* degradation study demonstrated that these microparticles also serve as digestible porogens to enhance material degradation in the presence of collagenase. Furthermore, in this environment, microparticle loading and crosslinking extent were shown to influence the rates of TGF- β 1 release and composite degradation. When utilized in the repair of rabbit osteochondral defects, OPF scaffolds were shown to undergo biocompatible degradation and to support healthy tissue in-growth. However, the incorporated TGF- β 1 was not shown to greatly influence tissue repair. Accordingly,

further investigations examined these hydrogel systems as carriers of TGF- β 1 and/or insulin-like growth factor (IGF-1) since these growth factors have been shown to synergistically promote chondrocyte proliferation and cartilage extracellular matrix synthesis *in vitro*. Surprisingly, individual delivery of IGF-1 appeared to enhance cartilage repair in rabbit osteochondral defects when compared to untreated defects, but delivery of TGF- β 1 with or without IGF-1 had no effect. These findings illustrate that the *in vitro* effects of growth factors, including the synergistic actions of multiple factors, may not directly translate to the wound healing environment. Furthermore, this research demonstrates the utility of these hydrogel systems in studying the effectiveness of various growth factor delivery regimes in soft tissue repair.

ACKNOWLEDGEMENTS

This research has been financially supported through a Whitaker Foundation Graduate Fellowship and by the National Institutes of Health. Numerous other individuals have contributed their advice, time, and expertise. I would particularly like to thank my advisor, Dr. Antonios G. Mikos, for the opportunity to work within his esteemed laboratory and for his professional guidance. I would also like to acknowledge the members of my committee for their generous advice and numerous contributions towards this work.

Furthermore, my colleagues, friends, and family deserve my heartfelt gratitude for their friendship and assistance over the years. And finally, to my mother, Rosemary Holland, who has forever been an unwavering support and a steadfast advocate of the values of higher education and enduring faith, thank you.

“And whatsoever you do in word or in deed, do all in the name of the Lord Jesus, giving thanks to God the Father through Him.” - *Colossians 3:17*

TABLE OF CONTENTS

Title Page	i
Abstract	ii
Acknowledgements	iv
Table of Contents	v
List of Tables	ix
List of Figures	xi
I. Review: Advances In Drug Delivery For Articular Cartilage	1
Abstract	1
Abbreviations	1
Introduction	2
Articular Cartilage Structure	2
Chondrocytes	3
Extracellular Matrix	3
Matrix Metalloproteinases	5
Important Signaling Molecules in Articular Cartilage	5
Growth Factors	6
Cytokines	11
Articular Cartilage Pathology	12
Partial Thickness Lesions	13
Full Thickness Lesions	13
Osteoarthritis	14
Drug Delivery Strategies	14
Regulation of Inflammatory Cytokines	15
Regulation of Matrix Degradation	18
Cellular Regulation	20
Conclusions	22
II. Specific Aims	24
III. <i>In Vitro</i> Release of Transforming Growth Factor- β 1 From Gelatin Microparticles Encapsulated in Biodegradable, Injectable Oligo(Poly(Ethylene Glycol) Fumarate) Hydrogels	25
Abstract	25
Abbreviations	26
Introduction	26
Experimental Methods	28
Gelatin Microparticle Fabrication	28
Microparticle Swelling	29
Microparticle Loading	30
OPF Synthesis	31
Gel Permeation Chromatography	32
Hydrogel and Composite Fabrication	32
Rheometry	33

Tensile Testing.....	34
Hydrogel and Composite Swelling Studies	34
Calculation of Molecular Weight between Crosslinks and Mesh Size.....	36
In Vitro TGF- β 1 Release Study	37
Statistical analysis.....	38
Results.....	38
Microparticle Swelling.....	38
GPC.....	39
Rheometry.....	39
Tensile Testing.....	39
Hydrogel Swelling	40
Hydrogel M_c and ξ	41
Composite Swelling.....	41
In Vitro TGF- β 1 Release Study	42
Discussion.....	49
Conclusions.....	54
 IV. Transforming Growth Factor- β 1 Release From Oligo(Poly(Ethylene Glycol) Fumarate) Hydrogels In Conditions Which Model the Cartilage Wound Healing Environment.....	55
Abstract.....	55
Abbreviations.....	56
Introduction.....	56
Experimental Methods.....	59
Assessment of Collagenase Activity.....	59
Gelatin Microparticle Fabrication.....	60
Microparticle Loading	60
OPF Synthesis.....	61
Gel Permeation Chromatography	62
Composite and Hydrogel Fabrication	62
In Vitro TGF- β 1 Release	63
Hydrogel and Composite Degradation.....	64
Statistical analysis.....	65
Results.....	65
Collagenase Activity in PBS.....	65
GPC.....	66
In Vitro TGF- β 1 Release and Material Degradation	67
Discussion.....	75
Conclusions.....	79
 V. Osteochondral Repair in the Rabbit Model Utilizing Bilayered, Degradable Oligo(Poly(Ethylene Glycol) Fumarate) Hydrogel Scaffolds	81
Abstract.....	81
Abbreviations.....	82
Introduction.....	82
Experimental Methods.....	85

Gelatin Microparticle Fabrication and Loading.....	85
OPF Synthesis.....	86
Scaffold Fabrication.....	86
Animal Surgery.....	88
Tissue Processing.....	90
Histological Scoring.....	91
Statistical analysis.....	92
Calculation of Average Histological Scores.....	92
ResultsAnimal Health & Macroscopic Joint Appearance at Recovery	95
Histological Appearance.....	95
Discussion.....	102
Conclusions.....	105
 VI. Dual Growth Factor Delivery From Degradable Oligo(Poly(Ethylene Glycol) Fumarate) Hydrogel Scaffolds for Cartilage Tissue Engineering.....	106
Abstract.....	106
Abbreviations.....	107
Introduction.....	107
Experimental Methods.....	110
Gelatin Microparticle Fabrication.....	110
Microparticle Loading	111
In Vitro Growth Factor Release from Gelatin Microparticles	112
OPF Synthesis and Characterization.....	114
Hydrogel and Composite Fabrication	114
Single and Dual Growth Factor Release from Hydrogels and Composites in Vitro	115
Statistical analysis.....	117
Results.....	117
In Vitro Growth Factor Release from Gelatin Microparticles	117
IGF-1 Release from Hydrogels and Composites in Vitro.....	121
Dual IGF-1 and TGF- β 1 Release from Hydrogels and Composites in Vitro	124
Discussion.....	128
Conclusions.....	132
 VII. Degradable Hydrogel Scaffolds for In Vivo Evaluation of Growth Factor Interactions in Cartilage Repair	134
Abstract.....	134
Abbreviations.....	135
Introduction.....	135
Results.....	137
In Vitro Growth Factor Release.....	137
Animal Health & Macroscopic Joint Appearance at Recovery	139
Histological Appearance.....	139
Histomorphometric Analysis	140
Discussion.....	149
Materials and Methods.....	152

Gelatin Microparticle Fabrication and Loading	152
OPF Synthesis	153
Scaffold Fabrication	153
Quantification of In Vitro Growth Factor Release	154
Animal Surgery	155
Tissue Processing	157
Histomorphometric Analysis	157
Statistical analysis	158
VIII. Summary	159
IX. Literature Cited	161
X. Appendix: Biodegradable Polymeric Scaffolds, Improvements in Bone Tissue Engineering through Controlled Drug Delivery	172
Abstract	172
Abbreviations	172
Introduction	173
Degenerative Bone Disorders	173
Bone Formation	174
Bone Remodeling by Osteoclasts and Osteoblasts	175
Regulatory Molecules	176
Critical Issues in Drug Delivery System Design	178
Polymeric Scaffolds for Bone Drug Delivery	179
Poly(lactic acid)	180
Poly(lactic-co-glycolic acid) Copolymers	184
Other Polyesters	186
Poly(lactic acid)-Poly(ethylene glycol) Block Copolymers	187
Additional Poly(ethylene glycol)-Based Materials	188
Polyanhydrides	189
Poly(propylene fumarate)	191
Future Directions	192
Conclusions	193
Appendix References	194

LIST OF TABLES

Table I-1: Regulatory effects of growth factors and cytokines in articular cartilage	9
Table III- 1: Parameters for OPF-gelatin microparticle composites.....	33
Table III- 2: Properties of OPF hydrogels	40
Table III- 3: <i>In vitro</i> TGF- β 1 release kinetics from gelatin microparticles	46
Table III- 4: TGF- β 1 burst release from OPF hydrogels and composites	46
Table III- 5: Phase 2 TGF- β 1 release rates from OPF hydrogels and composites	47
Table III- 6: Phase 3 TGF- β 1 release rates from OPF hydrogels and composites	47
Table III- 7: Cumulative TGF- β 1 release from OPF hydrogels and composites.....	47
Table IV- 1: Effect of pH and collagenase on TGF- β 1 release from microparticles.....	68
Table IV- 2: TGF- β 1 release from hydrogels and composites in PBS	69
Table IV- 3 TGF- β 1 release from hydrogels and composites in acidic buffer	71
Table IV- 4: TGF- β 1 release from hydrogels and composites in collagenase-containing PBS	73
Table V- 1: OPF scaffolds for osteochondral repair.....	84
Table V- 2: Histological scoring system.....	93
Table V- 3: Mean histological scores per formulation at 4 weeks	99
Table V- 4: Mean histological scores per formulation at 14 weeks	101
Table VI- 1: Composition of systems for IGF-1 release.....	112
Table VI- 2: Composition of systems for IGF-1 and TGF- β 1 release.....	113
Table VI- 3: IGF-1 release from microparticles	120
Table VI- 4: IGF-1 release from OPF hydrogels and composites.	122
Table VI- 5: IGF-1 and TGF- β 1 release from dual release systems.....	126

Table VII- 1: In vivo study design.....	137
Table VII- 2: Histological scoring system	145
Table A- 1: Biodegradable Polymers Utilized in Osteogenic Drug Delivery	183

LIST OF FIGURES

Figure III- 1: Fold swelling ratios for OPF composites	42
Figure III- 2: TGF- β 1 release from gelatin microparticles	43
Figure III- 3: TGF- β 1 release from OPF hydrogels.....	43
Figure III- 4: TGF- β 1 release from OPF3K composites crosslinked for 10 min	44
Figure III- 5: TGF- β 1 release from OPF3K composites crosslinked for 30 min	44
Figure III- 6: TGF- β 1 release from OPF10K composites crosslinked for 10 min	45
Figure IV- 1: Collagenase activity in PBS	66
Figure IV- 2: TGF- β 1 release and material degradation profiles in standard PBS.....	70
Figure IV- 3: TGF- β 1 release and material degradation profiles in acidic buffer	72
Figure IV- 4: TGF- β 1 release and material degradation profiles in collagenase-containing PBS	74
Figure IV- 5: Degradation of composites in the presence of collagenase.	79
Figure V- 1: Scaffold fabrication and implantation.....	88
Figure V- 2: Histological sections of osteochondral defects at 4 weeks post-surgery.	96
Figure V- 3: Histological sections of osteochondral defects at 14-week post-surgery.....	98
Figure VI- 1: Effect of gelatin IEP and crosslinking extent on growth factor release....	118
Figure VI- 2: IGF-1 release from OPF hydrogels and composites.....	123
Figure VI- 3: IGF-1 and TGF- β 1 release from OPF composites.....	125
Figure VII- 1: <i>In vitro</i> IGF-1 and TGF-1 release from OPF scaffolds	138
Figure VII- 2: Histological section displaying the thick fibrous tissue commonly observed at the neo-surface and that often accompanied un-remodeled cartilaginous regions in the subchondral zone.....	141
Figure VII- 3: Histological section displaying the most striking example of cartilaginous tissue remaining in the subchondral defect area	142

Figure VII- 4: Histological section displaying fibrocartilage in-growth near the chondral defect margins and significant subchondral restoration.....	143
Figure VII- 5: Histological section displaying excessive fibrous tissue growth into the joint space and significant subchondral restoration.	144
Figure VII- 6: Histological section displaying thin fibrous tissue growth along the surface of a joint with complete subchondral restoration.....	147
Figure VII- 7: Comparison of results following histomorphometric analysis.....	148

I. REVIEW: ADVANCES IN DRUG DELIVERY FOR ARTICULAR CARTILAGE[†]

Abstract

The complex structure of articular cartilage, the connective tissue lining diarthrodial joints, enables this tissue to dissipate compressive loads but also appears to hinder its repair ability. At best, both natural and surgical repair attempts replace the highly ordered extracellular matrix of native articular cartilage with fibrous repair tissue of inferior mechanical properties. Numerous bioactive molecules closely regulate the cellular processes in healthy and degenerative articular cartilage. Accordingly, this review outlines the roles of important signaling molecules in cartilage tissue. In addition, drug delivery strategies, aimed at utilizing these bioactive agents to prevent inflammation, to regulate extracellular matrix metabolism, and to control cellular activities, are discussed. As scientists gain further insight into the complex signaling cascades of articular cartilage, continued refinement of drug delivery systems is necessary to develop effective clinical therapies for articular cartilage repair.

Abbreviations

BMP, bone morphogenetic protein; CIF, cartilage inducing factor; DCMC, N,N-dicarboxymethyl chitosan; EGF, epidermal growth factor; FGF, fibroblast-derived growth factor; GAG, glycoasminoglycan; IGF, insulin-like growth factor; IL, interleukin; IGFBP, insulin-like growth factor binding protein; LAP, latency associated peptide; LTBP, latency binding protein; MMP, matrix metalloproteinase; MSC, mesenchymal stem cell; NSAID, non-steroidal anti-inflammatory drug; PDGF, platelet-derived growth factor; PLGA, poly(lactic acid-co-glycolic acid); TGF, transforming growth factor; TIMP, tissue inhibitor of metalloproteinase; TNF, tumor necrosis factor; VEGF, vascular endothelial growth factor;

[†] This chapter was published as the following article: TA Holland and AG Mikos, *Advances in Drug Delivery for Articular Cartilage*, J. Control. Release, 86, 1-12 (2003).

Introduction

The inability of cartilage to undergo successful repair has puzzled researchers and physicians for many years. However, as the knowledge and skills of biologists, engineers, and physicians merge, new strategies for treating degenerative cartilage are being investigated and may revolutionize treatment for articular cartilage lesions and osteoarthritis. Current therapies actually require surgical drilling or abrasion to deepen lesions for contact with cells and bioactive molecules of the bone marrow. Unfortunately, these rigorous techniques do not restore the native structure of cartilage and may lead to further tissue loss (1, 2). Recent research has increased our understanding of the growth factors and cytokines involved in both cartilage homeostasis and pathology. Utilizing this knowledge, novel therapies for treatment of articular cartilage defects are being investigated. To avoid potential complications with the use of these pluripotent molecules, new strategies must ensure localized delivery of safe levels of bioactive agents in a controlled manner. Understanding the physiology and pathology of articular cartilage, as well as the methodology and results of recent strategies, is necessary to further advance drug therapies for degenerative cartilage.

Articular Cartilage Structure

Injury to articular cartilage results in cell death, disruption of the extracellular matrix, and release of numerous signaling molecules. Although a classical wound healing response is initiated, articular cartilage lesions are repaired without complete restoration of the components and architecture of the native tissue (2, 3). To understand the shortcomings of the natural healing events and current clinical therapies, the physiology of healthy articular cartilage is briefly explored.

Chondrocytes

Although only a few millimeters in thickness, articular cartilage possesses a complex structure, allowing this tissue to absorb and dissipate mechanical shock in joints. The primary components of healthy articular cartilage, water, collagen, and proteoglycans, are maintained in a highly, ordered extracellular matrix by a sparse population of chondrocytes. In fact, chondrocytes compose less than 10% of the weight of articular cartilage (3, 4).

Chondrocytes originate from mesenchymal cells during fetal development as the majority of cartilage is remodeled into bone. At skeletal maturity, articular cartilage is the only remaining cartilaginous portion of the long bones. Accordingly, articular chondrocytes differ greatly from the chondrocytes capable of endochondral bone formation. A shift towards this later phenotype is observed in the progression of osteoarthritis as ossification replaces articular cartilage (5).

Articular chondrocyte metabolism involves primarily anaerobic processes due to the low oxygen pressure within this avascular tissue (4, 6). Low cellularity coupled with the slow rate of chondrocyte division contribute to cartilage degeneration, since invading fibroblasts rapidly divide and synthesize scar tissue before intrinsic repair may occur (7).

Extracellular Matrix

Water comprises approximately 75% of the wet weight of articular cartilage and interacts with negatively charged glycoasminoglycan (GAG) chains of proteoglycans (3). Aggrecan, the largest proteoglycan in articular cartilage, consists of a core protein with many GAG side chains, such as chondroitin sulfate, keratan sulfate, and heparan sulfate, which associate with hyaluronan, another GAG. These high molecular weight complexes attract water and generate a swelling pressure to counter compressive loads. Other

proteoglycans, such as decorin, biglycan, and fibromodulin, have one to two GAG chains which associate with collagen fibrils and may regulate collagen fiber formation (7-9). In addition to their importance in maintaining tissue structure, proteoglycans also function in molecular signaling as reservoirs and receptors for growth factors (9, 10) .

Respectively, proteoglycans and collagen comprise 15-30% and 50-73% of the solid extracellular matrix weight, intertwining to form a tight fiber network (3). Glycoproteins, such as fibronectin, also contribute to this network, serving as a link between cells and the extracellular matrix (11). Collagen fibers, predominately type II, but also types I, V, VI, IX, X and XI, impart tensile strength and immobilize proteoglycan molecules (7). Disruption of the collagen-proteoglycan network may be partially responsible for proteoglycan release in fibrillated cartilage (4).

Four distinct zones characterize the amount, orientation, and shape of matrix molecules and chondrocytes in articular cartilage (4, 7). Moving through these zones from the articulating surface towards the subchondral bone, water content decreases while proteoglycan content increases (3). The superficial zone, near the joint space, contains elongated chondrocytes and thin collagen fibers tangentially aligned to the surface. Directly beneath lies the intermediate zone in which rounded chondrocytes and larger diameter collagen fibers appear less aligned. Here, groups of chondrocytes, or chondrones, are encapsulated in lacunae, a specialized extracellular matrix enriched in hyaluronan, proteoglycans, fibronectin, and thin collagen fibers. In the deep zone, collagen fibers and columns of clustered, hypertrophic chondrocytes are oriented perpendicular to the articulating surface. Finally, the calcified zone contains rather small

cells, an abundance of calcium salts, and a thin vasculature network as the tissue transitions from cartilage to mineralized bone (3, 4, 7).

Matrix Metalloproteinases

A family of enzymes, known as matrix metalloproteinases (MMPs), plays an important role in the digestion of the extracellular matrix in both normal and degenerative articular cartilage. These enzymes target specific components of the extracellular matrix and may be activated through a number of signaling pathways. Collagenases (MMPs-1, -8, and -13), gelatinases (MMPs-2 and -9), and stromelysins (MMP-3 and -10) belong to this family and degrade collagen, aggrecan, fibronectin, laminin, and elastin. MMPs contain a Zn^{2+} ion at their active site and are stabilized by Ca^{2+} ions (12, 13).

The activity of MMPs is strictly regulated by a group of inhibitors, the tissue inhibitors of matrix metalloproteinases (TIMPs). At least four TIMPs exist and control MMP activity by binding to the active site of MMPs. TIMPs may also bind to additional sites on latent MMPs. Elevated levels of MMPs and TIMPs are found in patients with osteoarthritis and rheumatoid arthritis (13, 14).

Important Signaling Molecules in Articular Cartilage

Molecules involved in the regulation of cellular functions may be loosely classified by three categories - hormones, cytokines, and growth factors. Hormones are the chemical messengers synthesized by specialized endocrine glands and transported via body fluids to act on distant cells. Cytokines refer to molecules commonly secreted by immune cells to act on damaged or infected tissue. However, other cell types may secrete cytokines as well. Growth factors are synthesized and secreted by cells in a variety of tissues and generally act on nearby cells in a paracrine or autocrine fashion (15). Growth

factors are often secreted in a latent form and may bind to extracellular matrix components, requiring proteolytic cleavage for activation and cell receptor binding (16). As summarized in Table 1, a number of growth factors and inflammatory cytokines interact to maintain homeostasis in healthy cartilage. Imbalance in one or more of these important molecular signals appears to have a role in cartilage pathology (17, 18). Understanding the interplay between these signaling molecules is necessary for the design of new therapies aimed at manipulation of their expression in damaged articular cartilage.

Growth Factors

TGF- β s

The transforming growth factor (TGF) family includes a number polypeptides involved in the regulation of cell growth and differentiation and in wound healing (19). transforming growth factor- β , first identified by its ability to stimulate normal cells to grow and differentiate in soft agar, is found throughout the body and binds to at least three membrane receptors common to most cells (19-21). Three isoforms, TGF- β 1, TGF- β 2, and TGF- β 3, have been isolated from cartilage in mammals and shown to have a high affinity for the proteoglycan decorin (9, 21, 22). The TGF superfamily also includes two cartilage-specific proteins, cartilage-inducing factors A and B (CIF-A and CIF-B), which promote mesenchymal stem cell (MSC) differentiation along the chondrogenic phenotype. However, CIF-A appears to be identical to TGF- β 1, while CIF-B shares extensive structural homology to the TGF- β s (23, 24).

Active TGF- β 1, the most widely investigated molecule of this family, is a 25 kDa protein composed of two polypeptide chains held together by disulfide linkages. This molecule is first synthesized and secreted as 100 kDa precursor protein, composed of the

active TGF- β 1 subunit and a 75 kDa latency associated peptide (LAP). Dissociation from LAP is required before TGF- β 1 may bind to a TGF receptor (21, 22, 25). Additionally, noncovalently binding to a 200 kDa dimeric protein, known as latency binding protein (LTBP), appears necessary for storage of TGF in the extracellular matrix and its subsequent activation (25, 26).

TGF- β exerts various effects on a number of connective tissues depending on cell age and phenotype, culture conditions, and administered dose (19, 20). TGF- β 1 has been shown to promote the differentiation of MSCs to osteoblasts, osteoclasts, and chondrocytes (10, 27-31). In articular cartilage, TGF- β 1 promotes protein synthesis (32-35) and cell proliferation (36, 37) and inhibits the actions of MMPs (38-40). In addition to TGF- β 1's protective effect on articular cartilage, TGF- β 1 is known to promote chemotaxis and activation of inflammatory cells and, at high concentrations, has been implicated in fibrosis and osteophyte formation in articular cartilage defects (21, 41-43). Synergistic actions with other growth factors have also been reported (37, 44-46). TGF- β 2 appears to exert similar effects as TGF- β 1 (30).

BMPs

Bone morphogenetic proteins (BMPs), named for their ability to induce bone and cartilage formation, are a subfamily of the TGF superfamily (19). The effects of a number of BMPs on articular chondrocytes have been studied. In general, BMP-4,-6, and-7 appear to enhance the chondrogenic phenotype, as seen by an increase in type II collagen and proteoglycan synthesis and reduction in synthesis of type I collagen, the major organic component of bone (47-49). However, studies reveal that other members of the BMP family may promote the opposite effect on articular chondrocytes (48) and may

lead to osteophyte formation (42) and GAG release in articular cartilage (50). Additionally, comparison studies with BMPs and TGF- β s suggest that BMPs may not be as potent as TGF- β 1 in promoting proteoglycan synthesis and overcoming the effects of catabolic cytokines (42, 51).

IGFs

Insulin-like growth factors 1 and 2 (IGF-1 and IGF-2), which exhibit close homologies to insulin, have been isolated from a number of tissues, including articular cartilage. These growth factors were initially discovered as sulfation factors or somatomedins which promote sulfate incorporation into proteoglycans (33, 52). In articular cartilage, these growth factors act primarily in an anabolic fashion to increase proteoglycan and type II collagen synthesis (33, 38, 52, 53). IGF-1 also appears to influence cellular differentiation (54-56) and specific integrin expression (57).

IGF-1, also known as somatomedin C, is the predominant form of IGF in adults (15). Like TGF- β 1, IGF-1 and IGF-2 are synthesized in latent forms of 130 and 180 amino acid chains, respectively. Active IGF-1 is actually a single chain of 70 amino acids, while active IGF-2, also known as somatomedin A, is a chain of 67 amino acids (19). IGF activity is regulated by six known IGF binding proteins (IGFBPs). A number of these binding proteins are secreted by chondrocytes and regulate IGF by sequestering it from cell surface receptors. Recent research indicates that IGFBP-3 is maintained in articular cartilage through association with fibronectin and heparan sulfate proteoglycans in the pericellular matrix surrounding chondrocytes (58, 59).

Table I-1: Regulatory effects of growth factors and cytokines in articular cartilage

Regulatory Effect	Growth Factor/Cytokine	References
Chondrogenic differentiation of progenitor cells	TGF- β 1 IGF-1 PDGF	(10, 27-31, 60) (54-56) (31)
Chondrocyte proliferation	TGF- β 1 IGF-1 FGF EGF	(36, 37, 44, 61) (61) (44, 62, 63) (37)
Matrix synthesis	TGF- β 1 BMP-2, 4, 6, 7 IGF-1	(32-35, 39, 61) (42, 47-49) (33, 38, 52, 53, 61, 64)
MMP inhibition	TGF- β 1 IGF-1 IL-4, 6	(38, 40, 65) (65) (66, 67)
Chemotaxis of inflammatory cells	TGF- β 1 FGF	(21, 41) (68)
Ossification	TGF- β 1 BMP-2 FGF PDGF VEGF	(35, 41-43) (42) (43) (41) (69, 70)
MMP stimulation	FGF PDGF IL-1 β , 17, 18 TNF- α	(71, 72) (71) (71, 73-75) (71)
Matrix degradation	BMP-2 FGF PDGF EGF IL-1 β , 18 TNF- α	(50) (76-79) (41) (80) (34, 38, 40, 64, 73) (34, 81)

FGF

Heparan sulfate also stores fibroblast-derived growth factor (FGF) in the extracellular matrix of articular cartilage (72). FGF is an important mitogen for cells of mesodermal origin and plays an important role in angiogenesis, serving as a mitogen and chemoattractant for endothelial cells (19, 68). Although two forms of FGF exist, basic (b-FGF) and acidic (a-FGF), these 14-16 kDa proteins appear to exert similar effects (19). Early studies, in which FGF was seen to promote DNA synthesis (44) and cell proliferation in articular cartilage (62, 63), suggested FGF's anabolic role in cartilage tissue. However, these studies only evaluated the short term effects of FGF. In another study, rabbit articular chondrocytes cultured with 0.4 ng/ml bFGF experienced a change in morphology towards characteristics of flat, fibroblastic cells (45). More recently, FGF has been detected in osteophytes and throughout articular cartilage in osteoarthritic patients (43). FGF has also been shown to inhibit type II collagen and proteoglycan synthesis (76-79) and to induce synthesis of MMPs (71, 72).

PDGF, EGF, and VEGF

While TGF- β s, BMPs, IGFs, and FGF have been the most widely investigated growth factors isolated from cartilage, a number of growth factors, including platelet-derived growth factor (PDGF), epidermal growth factor (EGF), and vascular endothelial growth factor (VEGF), play an important role in healthy and injured articular cartilage. PDGF, a 30 kDa glycoprotein, is a known chemotractant and stimulant of macrophages and fibroblasts during wound healing (82). PDGF has also been shown to affect MSC differentiation (31), MMP expression (71), and ossification (41). EGF, a smaller 1.6 kDa protein, is sometimes considered a hormone since it circulates in the blood, and may therefore, act on a number of different cell types (19). In culture, EGF promotes short

term DNA synthesis and proliferation of chondrocytes (37) and a decrease in type II collagen expression (80). VEGF, a 23 kDa polypeptide, acts synergistically with bFGF in the induction of angiogenesis (19). VEGF is found in elevated levels in the osteoarthritic cartilage (70) and appears to be necessary for endochondral bone formation (69).

Cytokines

ILs

Recent research points to a family of cytokines, the interleukins (ILs), as important agents in articular cartilage repair. ILs, originally identified in the supernatants of human lymphocyte cultures, are also secreted by macrophages, fibroblasts, chondrocytes, and synovial cells and interact with a number of growth factors and signaling molecules to affect inflammation and wound healing (66, 82, 83). A number ILs, including IL-1, -4, -6, -10, and -17, are upregulated in osteoarthritic joints (74, 83).

Interleukin-1 (IL-1) appears to play a central role in cartilage degeneration. IL-1 is actually two proteins that bind to a common receptor. While IL-1 α is expressed as a membrane-associated protein, IL-1 β is secreted as a soluble protein, and thus, exerts a wide range of effects (82). IL-1 β , acts as an antagonist of TGF- β 1, suppressing expression of proteoglycans, type II collagen, and TIMP-1 in human articular chondrocytes cultures (34, 40). In addition, IL-1 β induces the expression of MMPs (71) and the subsequent degradation and loss of proteoglycans from articular cartilage explants (38, 64). IL-1 β also stimulates bFGF release and upregulates nitric oxide synthase, the enzyme responsible for synthesizing harmful nitric oxide radicals (75).

IL-18 exerts effects similar to IL-1 β , demonstrating ability to upregulate MMPs, enhance nitric oxide production, and stimulate GAG release from articular cartilage explants (73). IL-17 also upregulates MMP expression in chondrocytes culture (74).

However, other interleukins, such as IL-4 and IL-6, appear to regulate the catabolic effects of these molecules by enhancing TIMP-1 production in articular chondrocytes (66, 67). Moos et al. explored the interactions of several ILs and other signaling molecules and found a closely regulated pattern of expression among IL-1, 4, 10 and TGF- β 1. In particular, IL-1 β was shown to upregulate expression of TGF- β 1. However, no regulatory counterpart was identified for another inflammatory cytokine, tumor necrosis factor- α (TNF- α) (83).

TNF

TNF- α belongs to a group of cytokines which commonly exert cytotoxic effects on many cell types but may also exert stimulating influences. This group was originally named for its ability to regress some tumors in mice. TNF- α , a 17 kDa trimeric protein, is predominantly secreted by macrophages (82). TNF- α is expressed in osteoarthritic cartilage but not in normal articular cartilage (84). This cytokine shares many functions with IL-1 β , including suppression of proteoglycan synthesis, stimulation of collagen degradation, and induction of MMP expression, but appears to be less active than IL-1 β (34, 71, 81).

Articular Cartilage Pathology

The body's response to articular cartilage defects resulting from trauma upon impact or loading depends on the lesion depth. Partial defects do not penetrate the underlying subchondral bone, and therefore, do not contact the host of cells and bioactive molecules in the underlying bone marrow. Accordingly, an intrinsic response ensues as the surrounding cartilage independently attempts to regenerate new tissue. In contrast, full thickness defects penetrate the subchondral bone and contact the marrow. Thus, an

extrinsic response dominates the repair process as blood from the marrow delivers MSCs, fibroblasts, and inflammatory cells to the wound site (2, 4, 7, 85). In general, both partial thickness and full thickness articular cartilage lesions do not result in complete tissue regeneration and subsequent tissue degeneration at the wound site may lead to the onset of osteoarthritis (1).

Partial Thickness Lesions

With partial thickness lesions, chondrocyte proliferation and clustering near the defect site begins soon after joint trauma. However, migration of cells farther from the defect appears to be inhibited by entrapment in the dense extracellular matrix (4, 86). Newly formed superficial tissue forms a sloping shoulder at the side of the defect but fails to remodel and integrate with the surrounding cartilage. Accordingly, further abrasion of the articular surface during loading and exposure of the subchondral bone frequently results (4, 87).

Full Thickness Lesions

With full thickness lesions, blood from the marrow facilitates formation of a fibrin clot within approximately two days of the trauma (2). MSCs quickly penetrate the clot, differentiate into chondrocytes, and begin synthesizing proteoglycan and type II collagen-rich extracellular matrix. However, inflammatory cells release cytokines which initiate scar tissue deposition and promote angiogenesis. In general, fibrocartilage, which has decreased proteoglycan content and increased type I collagen content, fills the defect. This tissue may undergo further degeneration and become completely vascularized, leading to osteoarthritis (2, 3, 7, 85).

Osteoarthritis

Symptoms of osteoarthritis are similar to those of articular cartilage lesions, including persistent pain, swelling, and catching of the joint (1). Enhanced breakdown of the cartilage matrix coupled with reduced synthesis of matrix components by articular chondrocytes results in the destruction of joint cartilage (83). Decreased proteoglycan content and increased water content in articular cartilage, as well as, elevated concentrations of proteoglycans and fibronectin fragments in the synovial fluid are characteristic of osteoarthritis due to the upregulation of MMPs in degenerative chondrocytes (6, 65, 88, 89). As the articular surface becomes fibrillated, loose cartilage fragments may attach to the synovial membrane, become vascularized, and form bony growths, known as osteophytes. Angiogenesis from the synovium and underlying marrow is thought to result in ossification, the calcification of joint cartilage (90).

Drug Delivery Strategies

Current clinical treatments for articular cartilage lesions utilize arthroscopic techniques to contact the underlying bone marrow by abrasion or drilling, and thus, populate defects with blood, MSCs, and bioactive molecules (1). In severe cases, open joint surgery must be performed to completely replace the joint or to realign the joint and relieve contact stress at degenerative sites (90). However, each of these techniques inflicts further joint damage and typically results in fibrocartilage repair tissue (2).

To enhance the quality of tissue repair, an active area of research seeks to revolutionize the treatment of articular cartilage by administration of therapeutic agents. However, since many drugs, growth factors, and other bioactive molecules may act systemically to exert a spectrum of effects, clinical drug therapies must provide a means of targeting and localizing these agents to specific tissues. Furthermore, subcutaneous,

intravenous, or intra-articular delivery of growth factors or other agents frequently requires concentrations much higher than physiological levels due to molecular diffusion and protein deactivation. Accordingly, new drug therapies must develop highly efficient, controlled systems capable of safely delivering drugs to damaged tissues. The following section discusses drug delivery strategies aimed at regulating inflammatory cytokines, decreasing matrix degradation, and regulating the cellular activities in damaged articular cartilage.

Regulation of Inflammatory Cytokines

In articular cartilage defects, penetration of the subchondral bone appears to be necessary for the migration of important progenitor cells. However, contacting the bone marrow also allows rapid migration of inflammatory cells and blood cells which secrete a number of cytokines and initiate a wound healing response that may lead to cartilage destruction, vascularization, and ossification (91). Non-steroidal anti-inflammatory drugs (NSAIDs), appear to help alleviate the joint pain associated with inflammation but have numerous side effects and may actually enhance production of the catabolic cytokine IL-1 (18, 92). However, novel methods of regulating IL-1 and other catabolic signaling molecules are being investigated.

An obvious means of controlling IL-1 is to regulate its IL-receptor binding ability. One strategy for preventing receptor binding has examined polyclonal antibodies directed against IL-1 α and IL-1 β . In arthritic murine joints, IL antibodies were shown to prevent proteoglycan suppression for approximately two days. However, antibodies against TNF- α and IL-6 did not reduce proteoglycan synthesis (93). Another strategy to regulate IL-receptor binding centers on competition for receptor binding sites through the use of IL-1

receptor antagonist protein (IRAP), a protein with affinity for both forms of the IL-1 receptor. *In vitro* and *in vivo*, IRAP has been shown to reduce IL-1 stimulated proteoglycan loss (93, 94). However, clinical trials resulted in serious injection-site reactions in 62% of patients (95). Accordingly, strategies focusing on IL-receptor binding may not provide safe treatments due to these side effects and their lack of specificity to cartilage tissue.

Growth factors, such as the TGF- β s, BMPs, and IGFs, may offer an alternative means to counter the actions of IL-1, since these molecules seem to promote anabolic activities. *In vitro*, TGF- β 1 has been shown to overcome IL-1 suppression of proteoglycan synthesis and IL-1 stimulation of collagen and MMP release (39, 40). *In vivo* research demonstrates that three, 200 ng injections of TGF- β 1 over the course of four days were capable of overcoming suppression of proteoglycan synthesis in murine knee joints concurrently treated with 1 ng IL-1. Similar treatment with BMP-2 was not able to overcome IL-1 suppression (96, 97). IGF-1 has also been shown to counter the catabolic effects of IL-1 on proteoglycan synthesis in cartilage explants (64). However, osteoarthritic patients have elevated levels of IGF binding proteins which maintain stores of latent IGF-1 in extracellular matrix, and therefore, may limit IGF therapies *in vivo* (98).

Although TGF- β 1 appears to be a powerful moderator of IL-1, repeated 200 ng intra-articular injections of TGF- β 1 into murine knee joints were also shown to induce osteophytes (35). Therefore, TGF- β 1 must be administered in a controlled manner which ensures local delivery of low dosages. To achieve sustained release, biodegradable osteochondral implants composed of 50:50 poly(lactic acid-co-glycolic acid) (PLGA) polymers have been examined as drug carriers. During the fabrication process, polymer

and a TGF- β 1 solution were mixed and subjected to compression molding. These delivery vehicles were implanted to full thickness defects in rabbits. Fifty percent of implants loaded with TGF- β 1 improved the quality of tissue repair over unloaded implants, as assessed by histological evaluation. However, the neo-cartilage exhibited inferior mechanical properties when compared to normal cartilage (99). These investigators expanded their study to full thickness defects in goats and found similar results with incomplete cartilage restoration in all defects at 18 weeks (100). The activity and release profile of TGF- β 1 from these carriers was not examined but may be helpful in refining this and other delivery systems.

Alternative biodegradable carriers for TGF- β 1 and other drugs have been investigated and include polymer hydrogels and microparticles, as well as, collagen, fibrin, chitosan, and hyaluronan based materials (61, 101-108). For instance, collagen sponges, impregnated with high doses (5 μ g) of BMP-2, have been implanted into full thickness defects in rabbits. While untreated defects and defects treated with unloaded sponges resulted in fibrous tissue with clefts and fissures, defects with BMP-2 loaded sponges resulted in repair cartilage of seventy percent the normal thickness of articular cartilage and only mild fibrillation (104). It should be noted, however, that the remaining portion of BMP-2 treated defects were filled with bone tissue, a probable consequence of the high BMP concentration.

Microsphere drug encapsulation offers a non-invasive means of delivering growth factors and other regulatory molecules to degenerative cartilage. Unlike scaffolds, microparticles may be injected into defects to provide controlled drug release. Microspheres of *N,N*-dicarboxymethyl chitosan (DCMC), a copolymer of N-

acetylglucosamine and glucosamine, have been formulated and impregnated with BMP-7 to regulate the inflammatory response in full thickness rabbit articular cartilage lesions. Delivery of BMP-7 was able to stimulate chondrocyte proliferation and reduce vascularization and the influx of fibroblast-like cells into these lesions (108). Accordingly, while BMP-2 may not be capable of overcoming the catabolic effects of IL-1, other BMPs may prove to be effective.

PLGA microspheres loaded with paclitaxel, a chemotherapeutic agent that suppresses angiogenesis and cellular proliferation, have been tested assessed for their anti-inflammatory potential. Preliminary studies with intra-articular delivery of these microspheres to isolated equine metacarpophalangeal joints demonstrated biocompatibility and minimal disruption of the hemodynamic forces which might influence drug removal from the joint space (102). PLGA nanospheres have also been explored as carriers for local delivery of betamethasone, a water-soluble corticosteroid. In antigen-induced arthritic rabbits, phagocytosis of these nanospheres by synovial cells was able to reduce joint swelling (109). Although corticosteroids have a number of side effects, this study's use of nanospheres for drug localization via phagocytosis presents a novel delivery strategy.

Regulation of Matrix Degradation

Instead of concentrating on the catabolic signaling molecules involved in cartilage destruction, other researchers are examining the anabolic factors and matrix components which IL and other cytokines appear to influence. Thus, these strategies propose to enhance cartilage repair through delivery of protective growth factors and other matrix components to directly influence matrix metabolism (17, 33, 65).

To prevent proteoglycan loss from aged or injured articular cartilage, many researchers are focusing on the IGF-1 signaling cascade, since this factor has repeatedly demonstrated anabolic effects on matrix metabolism. IGF binding proteins, which regulate extracellular stores of IGF, are overexpressed in the cartilage and synovial fluid of patients with osteoarthritis and may hinder IGF-controlled processes (17). Martin et al. have investigated the effect of elevated IGF binding proteins on proteoglycan synthesis. This study revealed that increasing concentrations of IGF binding protein-3 (IGFBP-3) decrease *in vitro* matrix synthesis in rabbit articular chondrocytes. Addition of fibronectin, which associates with IGFBPs in the extracellular matrix, enhanced the destructive effects of IGFBP-3 (98). Further research demonstrates that these effects may be mitigated by IGF-1 analogs which have decreased affinity for IGFBPs but still activate IGF receptors to promote proteoglycan synthesis in articular cartilage explants (33). Thus, regulation of the IGF axis through peptide delivery may prove helpful in preventing proteoglycan loss. However, controlled peptide delivery of IGF-1 analogs remains to be investigated.

Other strategies aimed at suppressing degradation of cartilage matrix components include attempts to down-regulate MMPs and to up-regulate the tissue inhibitors of MMPs (TIMPs). In one study, both IGF-1 and TGF- β 1 were demonstrated to reduce MMP-1 and -8 activity and mRNA levels of MMP-1, 3, and 8. However, TGF- β 1 had a more potent effect on MMP activity and was also able to increase TIMP expression (65).

Additional research suggests that delivery of TIMPs to damaged articular cartilage may not prevent proteoglycan loss since TIMP expression is regulated by IL-1 β (40, 110). However, a synthetic inhibitor of MMPs has demonstrated potential in

preventing cartilage breakdown in IL-1 β -stimulated cartilage explants. This low molecular weight inhibitor contains a sequence which MMPs are known to cleave, as well as a hydroxamic acid moiety that binds to the zinc ion of MMP's active site (110). Although, this inhibitor was unable to fully reverse the catabolic effects of IL-1 β , its synthetic origin allows for possible modifications to improve its therapeutic effects and to develop a method of controlled delivery.

Another synthetic peptide (TP508), which has the receptor binding domain of thrombin, appears to have potential in articular cartilage repair. TP508 has been shown to promote collagen II expression (111) and has been incorporated into a controlled drug delivery system (112, 113). When applied to full thickness lesions in rabbits, collagen gels embedded with TP508-loaded PLGA microspheres resulted in enhanced GAG content and a smooth articular surface at eight weeks. Likewise, IGF-1 analogs or synthetic TIMP peptides may exhibit further therapeutic benefit for articular cartilage when combined with either a microsphere or nanosphere drug delivery system.

Cellular Regulation

The slow metabolic rates of chondrocytes and their entrapment within the dense extracellular matrix are believed to be significant factors undermining the low repair inability of articular cartilage. Accordingly, research has focused on the use of bioactive molecules to regulate the chemotaxis, proliferation, and differentiation of both articular chondrocytes and progenitor cells.

Repair of chondral defects by recruitment of progenitor cells from the synovial membrane, in contrast to the clinical technique of contacting bone marrow MSCs, has been investigated (60). In order to promote cell migration into porcine and rabbit

chondral defects, the enzymes chondroitinase ABC and trypsin were administered to the surface of defects. Like MMPs, chondroitinase ABC and trypsin digest the GAG chains and protein cores of proteoglycans. Although enzymatic treatment increased cell migration at four weeks, cell coverage only extended over the walls and floor of the defect and did not fill the central cavity. When enzymatic treatment was combined with the subsequent injection of 6 ng/ml TGF- β 1, coverage was improved to multiple cell layers but was still incomplete. However, enzymatic treatment followed by application of a fibrinogen/thrombin solution containing 6 ng/ml TGF allowed for complete filling of the defect cavity with cells and a fibrous extracellular matrix. Treatment of defects with enzymatic treatment and higher concentrations of other growth factors (IGF-1, EGF, and FGF) within the fibrin matrix did not appear to be as effective in cell recruitment (60). This study demonstrates the profound effect that local drug delivery from a scaffold, rather than free injections, may have on tissue repair.

This work was recently extended to porcine full thickness defects. However, a membrane barrier was used to prevent MSC infiltration from the underlying bone marrow. Additionally, a higher dose of TGF- β 1 (200 – 3200 ng/ml) was encapsulated in liposomes and added to the original fibrinogen/thrombin/TGF- β 1 solution (114). Thus, liposome-encapsulated TGF- β 1 was intended to provide sustained, localized drug delivery while the initial release of TGF- β 1 from the fibrin matrix served as a chemotactic agent for synovial cells. Liposomal TGF- β 1 concentrations between 200-900 ng/ml were reported to stimulate chondrogenesis in concentration dependent fashion. However, concentrations of TGF- β 1 above 900 ng/ml resulted in significant side effects, including osteophyte formation (114). Accordingly, this work provides valuable insight

into the effects that drug dose and delivery method may have on cartilage repair. Further knowledge may be gained from examining the release kinetics of TGF- β 1 from the matrix-embedded liposomes to develop correlations between cellular activities and release profiles.

Another pertinent study examined the potential of using photocrosslinked poly(ethylene oxide)-based hydrogels as carriers for both growth factors and chondrocytes for cartilage repair. TGF- β 1 and IGF-1 were encapsulated into PLGA microspheres and then mixed with a polymer/cell solution, prior to hydrogel photopolymerization. *In vitro* culture of these bovine articular chondrocyte constructs demonstrated a significant increase in GAG content and cell content after approximately two weeks. *In vitro* release profiles of PLGA microspheres embedded in cell-free hydrogels allowed for a comparison of release kinetics with trends in matrix synthesis and cell proliferation (61). Similar experiments with other drug delivery systems may provide useful information on the temporal sequence of cellular activation by these bioactive agents.

Conclusions

Numerous growth factors and cytokines have been isolated from articular cartilage and identified as important regulatory molecules in wound healing, matrix synthesis, and cellular migration, proliferation, and differentiation. Among these molecules, TGF- β 1, IGF-1, and members of the BMP family of proteins appear to exert mainly anabolic effects on articular cartilage. Catabolic cytokines, such as IL-1 and TNF- α , are implicated in many of the destructive events which lead to cartilage degeneration. Drug delivery strategies have concentrated on ways to regulate IL-1's destructive effects,

to prevent loss of important matrix molecules, and to promote chondrocyte proliferation in articular cartilage defects. Studies indicate TGF- β 1 as a potential therapeutic agent in each of these strategies. However, since pathological side effects have been associated with TGF- β 1 and other potential candidates, safe methods of sustained, localized delivery are necessary for clinical use of these molecules. Furthermore, a greater understanding of the required therapeutic dose and release kinetics associated with these drug systems will be important in effectively targeting specific molecular and cellular events.

II. SPECIFIC AIMS

Healthy articular cartilage, the thin tissue lining diarthrodial joints, plays a vital role in pain-free movement. However, adult articular cartilage exhibits a very limited intrinsic ability for repair, and current surgical treatments for articular cartilage lesions demonstrate incomplete restoration of tissue structure and function. Accordingly, this research seeks to develop biodegradable hydrogels as controlled drug delivery systems and to utilize these systems to explore the role of growth factors in cartilage repair.

Specifically, this work investigates the potential of oligo(poly(ethylene glycol) fumarate) (OPF) hydrogels as novel release systems towards the following objectives:

1. Determination of the effects of OPF mesh size and gelatin microparticle loading on protein release profiles to fabricate growth factor delivery systems with varying *in vitro* release kinetics
2. Further assessment of growth factor release rates and material degradation profiles in conditions that model the cartilage wound healing environment
3. Evaluation of the biocompatibility and biodegradability of these hydrogel systems in osteochondral defects
4. Extension of these systems for dual delivery of TGF- β 1 and insulin-like growth factor (IGF-1)
5. Investigation of the potential effects of TGF- β 1 and IGF-1 in osteochondral repair *in vivo*

III. *IN VITRO* RELEASE OF TRANSFORMING GROWTH FACTOR- β 1 FROM GELATIN MICROPARTICLES ENCAPSULATED IN BIODEGRADABLE, INJECTABLE OLIGO(POLY(ETHYLENE GLYCOL) FUMARATE) HYDROGELS[†]

Abstract

This research investigates the *in vitro* release of transforming growth factor- β 1 (TGF- β 1) from novel, injectable hydrogels based on the polymer oligo(poly(ethylene glycol) fumarate) (OPF). These hydrogels can be used to encapsulate TGF- β 1-loaded-gelatin microparticles and can be crosslinked at physiological conditions within a clinically relevant time period. Experiments revealed that OPF formulation and crosslinking time may be adjusted to influence the equilibrium swelling ratio, elastic modulus, strain at fracture, and mesh size of these hydrogels. Studies with OPF-gelatin microparticle composites revealed that OPF formulation and crosslinking time, as well as microparticle loading and crosslinking extent, influence composite swelling. *In vitro* TGF- β 1 release studies demonstrated that burst release from OPF hydrogels with a mesh size of 136 Å was approximately 53%, while burst release from hydrogels with a mesh size of 93 Å was only 34%. For hydrogels with a large mesh size (136 Å), encapsulation of loaded gelatin microparticles allowed burst release to be reduced to 29-32%, depending on microparticle loading. Likewise, final cumulative release after 28 days was reduced from 71% to 48-66% by encapsulation of loaded microparticles. However, inclusion of gelatin microparticles within OPF hydrogels of smaller mesh size (93Å) was seen to increase TGF- β 1 release rates. The equilibrium swelling ratio of the microparticle component of these composites was shown to be greater than the equilibrium swelling ratio of the OPF component. Therefore, increased release rates are the result of disruption

[†] This chapter was published as the following article: TA Holland, Y Tabata, and AG Mikos, *In Vitro Release of Transforming Growth Factor- β 1 from Gelatin Microparticles Encapsulated in Biodegradable, Injectable Oligo(Poly(Ethylene Glycol) Fumarate) Hydrogels*, *J. Control. Release*, 91, 299-313 (2003).

of the polymer network during swelling. These combined results indicate that the kinetics of TGF- β 1 release can be controlled by adjusting OPF formulation and microparticle loading, factors affecting the swelling behavior these composites. By systematically altering these parameters, *in vitro* release rates from hydrogels and composites loaded with TGF- β 1 at concentrations of 200 ng/ml can be varied from 13–170 pg TGF- β 1/day for days 1-3 and from 7–47 pg TGF- β 1/day for days 6-21. Therefore, these studies demonstrate the potential of these novel hydrogels and composites in the sustained delivery of low dosages of TGF- β 1 to articular cartilage defects.

Abbreviations

GA, glutaraldehyde; IEP, isoelectric point; OPF, oligo(poly(ethylene glycol) fumarate); OPF3K, OPF synthesized with PEG of molecular weight 3350; OPF10K, OPF synthesized with PEG of molecular weight 10,000; OPF3K-10min, OPF3K crosslinked for 10 min; OPF3K-30min, OPF3K crosslinked for 30 min; PBS, phosphate buffered saline; PEG, poly(ethylene glycol); TGF- β 1, transforming growth factor- β 1;

Introduction

Advances in the fields of biology and cell and molecular engineering have allowed scientists to identify numerous bioactive agents, including members of the transforming growth factor, bone morphogenic protein, and insulin-like growth factor families, which are important to the maintenance and repair of articular cartilage (17, 18). Since articular cartilage lesions typically remain unhealed and often lead to further tissue degeneration and the onset of osteoarthritis (1), understanding the physiological role of these proteins in the wound healing cascade is of critical importance in advancing the treatment of articular cartilage defects. Most of the research in this field has centered on examining the *in vitro* effects which these molecules have on chondrocytes cultured in the presence of one or more growth factors or cytokines (115). However, as the fields of

tissue engineering and biomaterials merge with molecular and cellular biology, new drug delivery vehicles can be utilized to study the *in vivo* effect of these molecules on articular cartilage repair. Accordingly, this paper details the design and development of a novel, biodegradable hydrogel for the controlled delivery of transforming growth factor- β 1 (TGF- β 1) to articular cartilage.

A host of tissue scaffolds have been examined for articular cartilage repair, including synthetic poly(glycolic acid) (PGA) and poly(L-lactic acid) (PLLA) polymer meshes, as well as constructs derived from natural materials such as collagen, fibrin, and hyaluronic acid (116). Hydrophilic materials that can be processed into hydrogels are among the most promising candidates for cartilage repair, since cartilage itself has a water content of approximately 75% (3, 117). Although natural materials such as gelatin, collagen, and hyaluronic acid can be formulated into gels, synthetic polymer hydrogels are often preferred since these materials can be easily reproduced with tailored mechanical, physical, and chemical properties (118). Biomaterials formulated to serve as both tissue scaffolds and drug delivery vehicles for articular cartilage should be both biodegradable and biocompatible. Additionally, these materials must offer a means for preserving drug bioactivity during processing and for controlled release of therapeutic drug levels *in vivo*.

The research presented here examines the material properties which influence the *in vitro* release kinetics of transforming growth factor- β 1 (TGF- β 1) from novel oligo(poly(ethylene glycol) fumarate) (OPF) hydrogels. OPF, a water soluble polymer, can be injected into a defect site and crosslinked *in situ* at physiological conditions. These hydrogels have been shown to be biocompatible and biodegradable (119, 120).

Furthermore, as this research demonstrates, gelatin microparticles can be loaded with TGF- β 1 after microparticle fabrication and then be encapsulated within OPF hydrogels to provide greater control over drug release. Previous research has shown that *in vivo* protein release from gelatin microparticles is dependent on enzymatic degradation of gelatin (121). Accordingly, OPF hydrogels with encapsulated gelatin microparticles offer a means of delivering TGF- β 1 to articular cartilage as key enzymes in the wound healing process initiate tissue remodeling.

Before such a delivery device is examined *in vivo*, the kinetics of *in vitro* release should first be investigated so that tissue response may be correlated with the time course of drug delivery. Consequently, the goal of this research was to systematically explore the material properties of OPF hydrogels and OPF-gelatin microparticle composites which may influence *in vitro* TGF- β 1 release. Specifically, the objectives of this work were as follows:

1. To investigate the effects of OPF formulation and crosslinking time on hydrogel swelling, mechanical properties, and mesh size.
2. To evaluate the effects of microparticle loading and crosslinking extent on the swelling properties of OPF-gelatin microparticle composites.
3. To determine whether the *in vitro* release profiles of TGF- β 1 could be altered by varying OPF formulation and crosslinking time, microparticle loading, and microparticle crosslinking extent.

Experimental Methods

Gelatin Microparticle Fabrication

Acidic gelatin (Nitta Gelatin Inc., Osaka, Japan) with an isoelectric point (IEP) of 5.0 was used for microparticle fabrication according to a previously established method (122). Briefly, 5 g gelatin was dissolved in 45 ml ddH₂O by mixing and heating (60°C).

This aqueous gelatin solution was added dropwise to 250 ml olive oil while stirring at 500 rpm. The temperature of the emulsion was then decreased to approximately 15°C with constant stirring. After 30 min, 100 ml chilled acetone (4°C) was added to the emulsion. After 1 hour, the resulting microspheres were collected by filtration and washed with acetone to remove residual olive oil.

Microspheres were crosslinked by incubation in a 0.1 wt% solution of Tween 80 (Sigma, St. Louis, MO) in ddH₂O containing either 10 mM or 40 mM glutaraldehyde (GA) (Sigma, St. Louis, MO). This crosslinking reaction was maintained at 15°C for approximately 15 h while stirring at 500 rpm. Crosslinked microparticles were collected by filtration, washed with ddH₂O, and then agitated in a 25 mM glycine solution to block residual aldehyde groups of unreacted GA. After 1 hour, microparticles were again collected by filtration, washed with ddH₂O, and then vacuum dried overnight. After drying, the microparticles were sieved to obtain particles 50-100 μ m in size.

Microparticle Swelling

Gelatin microparticle crosslinking extent was assessed by examining microparticle swelling in 0.01 M phosphate buffered saline (PBS) at pH 7.4. Specifically, 50 mg gelatin microparticles were swollen overnight in 20 ml PBS while agitated on a shaker table at 100 rpm. After 24 h, the swollen microparticles were collected on filter paper to remove surface water and placed in a vial of known weight (W_v). The weight of the swollen microparticles and vial was then recorded ($W_{s,v}$). After vacuum drying for 24 h, the weight of the dry microparticles and vial was recorded ($W_{d,v}$). Accordingly, the fold swelling ratio (S) of gelatin microparticles was calculated as follows,

$$S = \frac{W_{s,v} - W_{d,v}}{W_{d,v} - W_v}$$

This ratio provides an indication of how water is absorbed per g microparticle. Fold swelling ratios for microparticles crosslinked with 10 and 40 mM GA were determined with $n = 5$ for each experiment.

Volumetric equilibrium swelling ratios of loaded-gelatin microparticles were estimated by the following equation,

$$Q = \frac{1 + Sp}{1 + sp}$$

where S is the fold swelling ratio (defined above), s is the ratio of drug solution (ml) per g microparticles used in microparticle loading (5 ml/g as described below), and ρ is the density of dry microparticles (g/ml).

Microparticle Loading

For release studies, microparticles were loaded with TGF- β 1 by swelling in aqueous TGF- β 1 solutions at pH 7.4 according to established methods (122, 123). At this pH, TGF- β 1 (with an IEP of 9.5) is positively charged, and therefore, forms a polyionic complexation with negatively charged acidic gelatin (IEP of 5.0) (124). Solutions of TGF- β 1 were composed of I^{125} labeled-TGF- β 1 (Perkin Elmer Life Sciences, Boston, MA) and unlabeled-TGF- β 1 (R&D Systems, Minneapolis, MN) in a mass ratio of 0.06 to allow for detection of drug release. The TGF- β 1 concentration in the swelling solutions was varied according to the microparticle/polymer ratio of composites to achieve a final TGF- β 1 concentration of 200 ng/ml. This concentration of TGF- β 1 has been shown to be therapeutic in the treatment of full and partial thickness rabbit and porcine defects when encapsulated in liposomes (105, 114).

Specifically, microparticle loading was performed by adding 5 μ l of TGF- β 1 solution per mg microparticle to dried microparticles. This solution volume is below the microparticles' theoretical, equilibrium swelling volume to allow for complete drug absorption. The resulting mixture was vortexed and incubated at 4°C for 15h. For composite swelling studies, TGF- β 1-free microparticles were prepared in a similar method using PBS. Accordingly, all experimental measurements, unless otherwise stated, were begun with microparticles in this initial, partially-swollen state.

OPF Synthesis

Two formulations of OPF were synthesized according to a method developed in our laboratory by varying the molecular weight of the initial poly(ethylene glycol) (PEG) (125). PEG, with initial average molecular weight 3350 (Dow, Midland, MI) and 10,000 (Aldrich, Milwaukee, WI) was used to synthesize OPF3K and OPF10K, respectively. Approximately 50 g PEG was first azeotropically distilled in toluene to remove residual water and then dissolved in 500 ml distilled methylene chloride. The resulting PEG solution was placed in an ice bath and stirred while 0.9 moles triethylamine (TEA, Acros, Pittsburgh, PA) per mole PEG and 1.8 moles distilled fumaryl chloride per mole PEG were added dropwise. The reaction was maintained in a nitrogen environment. Upon completion of reagent addition, the reaction vessel was removed from the ice bath and stirred at room temperature.

After 48 h, polymer purification was begun with the removal of methylene chloride by rotary evaporation. The OPF was then dissolved in ethyl acetate and vacuum-filtered to remove the salt precipitate formed by the reaction of chloride with TEA. Finally, OPF was recrystallized twice in ethyl ether, and the resulting powder vacuum

dried for approximately 8 h. Dry, purified polymer was stored in a sealed vessel at -20°C until use.

Gel Permeation Chromatography

OPF molecular weights were determined by gel permeation chromatography (GPC) (Model 410; Waters, Milford, PA). Samples of both the initial PEG and final OPF were dissolved in chloroform and filtered before injection into a Waters column (50-100,000 Da range). The GPC was operated at a flow rate of 1 ml/min. Molecular weights were determined from elution time based on a calibration curve generated with PEG standards. Samples were run in triplicate.

Hydrogel and Composite Fabrication

OPF hydrogels, with no microparticle component, and OPF-gelatin microparticle composites were fabricated using the same procedure. For swelling and release studies, the effects of OPF formulation (initial PEG molecular weight and crosslinking time), microparticle loading, and microparticle crosslinking extent were examined at the values as shown in Table 1. To formulate hydrogels and composites, 0.15 g OPF was dissolved in 395 μ l of PBS containing 14 mg N,N'-methylene bisacrylamide (Sigma, St. Louis, MO) as a crosslinking agent. Then the appropriate amount of microspheres (0, 8, or 32 mg) was added to this polymer solution with an additional 118 μ l PBS. The resulting mixture was thoroughly vortexed. Finally, 51 μ l of 0.3 M tetramethylethylenediamine (in PBS) (Sigma, St. Louis, MO) and 51 μ l of 0.3 M ammonium persulfate (in PBS) (Sigma, St. Louis, MO) were added to initiate crosslinking accordingly to established procedures for OPF hydrogel crosslinking (126). After vortexing, the suspension was injected into a Teflon mold and incubated at 37°C. After either 10 or 30 min, the resulting crosslinked

hydrogel or crosslinked composite was removed and swollen in PBS or ddH₂O prior to use. The abbreviations OPF3K-10min, OPF3K-30min, and OPF10K-10min refer to the OPF formulation and crosslinking time used in fabricating hydrogels and composites.

Table III- 1: Parameters for OPF-gelatin microparticle composites

OPF Formulation		OPF3K-10 min	OPF3K-30 min	OPF10K-10 min
g Microparticle g Polymer	High	0.20	0.20	0.20
	Low	0.05	0.05	0.05
GA Concentration for Microparticle Crosslinking	High	40 mM	40 mM	40 mM
	Low	10 mM	10 mM	10 mM

Rheometry

A rheometer (Model AR1000; TA Instruments, New Castle, DE) was used to measure the complex viscosity of OPF3K and OPF10K hydrogels during the crosslinking reaction. A flat, parallel plate geometry (0.8 cm in diameter) was attached to the motor spindle and aligned with the sample well. Polymer and initiator solutions were combined as described above, and then 750 μ l of this solution was injected into the sample well and maintained at 37°C. The flat plate was then lowered to a gap height of 11,000 μ m above the sample and allowed to oscillate, applying a sinusoidal stress wave to the sample. The resulting strain wave was measured and used to calculate viscosity (η) by the equation, $\omega = \mu\gamma$, where σ and γ represent the shear stress and strain rate. Calculations were performed using Rheology Solutions Software (TA Instruments, New Castle, DE). To prevent hydrogel dehydration during the duration of the experiment, the hydrogel surface was wetted with PBS approximately every 60 s. Gelation time was defined as the length of time required until less than 1% change in complex viscosity was observed. Experiments were conducted in triplicate for each OPF formulation.

Tensile Testing

For tensile testing, the polymer and initiator solutions were combined as previously described and then injected into a dog-bone shaped Teflon mold, with dimensions specified by ASTM D638-98. Hydrogels formed from OPF10K were removed from the mold after 10 min of incubation at 37°C, while OPF3K hydrogels were removed from the mold after 10 or 30 min of incubation at 37°C. All hydrogels were immediately swollen in ddH₂O for approximately 24 h.

An Instron testing machine (Model 5565, Canton, MA), equipped with a 50 N load cell, was used to perform hydrogel tensile testing, according to ASTM D638-98. Hydrogels were pulled at a rate of 25 mm/min to ensure fracture between 0.5 – 5 min. Specimens were misted with ddH₂O to maintain hydration throughout the experiment. Load-displacement curves were recorded and converted to stress-strain curves using the known initial cross-sectional area of the specimens. Tensile modulus was calculated as the slope of the initial portion of the stress-strain curve. Strain at fracture (α) was determined by the equation,

$$\alpha = (L - L_0)/L_0,$$

where L_0 and L represent the initial and final specimen length, respectively. Strength at fracture (τ) was also determined for each specimen. The tensile properties of both OPF3K-30min and OPF10K-10min hydrogels were examined with $n = 5$ for each OPF formulation.

Hydrogel and Composite Swelling Studies

The volumetric swelling ratios of OPF3K and OPF10K hydrogels crosslinked for 30 and 10 min, respectively, were determined using a hanging pan balance according to established procedures (127, 128). Crosslinking was performed as described above, and

then a cork bore was used to cut hydrogels of appropriate dimensions (10 mm in diameter and 1 mm in thickness). The volumetric swelling ratio (Q) of these hydrogels was determined by the following equation,

$$Q = (1 - \phi) \frac{v_r}{v_s}$$

where ϕ represents the hydrogel sol fraction. The parameters, v_s and v_r , respectively represent the polymer volume fraction in the hydrogel after swelling and the polymer volume fraction in the hydrogel after crosslinking but before swelling. These parameters were calculated using the following equations,

$$v_s = \frac{W_{a,d} - W_{n,d}}{W_{a,s} - W_{n,s}} \quad v_r = \frac{W_{a,d} - W_{n,d}}{W_{a,r} - W_{n,r}}$$

where $W_{a,r}$ and $W_{n,r}$, respectively represent the weight of the crosslinked hydrogel (before swelling) in air or in the non-solvent hexane. $W_{a,s}$ and $W_{n,s}$ correspond to weight of the crosslinked hydrogel in air or in hexane after swelling for 24 h. $W_{a,d}$ and $W_{n,d}$ are the weights of the crosslinked hydrogel in air or in hexane after swelling 24 h and then vacuum drying for 24 h. The hydrogel sol fraction was calculated by the equation,

$$\phi = \frac{\kappa W_{a,r} - W_{a,d}}{\kappa W_{a,r}},$$

where κ represents the weight fraction of polymer in the solution just prior to crosslinking. For all formulations, $\kappa = 0.21$. Experiments were conducted with $n = 5$ for both OPF3K and OPF10K hydrogels.

Folding (mass) swelling ratios (S) for OPF hydrogels and OPF-gelatin microparticle composites were also determined using a method similar to the technique for analyzing microparticle swelling. After crosslinking, a cork bore was used to obtain

hydrogels and composites with the same dimensions (3 mm in diameter and 1 mm in thickness) as those used for release studies. Fold swelling was calculated by the formula,

$$S = \frac{W_{a,s} - W_{a,d}}{W_{a,d}}$$

The effects of OPF formulation, microparticle loading, and microparticle crosslinking extent on S were examined according to the parameters in Table 1. Fold swelling experiments were conducted with n = 6 for all formulations.

Calculation of Molecular Weight between Crosslinks and Mesh Size

The molecular weight between crosslinks (M_c) of OPF3K and OPF10K hydrogels crosslinked for 30 and 10 min, respectively, were calculated using previously established theories which assume a Gaussian distribution of chain lengths between crosslinks (128, 129). This method for M_c determination has been previously used to characterize OPF-PEG diacrylate hydrogels (127). The formula for M_c , based on these assumptions, is given by

$$\frac{1}{M_c} = \frac{\tau}{\alpha - (1/\alpha^2)} \cdot \frac{Q^{1/3}}{RTC} + \frac{2}{M_n}$$

where R is the gas constant (8.31 kPa·L/mol·K), T is the temperature at which tensile testing was conducted (298 K), C is the mass concentration of polymer in solution before crosslinking (0.27 kg/L), and M_n is the OPF number average molecular weight. The parameters τ , α , and Q correspond to previously defined mechanical and swelling properties of these hydrogels.

Mesh size (ξ) was also determined for these OPF hydrogels according the following equation,

$$\xi = (v_{2,s})^{1/3} \left(\overline{r_0^2} \right)^{1/2}$$

where $\overline{r_0^2}$ is the end to end distance of polymer chains in the unperturbed state (128). $\overline{r_0^2}$

is estimated from the characteristic ratio (C_n), given by

$$C_n = \frac{\overline{r_0^2} \cdot M_r}{\ell^2 \cdot 3M_c}$$

where $\ell = 1.47 \text{ \AA}$, the weighted average of C-C and C-O bond lengths. C_n is taken to be 4.0 for PEG (130). M_r is the molecular weight of the polymer repeating unit (44 g/mol). Error propagation methods were used to determine standard deviations for M_c and ξ (131).

In Vitro TGF- β 1 Release Study

Finally, the *in vitro* release of TGF- β 1 from gelatin microparticles, OPF hydrogels, and OPF-gelatin microparticle composites was examined over the course of 28 days. To examine TGF- β 1 release from microparticles, 5 mg of 10 or 40 mM GA microparticles were loaded, as previously described, and incubated in 3 ml PBS at 37°C. OPF3K and OPF10K hydrogels were loaded with TGF- β 1 just prior to crosslinking by replacing 40 μ l of the 118 μ l PBS addition with a solution of TGF- β 1. Composites were formulated with loaded gelatin microspheres as described above and according to the parameters outlined in Table 1. Both hydrogels and composites were crosslinked between two Teflon plates at 37°C for the designated time (10 or 30 min), and then gels of appropriated dimensions (3 mm in diameter and 1 mm in thickness) were obtained using a cork bore. These gels were placed in 3 ml PBS and incubated at 37°C. All specimens were agitated on a shaker table (70 rpm). After 0.5, 1, 2, 3, 6, 10, 14, 18, 21, and 28 days, the supernatant of each specimen was collected and analyzed for radioactivity using a gamma counter (Cobra II

Autogamma, Packard, Meridian, CT). The amount of TGF- β 1 in the supernatant was determined by correlation to a standard curve.

Cumulative release was determined by normalizing the total TGF- β 1 released at each time point with the sum of the total TGF- β 1 released over the course of 28 days and the TGF- β 1 remaining in the gel at day 28. Release rates were determined by taking the slope of the percent cumulative release curve for each sample over the stated range and averaging the resultant slopes for each formulation. Accordingly, rates are stated in terms of the change in the percent cumulative release per day. For all formulations of microparticles, hydrogels, and composites, n was initially 6. However, some samples were damaged in the collection of supernatant, resulting in an n of 4 to 6.

Statistical analysis

Results were statistically compared using the F test and Tukey's multiple comparison test ($p < 0.05$). Additionally, a factor effects analysis (132) was used to analyze the potential single factor effects of OPF formulation (crosslinking time and initial PEG molecular weight), microparticle loading, and microparticle crosslinking extent on composite swelling ($p < 0.05$). Values are reported as average \pm standard deviation.

Results

Microparticle Swelling

Gelatin microparticles formulated with 10 mM GA were found to exhibit a fold swelling ratio of 12.2 ± 0.9 . The swelling ratio of microparticles crosslinked with 40 mM GA was found to be 10.5 ± 0.4 , significantly lower than the value for 10 mM GA

microparticles. Volumetric equilibrium swelling ratios (Q) for loaded 10 and 40 mM GA microparticles were estimated to be 2.0 and 1.8, respectively.

GPC

GPC analysis confirmed the number average molecular weights of the initial PEG to be $2,850 \pm 30$ and $8,580 \pm 180$. The OPF synthesized with these PEG samples was determined to be of initial number average molecular weight $5,200 \pm 110$ (OPF3K) and $10,240 \pm 390$ (OPF10K), respectively. The polydispersity indices of OPF3K and OPF10K were determined to be 1.51 ± 0.02 and 1.15 ± 0.02 , respectively.

Rheometry

Rheometry experiments demonstrated that OPF3K hydrogels require longer crosslinking times than OPF10K hydrogels to achieve complete gelation at 37°C. The gelation time for OPF3K hydrogels was 28.8 ± 2.0 min, while the gelation time for OPF10K hydrogels was only 10.5 ± 0.2 min. After 10 min, the viscosity of OPF3K hydrogels reached approximately 23% of their final viscosity. However, after 10 min of crosslinking at 37°C, OPF3K hydrogels retained their structure when removed from a mold and swollen. Therefore, both OPF3K hydrogels crosslinked for 10 min and 30 min were examined as drug delivery vehicles. Since OPF10K hydrogels are fully crosslinked after 10 min, the effects of a longer crosslinking time were not explored for these hydrogels.

Tensile Testing

Although, both OPF3K hydrogels crosslinked for 10 min and 30 min retain their structural integrity for several days while swollen in PBS, OPF3K hydrogels crosslinked for 10 min did not possess the mechanical integrity required for tensile testing according

to ASTM D638-98. Accordingly, tensile testing of these hydrogels was not feasible. Tensile testing of OPF3K and OPF10K hydrogels crosslinked for 30 and 10 min, respectively, revealed that OPF3K hydrogels possess a significantly higher elastic modulus (55.6 ± 16.5) than OPF10K hydrogels (20.0 ± 1.4 , see Table 2). However, OPF3K hydrogels achieve a significantly lower strain at fracture (0.19 ± 0.05) than OPF10K hydrogels (0.46 ± 0.08). Stress at fracture did not vary between OPF3K (10.4 ± 2.7) and OPF10K (9.5 ± 0.8) hydrogels.

Table III- 2: Properties of OPF3K-10 hydrogels (crosslinked for 10 and 30 min) and OPF10K hydrogels (crosslinked for 10 min), respectively. Mechanical and swelling properties were statistically compared with asterisks indicating the greater value ($p < 0.05$).

Hydrogel Formulation	OPF3K-10min	OPF3K-30min	OPF10K-10min
Elastic Modulus (kPa)	n/a	55.6 ± 16.5 *	20.0 ± 1.4
Strain at Fracture (α)	n/a	0.19 ± 0.05	0.46 ± 0.08 *
Stress at Fracture (τ , kPa)	n/a	10.4 ± 2.7	8.5 ± 0.8
Volumetric Swelling Ratio (Q)	1.3 ± 0.1	1.2 ± 0.0	3.3 ± 0.2 *
Fold Swelling Ratio (S)	18.2 ± 4.0	15.5 ± 4.1	25.3 ± 2.4 *
Molecular Weight Between Crosslinks (M_c , g/mol)	n/a	2380 ± 70	4620 ± 160
Mesh Size (ξ , Å)	n/a	93 ± 3	136 ± 3

Hydrogel Swelling

Hydrogel swelling experiments revealed a significant difference in both the volumetric (Q) and fold swelling (S) ratios of OPF3K hydrogels and OPF10K hydrogels (Table 2). OPF10K hydrogel swelling ratios ($Q = 3.3 \pm 0.2$, $S = 25.3 \pm 2.4$) were significantly greater than both OPF3K hydrogels crosslinked for 10 min (OPF3K-10min) ($Q = 1.3 \pm 0.1$, $S = 18.2 \pm 4.0$) and OPF3K hydrogels crosslinked for 30 min (OPF3K-30min) ($Q = 1.2 \pm 0.0$, $S = 15.5 \pm 4.1$). However, statistical differences were not observed in the volumetric and fold swelling ratios of OPF3K-10min and OPF3K-30min hydrogels.

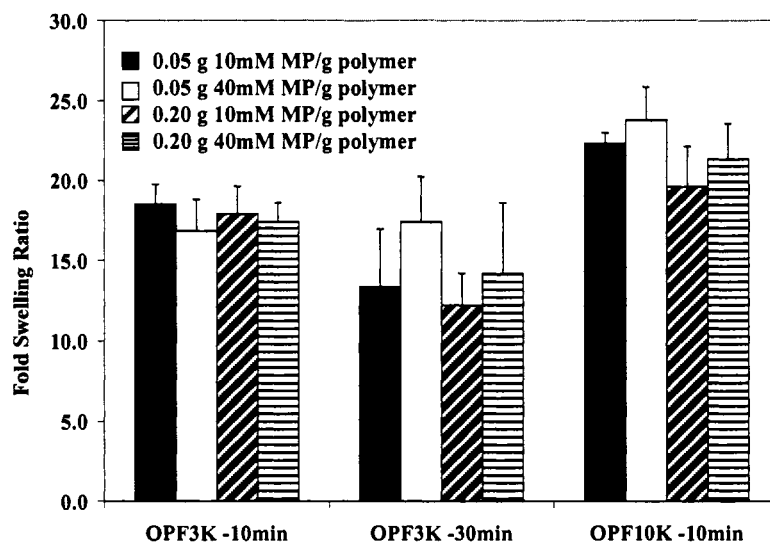
Hydrogel M_c and ξ

Combining the results of tensile testing and volumetric swelling experiments, the molecular weight between crosslinks (M_c) and mesh size (ξ) of OPF hydrogels was determined (Table 2). For OPF3K-30min hydrogels, M_c was determined to be 2380 ± 70 g/mol, while ξ was found to be 99 ± 3 Å. For OPF10K-10min hydrogels, M_c was determined to be 4620 ± 160 g/mol, and ξ was found to be 136 ± 3 Å. Since tensile testing of OPF3K hydrogels crosslinked for 10 min was not feasible, M_c and ξ were not determined for this formulation.

Composite Swelling

Fold swelling ratios (S) for OPF-gelatin microparticle composites are shown in Figure 1. A factor effects analysis was used to identify parameters of composites that significantly influence swelling. Using this method to compare to fold swelling data for composites formulated with OPF3K-10min and OPF3K-30 min, only crosslinking time was found to significantly influence swelling ($p < 0.05$). Microparticle loading and microparticle crosslinking extent were not significant factors affecting fold swelling. However, when a factor effects analysis was used to compare fold swelling data for composites formulated with fully crosslinked OPF (OPF3K-30min and OPF10K-10min), OPF formulation, microparticle loading, and microparticle crosslinking extent were found to be significant factors affecting swelling ($p < 0.05$).

Figure III- 1: Fold swelling ratios for OPF-gelatin microparticle composites. Parameters of composites correspond to Table 1. Error bars represent \pm standard deviation with $n = 6$ for all formulations.



In Vitro TGF- β 1 Release Study

The cumulative release profiles of gelatin microparticles, OPF hydrogels, and OPF-gelatin microparticle composites (Figures 2-6) were divided into four phases to allow for quantitative comparison between formulations. Similar methods have been used to describe TGF- β 1 release profiles from other polymeric materials (106). A burst release during the first 24 h (phase 1) was observed for all formulations. A period of continued moderate to slow release then ensued. To better describe the release profiles of some formulations, this period was divided into phase 2 (days 1-3) and phase 3 (days 6-21), with phase 2 release rates generally exceeding phase 3 release rates. Finally, release during days 21-28 (phase 4) appeared to be greatly influenced by the extent of OPF degradation. Therefore, the burst release after day 1, release rates for phases 2 and 3, and final cumulative release after day 28 were calculated as described above for all formulations.

Figure III- 2: Percent cumulative TGF- β 1 release from gelatin microparticles crosslinked with either 10 or 40 mM GA. Error bars represent \pm standard deviation with n = 4 to 6.

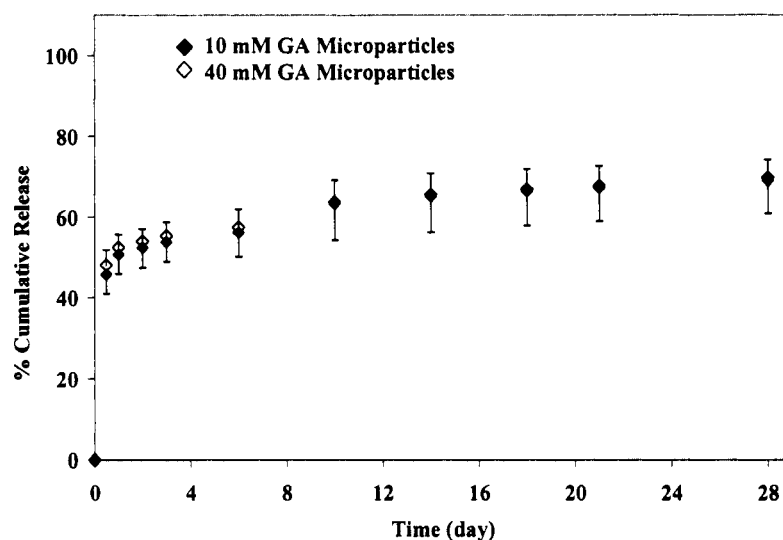


Figure III- 3: Percent cumulative TGF- β 1 release from OPF3K hydrogels (crosslinked for 10 and 30 min) and OPF10K hydrogels (crosslinked for 10 min). Error bars represent \pm standard deviation with n=4 to 6 for all formulations.

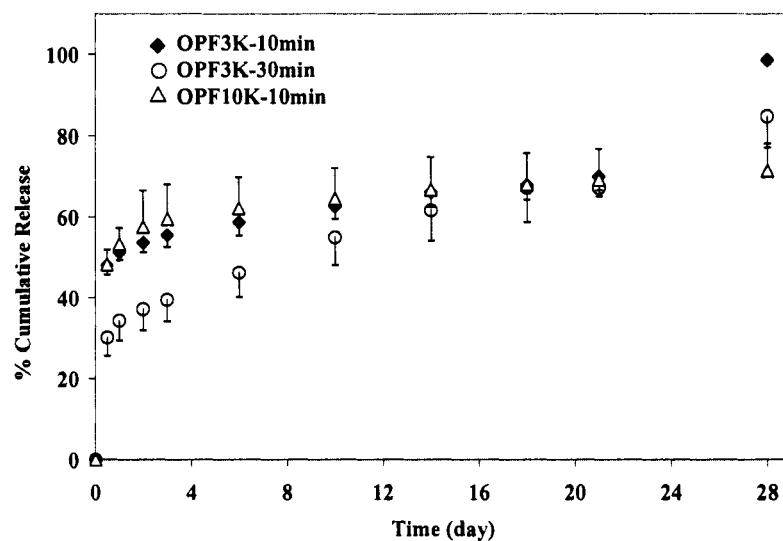


Figure III- 4: Percent cumulative TGF- β 1 release from OPF3K-gelatin microparticle composites crosslinked for 10 min. Error bars represent \pm standard deviation with n=4 to 6 for all formulations.

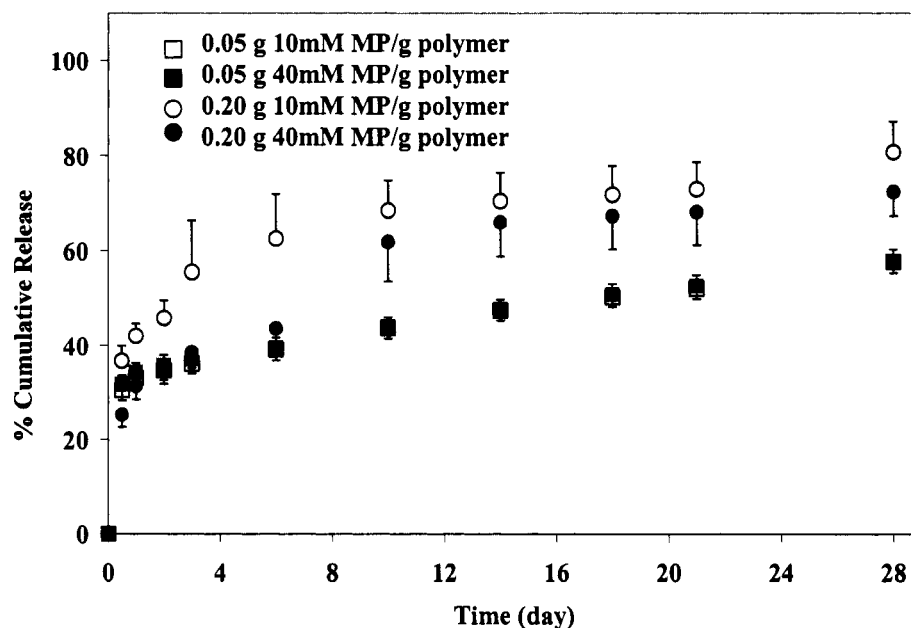


Figure III- 5: Percent cumulative TGF- β 1 release from OPF3K-gelatin microparticle composites crosslinked for 30 min. Error bars represent \pm standard deviation with n=4 to 6 for all formulations.

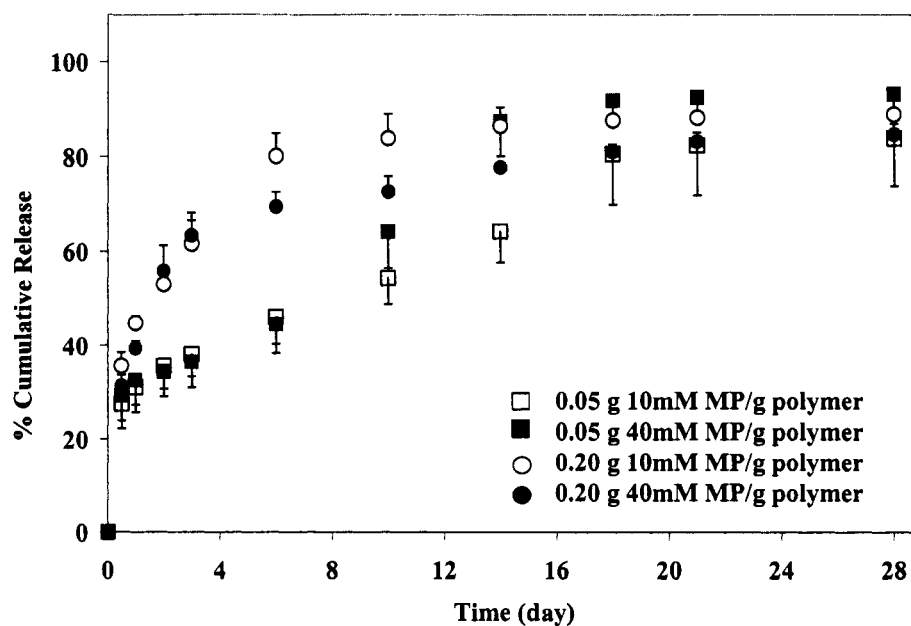
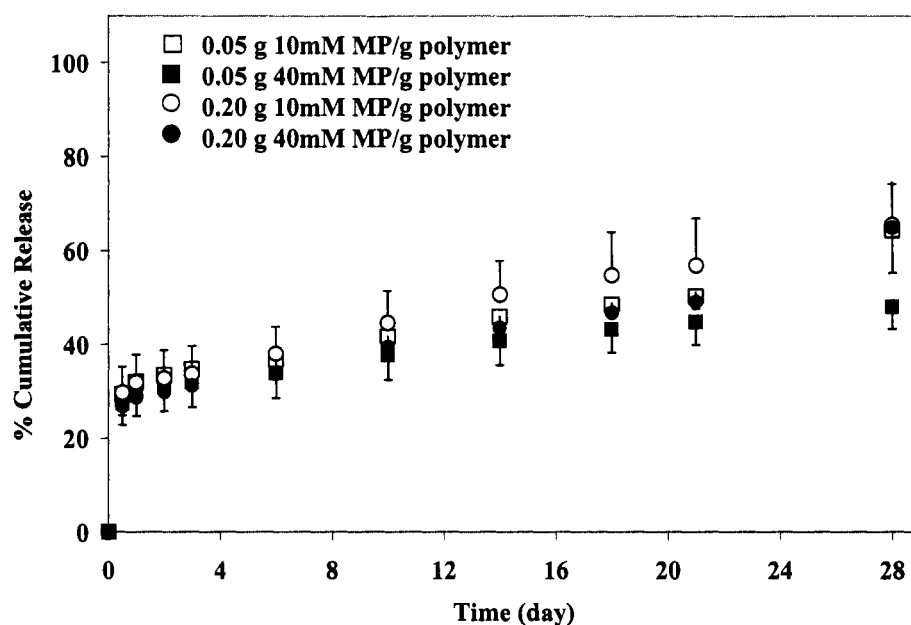


Figure III- 6: Percent cumulative TGF- β 1 release from OPF10K-gelatin microparticle composites crosslinked for 10 min. Error bars represent \pm standard deviation with $n=4$ to 6 for all formulations.



TGF- β 1 Release Kinetics for Gelatin Microparticles

The TGF- β 1 release profiles of gelatin microparticles were not affected by microparticle crosslinking extent (Figure 2). No significant differences were seen in either burst release or final cumulative release values from the two microparticle formulations. Microparticles crosslinked with 10 mM GA exhibited a burst release of $50.7 \pm 4.8\%$ after 1 day and a final cumulative release of $69.1 \pm 8.0\%$ after 28 days (Table 3). Microparticles crosslinked with 40 mM GA exhibited a burst release of $52.4 \pm 3.2\%$ after 1 day and a final cumulative release of $69.8 \pm 4.6\%$ after 28 days. Both microparticle formulations exhibited a phase 2 release rate of approximately 1.5% per day and phase 3 release rate of 0.7% per day, further indicating that microparticle crosslinking extent does not affect *in vitro* release kinetics.

TGF- β 1 Release Kinetics for OPF Hydrogels

As shown in Figure 3, OPF hydrogels fabricated with a crosslinking time of 10 minutes exhibited similar TGF- β 1 release profiles. For both OPF3K-10min and OPF10K-10min hydrogels, an initial burst release of approximately 50% (Table 4) was followed by a phase 2 release rate of approximately 2-3% per day (Table 5) and phase 3 release of < 1% per day (Table 6). However, the loosely crosslinked network of OPF3K-10min hydrogels appeared to be more susceptible to hydrolytic degradation than fully crosslinked OPF10K-10min hydrogels. Gel fragmentation and bleaching of their initial brownish color, evidence of degradation, was visible by day 14 for OPF3K-10min hydrogels. By day 28, OPF3K-10min hydrogels were completely degraded resulting in much higher final cumulative release for these hydrogels ($98.6 \pm 0.9\%$, see Table 7) than OPF10K-10min hydrogels ($71.5 \pm 6.7\%$).

Table III- 3: *In vitro* TGF- β 1 release kinetics from gelatin microparticles initially crosslinked with 10 or 40 mM GA.

Microparticle Crosslinking Extent	10 mM GA	40 mM GA
Burst Release (%)	50.7 ± 4.8	52.4 ± 3.2
Final Cumulative Release (%)	69.1 ± 8.0	69.8 ± 4.6
Release Rate (%/day) for Phase 2 (Days 1-3)	1.6 ± 0.2	1.4 ± 0.2
Release Rate (%/day) for Phase 3 (Days 6-21)	0.7 ± 0.2	0.6 ± 0.1

Table III- 4: Percent cumulative TGF- β 1 release after 1 day from OPF hydrogels and OPF-gelatin microparticle composites. OPF3K and OPF10K composites formulated with a crosslinking time of 10 min exhibited a significantly lower burst release than their corresponding hydrogels (*, $p < 0.05$). OPF3K composites formulated with a crosslinking time of 30 min exhibited a similar or greater (**, $p < 0.05$) burst release than their corresponding hydrogel.

Microparticle Content		Polymeric Content		
$\frac{\text{g Microparticle}}{\text{g Polymer}}$	Microparticle Crosslinking Extent (mM GA)	OPF3K-10min	OPF3K-30min	OPF10K-10min
0.00	-	51.3 ± 1.9	34.4 ± 5.0	53.4 ± 4.0
0.05	10 mM	33.2 ± 2.2 *	31.1 ± 5.3	32.1 ± 4.5 *
0.05	40 mM	34.4 ± 1.9 *	32.6 ± 5.3	30.0 ± 5.2 *
0.20	10 mM	42.0 ± 2.6 *	44.8 ± 1.5 **	31.9 ± 5.9 *
0.20	40 mM	31.4 ± 2.9 *	39.4 ± 1.6	28.7 ± 1.3 *

Table III- 5: Phase 2 (days 1-3) TGF- β 1 release rates from OPF hydrogels and OPF-gelatin microparticle composites. Rates are stated as change in percent TGF- β 1 released per day.

Microparticle Content		Polymeric Content		
<u>g Microparticle</u> <u>g Polymer</u>	Microparticle Crosslinking Extent (mM GA)	OPF3K-10min	OPF3K-30min	OPF10K-10min
0.00	-	2.1 ± 1.1	2.6 ± 0.5	3.1 ± 2.4
0.05	10 mM	1.5 ± 0.1	3.5 ± 0.9	1.3 ± 0.2
0.05	40 mM	1.5 ± 0.2	2.0 ± 0.2	1.0 ± 0.1
0.20	10 mM	6.8 ± 4.2	8.5 ± 2.7	1.0 ± 0.2
0.20	40 mM	3.6 ± 0.5	12.0 ± 2.3	1.3 ± 0.1

Table III- 6: Phase 3 (days 6-21) TGF- β 1 release rates from OPF hydrogels and OPF-gelatin microparticle composites. Rates are stated as change in percent TGF- β 1 release per day.

Microparticle Content		Polymeric Content		
<u>g Microparticle</u> <u>g Polymer</u>	Microparticle Crosslinking Extent (mM GA)	OPF3K-10min	OPF3K-30min	OPF10K-10min
0.00	-	0.7 ± 0.1	1.5 ± 0.1	0.5 ± 0.1
0.05	10 mM	0.9 ± 0.0	2.6 ± 0.5	0.9 ± 0.2
0.05	40 mM	0.9 ± 0.0	3.3 ± 0.4	0.7 ± 0.1
0.20	10 mM	0.6 ± 0.2	0.5 ± 0.2	1.3 ± 0.9
0.20	40 mM	1.5 ± 0.3	0.9 ± 0.3	1.0 ± 0.0

Table III- 7: Final percent cumulative TGF- β 1 release after 28 days from OPF hydrogels and OPF-gelatin microparticle composites. Asterisks indicate composites with a lower final cumulative release than their corresponding hydrogel ($p < 0.05$).

Microparticle Content		Polymeric Content		
<u>g Microparticle</u> <u>g Polymer</u>	Microparticle Crosslinking Extent (mM GA)	OPF3K-10min	OPF3K-30min	OPF10K-10min
0.00	-	98.6 ± 0.9	84.8 ± 7.6	71.5 ± 6.7
0.05	10 mM	57.7 ± 2.3 *	84.0 ± 10.0	64.5 ± 9.1
0.05	40 mM	57.7 ± 2.8 *	93.4 ± 3.4	48.2 ± 4.8 *
0.20	10 mM	80.8 ± 6.4 *	89.0 ± 3.1	65.6 ± 8.7
0.20	40 mM	72.5 ± 5.1 *	84.8 ± 2.3	65.0 ± 9.6

By extending the crosslinking time for OPF3K hydrogels to 30 min, hydrogel burst release was reduced to $34.4 \pm 5.0\%$ (Table 4). These hydrogels exhibited similar phase 2 and 3 release rates to hydrogels fabricated with a crosslinking time of 10 min. Final cumulative release for OPF3K-30min hydrogels ($84.8 \pm 7.6\%$, see Table 7) appeared to be similar to final cumulative release values for OPF10K-10min hydrogels.

Both of these fully crosslinked hydrogels remained intact through day 21 and exhibited only minimal signs of fragmentation and color loss by day 28.

TGF- β 1 Release Kinetics for OPF3K-10min Composites

Encapsulation of loaded gelatin microparticles within composites fabricated with OPF3K crosslinked for 10 min allowed for reduction in cumulative TGF- β 1 release when compared to OPF3K-30min hydrogels. All composites formulated with OPF3K-10min exhibited significantly lower burst release (Table 4) and final release values (Table 7) than OPF3K-10min hydrogels. Although some evidence of OPF degradation was seen by day 18, the gelatin component of these composites was hydrolytically stable, and thus, prevented the high cumulative release values observed with OPF3K-10min hydrogels. However, high microparticle loading (0.20 g microparticles/ g polymer) appeared to elevate phase 2 release rates (Table 5) and resulted in higher final cumulative release values (Table 7) than composites with low microparticle loading. Accordingly, these results indicate that while microparticle encapsulation allows for reduction of burst release within these loosely crosslinked gels, microparticle loading may increase the rate of further release.

TGF- β 1 Release Kinetics for OPF3K-30min Composites

Microparticle encapsulation within hydrogels of a small mesh size does not appear to further reduce burst release, as evident in the results of studies with OPF3K-30min composites. At low microparticle loading, burst release values from composites formulated with OPF3K-30min were similar to burst release values from OPF3K-30min hydrogels (Table 4) and OPF3K-10min composites. However, at higher microparticle loading, burst release increased and was shown to be significantly greater than the burst

release from OPF3K-30min hydrogels for one formulation. High microparticle loading also increased phase 2 release rates in OPF3K-30min composites (Table 5) and directly correlated with signs of degradation, including gel fragmentation and color loss, as early as day 10. Since only minimal degradation was observed with OPF3K-30min hydrogels by day 28, these combined results indicate that microparticle encapsulation may alter the physical structure of highly crosslinked networks, leading to enhanced hydrolysis and thus increased drug release.

TGF- β 1 Release Kinetics for OPF10K-10min Composites

Like OPF3K-10min composites, microparticle encapsulation within OPF10K-10min hydrogels again allowed for reduction of TGF- β 1 release after day 1 and day 28 when compared to OPF10K hydrogels (Tables 4 and 7). Burst release values for all composite formulations were significantly lower than burst release values from OPF10K-10min hydrogels. Additionally, final cumulative release values were consistently (though not significantly) lower for all OPF10K-10min composites when compared to final cumulative release from OPF10K-10min hydrogels. Slightly elevated phase 3 rates (Table 6) were observed for composites with high microparticle loading. Microparticle encapsulation did not appear to alter OPF10K degradation. Thus, for OPF hydrogels with a large mesh size (OPF3K-10min and OPF10K-10min), introduction of a microparticle component appears to reduce burst release while increasing the rate of subsequent release.

Discussion

Rheometry, tensile testing, and swelling experiments allowed for the determination of key OPF hydrogel parameters. At 37°C, both OPF3K and OPF10K can be crosslinked into hydrogels which maintain their shape and structure within a clinically

relevant time frame. However, OPF3K hydrogels require a longer incubation time (30 min) than OPF10K (10 min) to achieve full crosslinking. Tensile testing and swelling experiments with OPF3K and OPF10K hydrogels crosslinked for 30 and 10 min, respectively, allowed for mesh size (ξ) determination. From these calculations, it is clearly seen that the mesh size of OPF hydrogels is determined by the parent PEG molecular weight used during OPF synthesis. These findings agree with previous investigations in our laboratory for OPF-PEG diacrylate hydrogels (127). Furthermore, these results demonstrate the OPF hydrogel swelling and mechanical properties can be tailored by adjusting OPF formulation.

Using the mechanical properties and volumetric swelling ratios of these hydrogels, the approximate mesh size of OPF3K hydrogels crosslinked for only 10 min may be inferred. Although OPF3K-10min hydrogels exhibit only a slightly higher volumetric swelling ratio ($Q = 1.3 \pm 0.1$), than OPF3K-30min hydrogels ($Q = 1.2 \pm 0.0$), these loosely crosslinked hydrogels possess much less mechanical integrity than fully crosslinked OPF3K hydrogels. Accordingly, the observed volumetric swelling ratio of OPF3K-10min hydrogels may be restricted by the presence of entangled, yet uncrosslinked, polymer chains. Thus, the mesh size of OPF3K-10min hydrogels may be presumed to be similar to that of OPF10K-10min hydrogels. The observed TGF- β 1 release profiles for these hydrogels support this assumption, since OPF10K-10min and OPF3K-10min hydrogels exhibited similar initial release kinetics.

The utility of these hydrogels was further explored through encapsulation of gelatin microparticles within the OPF network. Swelling studies with composites further confirmed the effect of crosslinking time on OPF3K swelling. When fold swelling values

of OPF3K-10min and OPF3K-30min composites were compared, only crosslinking time was identified as a significant factor affecting swelling. However, when the fold swelling values of fully crosslinked OPF10K-10min and OPF3K-30min composites were compared, OPF formulation, microparticle loading, and microparticle crosslinking extent were found to be significant factors effect swelling.

While OPF formulation and microparticle loading within composites were also shown to affect *in vitro* TGF- β 1 release, microparticle crosslinking extent did not appear to influence TGF- β 1 release. These results directly correlate with findings that suggest that release of TGF- β 1 complexed with gelatin microparticles is dependent on enzymatic degradation (121). Since gelatin is not susceptible to degradation by simple hydrolysis, the crosslinking extent, and thus equilibrium swelling ratio, of gelatin microparticles did not influence the *in vitro* TGF- β 1 release kinetics. However, *in vivo*, microparticle crosslinking extent may influence the rate of enzymatic gelatin degradation, altering release kinetics. Initial burst release from these microparticles is presumed to be due to release of any TGF- β 1 which was not complexed with the acidic gelatin during microparticle loading. Minimal further release was observed over the course of 28 days with low rates of TGF- β 1 release (< 2% per day for phase 2 and < 1% per day for phase 3). Similar *in vitro* release profiles have been observed with gelatin microparticles loaded with other growth factors (122, 124).

With all hydrogel formulations, an initial burst release was expected as hydrogels reached their equilibrium swelling states. Both OPF3K-10min and OPF10K-10min hydrogels, presumed to possess similar mesh sizes, exhibited approximately 50% burst release. For OPF3K-30min hydrogels, which possess a smaller mesh size, burst release

was reduced to only 35%. This value was found to be significantly lower than the burst release of hydrogels with a larger mesh size (OPF3K-10min and OPF10K-10min) and lower than the burst release for gelatin microparticles alone ($p < 0.05$), indicating that burst release is diffusionally controlled. *In vitro* release of TGF- β 1 from OPF hydrogels generally exhibited linear kinetics during phases 2 and 3. However, after approximately 21 days, TGF- β 1 release kinetics were directly dependent on hydrogel degradation, as evident in the high final cumulative release values for OPF3K-10min hydrogels, whose loosely crosslinked network was susceptible to hydrolysis. Future investigations are needed to quantitatively correlate hydrogel degradation with TGF- β 1 release.

Release study results with composites indicated that release kinetics may be tailored by varying OPF formulation and crosslinking, as well as microparticle loading. As expected, complete (100%) TGF- β 1 release was not achieved within the 28 day period for any composite formulation, since loaded gelatin microparticles are resistant to hydrolytic degradation. The observed kinetic profiles of composites appear to be greatly influenced by the swelling characteristics of both their polymer and microparticle components.

Addition of a microparticle component to hydrogels with large mesh sizes (OPF3K-10min and OPF10-10min), allowed for reduction of TGF- β 1 release burst release to approximately 30-40%. However, microparticle encapsulation within hydrogels of smaller mesh size did not reduce TGF- β 1 burst release beyond the low value achieved with OPF3K-30min hydrogels. In fact, at high microparticle loading within OPF3K-30min composites, burst reduce was seen to increase. These trends can be understood by

examining the volumetric swelling ratios (Q) of the OPF and gelatin components within composites.

As previously discussed the true volumetric swelling ratio of the crosslinked network of OPF3K-10min hydrogels ($Q = 1.3 \pm 0.1$) is most likely underestimated by the presence of uncrosslinked polymer chains. Over time, these loose polymer chains may be easily hydrolyzed to yield a volumetric swelling ratio of approximate magnitude to that of OPF10K-10min hydrogels ($Q = 3.3 \pm 0.2$). Accordingly, the polymeric component of composites formulated with OPF crosslinked for 10 min achieves greater volumetric swelling at equilibrium than encapsulated microparticles ($Q = 2.0$ for 10mM GA microparticles and 1.8 for 40 mM GA microparticles). However, OPF3K-30min hydrogels have a lower volumetric swelling ratio ($Q = 1.2 \pm 0.0$) than gelatin microparticles. Consequently, microparticles encapsulated within OPF3K crosslinked for 30 min may exert forces on the polymer network, leading to enhanced gel fragmentation and degradation, and thus, increased burst release and phase 2 release rates.

This work demonstrates that gelatin microparticles and OPF can be combined to form novel drug delivery vehicles for TGF- β 1. By altering microparticle loading and the parameters which effect hydrogel swelling (crosslinking time and OPF formulation), unique release profiles (Figures 2-6) are obtained with distinct delivery dosages after 28 days and dynamic release kinetics. Furthermore, the degradation of these delivery vehicles may be manipulated by varying composite parameters. This dual ability to control both drug delivery from and degradation of these new biomaterials confirm their potential in studying the effects of TGF- β 1 release kinetics on cartilage repair.

Conclusions

This research demonstrates that OPF hydrogels and OPF-gelatin microparticle composites can be utilized as injectable biomaterials for the controlled delivery of TGF- β 1 to articular cartilage defects. Specifically, these studies show that hydrogels with different degradation times and swelling and mechanical properties may be formulated by varying OPF formulation and crosslinking time. Furthermore, we have shown that gelatin microparticles, loaded post-fabricationally with TGF- β 1, can be encapsulated within these hydrogels. Finally, *in vitro* release studies demonstrate that the swelling properties of both the OPF and gelatin components of these biomaterials influence the kinetics of TGF- β 1 release. Therefore, unique *in vitro* TGF- β 1 release profiles may be obtained by altering microparticle loading and OPF formulation and crosslinking time.

IV. TRANSFORMING GROWTH FACTOR- β 1 RELEASE FROM OLIGO(POLY(ETHYLENE GLYCOL) FUMARATE) HYDROGELS IN CONDITIONS WHICH MODEL THE CARTILAGE WOUND HEALING ENVIRONMENT[†]

Abstract

This research demonstrates that controlled material degradation and transforming growth factor- β 1 (TGF- β 1) release can be achieved by encapsulation of TGF- β 1-loaded gelatin microparticles within the biodegradable polymer oligo(poly(ethylene glycol) fumarate) (OPF), so that these microparticles function as both a digestible porogen and a delivery vehicle. Release studies performed with non-encapsulated microparticles confirmed that at normal physiological pH, TGF- β 1 complexes with acidic gelatin, resulting in slow release rates. At pH 4.0, this complexation no longer persists, and TGF- β 1 release is enhanced. However, by encapsulating TGF- β 1-loaded microparticles in a network of OPF, release at either pH can be diffusionally controlled. For instance, after 28 days incubation at pH 4.0, final cumulative release from non-encapsulated microparticles crosslinked in 10 mM and 40 mM glutaraldehyde (GA) was $75.4 \pm 1.6\%$ and $76.6 \pm 1.1\%$, respectively. However, when either microparticle formulation was encapsulated in an OPF hydrogel (noted as OPF-10 mM and OPF-40 mM, respectively), these values were reduced to $44.7 \pm 14.6\%$ and $47.4 \pm 4.7\%$. More interestingly, release studies, in conditions which model the expected collagenase concentration of injured cartilage, demonstrated that by altering the microparticle crosslinking extent and loading within OPF hydrogels, TGF- β 1 release, composite swelling, and polymer loss could be systematically altered. Composites encapsulating less crosslinked microparticles (OPF-10

[†] This chapter was published as the following article: TA Holland, JKV Tessmar, Y Tabata, and AG Mikos, Transforming Growth Factor- β 1 Release From Oligo(Poly(Ethylene Glycol) Fumarate) Hydrogels In Conditions Which Model the Cartilage Wound Healing Environment, J. Control. Release, 94, 101-114 (2004).

mM) exhibited 100% release after only 18 days and were completely degraded by day 24 in collagenase-containing PBS. Hydrogels encapsulating 40 mM GA microparticles did not exhibit 100% release or polymer loss until day 28. Hydrogels with no microparticle component demonstrated only $79.3 \pm 9.2\%$ release and $89.2 \pm 3.4\%$ polymer loss after 28 days in enzyme-containing PBS. Accordingly, these studies confirm that the rate of TGF- β 1 release and material degradation can be controlled by altering key parameters of these novel, in situ crosslinkable biomaterials, so that TGF- β 1 release and scaffold degradation may be tailored to optimize cartilage repair.

Abbreviations

10 mM microparticles, gelatin microparticles crosslinked in 10 mM glutaraldehyde; 40 mM microparticles, gelatin microparticles crosslinked in 40 mM glutaraldehyde; GA, glutaraldehyde; IEP, isoelectric point; MMP, matrix metalloproteinase; OPF, oligo(poly(ethylene glycol) fumarate); OPF-10 mM composites, OPF hydrogels encapsulating 10 mM microparticles; OPF-40 mM composites, OPF hydrogels encapsulating 40 mM microparticles; PBS, phosphate buffered saline; PEG, poly(ethylene glycol); TGF- β 1, transforming growth factor- β 1.

Introduction

Lesions to articular cartilage, the connective tissue lining diarthrodial joints, frequently result from sports injuries, accidents, and other joint traumas. Unfortunately, when these lesions occur in adults, the surrounding tissue generally fails to undergo successful repair (2, 3). Further cartilage degeneration may result if this thin tissue layer can no longer dissipate compressive loads, leaving the joint susceptible to further damage upon loading. The complex structure of articular cartilage enables this tissue to serve its important biomechanical role, but simultaneously appears to hinder repair, as lesions often progress into osteoarthritis (1).

Articular cartilage is an avascular tissue with low cellularity, high water content, and a dense extracellular matrix (7). To enhance cartilage repair, current clinical therapies actually require surgical drilling or abrasion through this matrix and into the underlying subchondral bone to contact the cells and bioactive molecules of the bone marrow. Unfortunately, these rigorous techniques require initial deepening of lesions, without achieving complete tissue restoration and often leading to further tissue loss (1, 2).

As an alternative to these harsh surgical techniques, we have developed novel, injectable drug delivery vehicles to enhance cartilage repair through the controlled release of a therapeutic protein, transforming growth factor- β 1 (TGF- β 1). These release systems are based on oligo(poly(ethylene glycol) fumarate) (OPF), a synthetic polymer which can be used to fabricate biodegradable and biocompatible hydrogels (120, 133). OPF, a water soluble polymer, can be injected into a defect site and crosslinked *in situ* at physiological conditions, thereby eliminating the need for invasive surgeries. Previous research has demonstrated that *in vitro* TGF- β 1 release from OPF hydrogels can be diffusionally controlled by altering the hydrogel mesh size, a material parameter dependent on the poly(ethylene glycol) (PEG) length in OPF's backbone structure (134). Furthermore, we have demonstrated that encapsulation of TGF- β 1-loaded gelatin microparticles in an OPF network minimizes the burst release commonly associated with hydrogel delivery systems (134).

The use of degradable, gelatin microparticles in delivery systems for articular cartilage not only allows for further control over drug release, but also enables these hydrogels to become porous, and thus, serve as potential scaffolds for tissue growth. Numerous synthetic and natural materials have been investigated as drug delivery

vehicles (16, 115, 135), but in order for these biomaterials to function as tissue scaffolds, supporting complete tissue repair, they must degrade on the time scale associated with tissue ingrowth. Gelatin is enzymatically degraded by a number of matrix metalloproteinases (MMPs), the enzymes which are upregulated in injured articular cartilage (12-14). Thus, encapsulation of gelatin microparticles within the OPF network should provide a means of enhancing the rate of hydrogel degradation, depending on both the microparticle loading within these hydrogels and the local enzyme concentration. Accordingly, this work investigates simultaneous use of gelatin microparticles as both a TGF- β 1 delivery vehicle and as a digestible porogen.

To analyze the resulting TGF- β 1 release and the degradation of these OPF-gelatin microparticle composites, a series of *in vitro* experiments were performed in the presence and absence of a gelatin degrading enzyme at normal, physiological pH. Composites in these studies contained microparticles crosslinked in either high or low concentrations of glutaraldehyde (GA) to alter microparticle crosslinking extent. Since alterations in the release profiles of some polymeric drug carriers have been observed at low pH (106), *in vitro* release and degradation experiments were also performed in an acidic environment to model the reduced pH commonly associated with inflammation in damaged tissues. Specifically, the objectives of this work were to investigate the effects of microparticle crosslinking extent and microparticle loading on TGF- β 1 release, swelling, and polymer loss when these OPF scaffolds were incubated in buffers which model healthy (phosphate buffered saline, PBS), inflamed (acidic buffer), and injured (enzyme-containing PBS) articular cartilage.

Experimental Methods

Assessment of Collagenase Activity

To examine the effects of microparticle loading and crosslinking extent on TGF- β 1 release from hydrogels in the wound healing environment, *in vitro* release and degradation experiments were performed in enzyme-containing PBS and enzyme-free PBS. Several matrix metalloproteinases (MMPs) in articular cartilage are known to target collagen, the protein from which gelatin is derived. Accordingly, bacterial collagenase 1A (E.C. 3.4.24.3, Sigma, St. Louis, MO) was utilized in this study at a concentration of 373 ng/ml to model MMP-1 (tissue collagenase) concentrations in the synovial fluid of patients with osteoarthritis (136). Collagenase 1A is known to digest gelatin as it recognizes the sequence -X-Gly-Pro-R-, where X is a neutral amino acid (137).

To determine the frequency of buffer exchanges for release and degradation experiments, the decrease in the enzymatic activity of collagenase 1A at a concentration of 373 ng/ml in PBS was assessed using the EnzChek Gelatinase/Collagenase Assay Kit (Molecular Probes, Eugene, OR). After various incubation periods at 37°C, 180 μ l of enzyme-containing buffer was added to 20 μ l of a 100 μ g/ml solution of fluorescein conjugated gelatin in PBS. This conjugated gelatin is heavily labeled with fluorescein so that its fluorescence is normally quenched, but after digestion by collagenase it yields highly fluorescent peptides. A microplate reader (FLx800, BIO-TEK Instrument, Winooski, VT) set for excitation at 485 ± 10 nm and emission detection at 530 ± 15 nm was used to quantify fluorescence. Values were corrected for background fluorescence of the fluorescein labeled gelatin by subtracting the fluorescence value of 20 μ l of non-digested gelatin solution in 180 μ l of enzyme-free PBS. Experiments were conducted in triplicate.

Gelatin Microparticle Fabrication

Acidic gelatin (Nitta Gelatin Inc., Osaka, Japan) with an isoelectric point (IEP) of 5.0 was used for microparticle fabrication according to a previously established method (122). Briefly, 5 g gelatin was dissolved in 45 ml distilled, deionized water (ddH₂O) by mixing and heating (60°C). This aqueous gelatin solution was added dropwise to 250 ml olive oil while stirring at 500 rpm. The temperature of the emulsion was then decreased to approximately 15°C with constant stirring. After 30 min, 100 ml chilled acetone (4°C) was added to the emulsion. After 1 hour, the resulting microspheres were collected by filtration and washed with acetone to remove residual olive oil.

Microspheres were crosslinked by incubation in a 0.1 wt% solution of Tween 80 (Sigma, St. Louis, MO) in ddH₂O containing either 10 mM or 40 mM glutaraldehyde (GA) (Sigma, St. Louis, MO). Hereafter, these microparticles are referred to as 10 mM microparticles and 40 mM microparticles. This crosslinking reaction was maintained at 15°C for approximately 15 h while stirring at 500 rpm. Crosslinked microparticles were collected by filtration, washed with ddH₂O, and then agitated in a 25 mM glycine solution to block residual aldehyde groups of unreacted GA. After 1 hour, microparticles were again collected by filtration, washed with ddH₂O, and then vacuum dried overnight. After drying, the microparticles were sieved to obtain particles 50-100 µm in size.

Microparticle Loading

For release studies, microparticles were loaded with TGF-β1 by swelling in aqueous TGF-β1 solutions at pH 7.4 according to established methods (122, 123). At this pH, TGF-β1 (with an IEP of 9.5) is positively charged, and therefore, forms a polyionic complexation with negatively charged acidic gelatin (IEP of 5.0) (124). Solutions of

TGF- β 1 were composed of I^{125} labeled-TGF- β 1 (Perkin Elmer Life Sciences, Boston, MA) and unlabeled-TGF- β 1 (R&D Systems, Minneapolis, MN) in a mass ratio of approximately 0.06 to allow for detection of TGF- β 1 release. The final TGF- β 1 concentration in crosslinked hydrogels and composites prior to swelling was approximately 200 ng/ml. This concentration of TGF- β 1 has been shown to be therapeutic in the treatment of full and partial thickness rabbit and porcine articular cartilage defects when encapsulated in liposomes (105, 114).

Microparticle loading was achieved by adding 5 μ l of TGF- β 1 solution per mg microparticle to dried microparticles. This solution volume is below the microparticles' theoretical, equilibrium swelling volume to allow for complete drug absorption. The resulting mixture was vortexed and incubated at 4°C for 15h. For degradation studies, TGF- β 1-free microparticles were prepared in a similar method using PBS to partially-swell microparticles before encapsulating them in the hydrogels.

OPF Synthesis

Poly(ethylene glycol) (PEG), with initial average molecular weight 10,000 (Aldrich, Milwaukee, WI) was used to synthesize OPF according to a method developed in our laboratory (125). Approximately 50 g PEG was first azeotropically distilled in toluene to remove residual water and then dissolved in 500 ml anhydrous methylene chloride. The resulting PEG solution was placed in an ice bath and stirred while 1.8 moles triethylamine (TEA, Acros, Pittsburgh, PA) per mole PEG and 0.9 moles distilled fumaryl chloride per mole PEG were added dropwise. The reaction was maintained in a nitrogen environment. Upon completion of reagent addition, the reaction vessel was removed from the ice bath and stirred at room temperature.

After 48 h, polymer purification was begun with the removal of methylene chloride by rotary evaporation. The OPF was then dissolved in ethyl acetate and vacuum-filtered to remove the salt precipitate formed by the reaction of chloride with TEA. Finally, OPF was recrystallized twice in ethyl acetate, and the resulting powder was vacuum dried for approximately 8 h. Dry, purified polymer was stored in a sealed vessel at -20°C until use.

Gel Permeation Chromatography

OPF molecular weight was assessed by gel permeation chromatography (GPC) on a system (Waters, Milford, MA) consisting of a pump (Model 510), injection module (Model 717) and refractive index detector (Model 410). Samples of both the initial PEG and final OPF were dissolved in chloroform, filtered using a chloroform resistant filter, and then analyzed using a Waters Styragel HR 4E column (50-100,000 Da range). The GPC was operated at a flow rate of 1 ml/min. Molecular weights were calculated from elution time using Empower GPC Software (Waters, Milford, MA) and a calibration curve generated with PEG standards. Samples were run in triplicate.

Composite and Hydrogel Fabrication

Gelatin microparticles, crosslinked with either 10 or 40 mM GA, were encapsulated in OPF hydrogels following an established technique (134) to form OPF-10 mM or OPF-40 mM composites, respectively. Briefly, 0.15 g OPF was dissolved in 395 μ l of PBS containing 14 mg N,N'-methylene bisacrylamide (Sigma, St. Louis, MO) as a crosslinking agent. Then 0.2 g gelatin microparticles per g OPF were added to the polymer solution with an additional 118 μ l PBS. The resulting mixture was thoroughly vortexed. Finally, 51 μ l of 0.3 M tetramethylethylenediamine (in PBS) (Sigma, St. Louis,

MO) and 51 μ l of 0.3 M ammonium persulfate (in PBS) (Sigma, St. Louis, MO) were added to initiate crosslinking. After vortexing, the suspension was injected into a Teflon mold and incubated at 37°C. After 10 minutes incubation, this formulation of OPF forms a crosslinked hydrogel, enabling the embedding of gelatin microparticles within the polymer network (134). This procedure was also utilized to crosslink hydrogels with no microparticle component. After completion of crosslinking, both composites and hydrogels were removed from the mold, and a cork bore used to cut discs of approximately 3 mm in diameter and 1 mm in thickness.

In Vitro TGF- β 1 Release

Hydrogel and composite discs were placed into 3 ml of one of the following isotonic buffers, PBS (pH 7.4), a citrate buffer (pH 4.0), or PBS (pH 7.4) containing approximately 373 ng collagenase 1A per ml. Both formulations of TGF- β 1-loaded gelatin microparticles (5 mg) were also placed into each of these buffers. All specimens were agitated on a shaker table (70 rpm) at 37°C. The supernatant of each specimen was collected and replaced by fresh buffer after day 1, 2, 3, 6, 10, 14, 18, 21, 24, and 28. A three to four day interval between buffer changes was utilized to maintain an enzyme activity level of at least 25% of its initial activity as assessed by the collagenase assay (described above).

At each time point, the supernatant of specimens was analyzed for radioactivity using a gamma counter (Cobra II Autogamma, Packard, Meridian, CT). The amount of TGF- β 1 in the supernatant was determined by correlation to a standard curve. Cumulative release was determined by normalizing the total TGF- β 1 released at each time point with the sum of the total TGF- β 1 released over the course of 28 days and the TGF- β 1

remaining in the gel at day 28. Release rates were determined by taking the slope of the percent cumulative release curve for each sample over the stated range and averaging the resultant slopes for each formulation. Accordingly, rates are stated in terms of the change in the percent cumulative release per day. For all treatments, n was initially 6. However, some samples were damaged during the collection of supernatant, resulting in an n of 5 for some formulations.

Hydrogel and Composite Degradation

TGF- β 1-free hydrogels and composites were prepared and maintained as described above for TGF- β 1 release studies to facilitate parallel assessment of material degradation. The supernatant of each specimen was exchanged using the previously mentioned schedule. At days 1, 3, 6, 14, 18, 21, 24, and 28, specimens (n = 3 to 4 for each treatment) were removed from the buffers for measurement. The wet weight (W_w) immediately upon removal from the buffer and dry weight (W_d) after 24 hours of vacuuming drying were recorded for each specimen. Accordingly, the fold swelling ratio of hydrogels and composites at each time point were calculated by the equation,

$$\text{Swelling Ratio} = \frac{W_w - W_d}{W_d}$$

This value provides a means of assessing the ratio of water (g) per g of dry polymer in each gel at the corresponding time point. Additionally, the percent polymer loss at each time point was determined from the equation,

$$\% \text{ Polymer Loss} = \frac{\kappa W_x - W_d}{\kappa W_x} \times 100$$

where W_x is the initial weight of the crosslinked hydrogel or composite (before placement in buffer), and κ is the theoretical fraction of OPF and gelatin initially present in each specimen ($\kappa = 0.21$ for hydrogels and 0.20 for composites).

Due to difficulty in handling, non-encapsulated microparticles were not included as experimental groups in this extended degradation study. However, the fold swelling ratios of both formulations of microparticles were determined after 24 h swelling in each of the buffers ($n = 6$).

Statistical analysis

Polymer loss, swelling, cumulative release values, and release rates for scaffold formulations (hydrogel, OPF-10 mM, and OPF-40 mM) in each buffer were statistically compared using the F test and Tukey's multiple comparison test ($p < 0.05$) (132). Likewise, values for the two microparticle formulations were statistically compared. Microparticles were not statistically compared to scaffolds since the total amount of collagenase substrate (gelatin) per sample was not constant between microparticle and scaffold samples. Additional statistical comparisons were performed, as stated, between buffers for a single experimental group using the F test and Tukey's multiple comparison test. Values are reported as average \pm standard deviation.

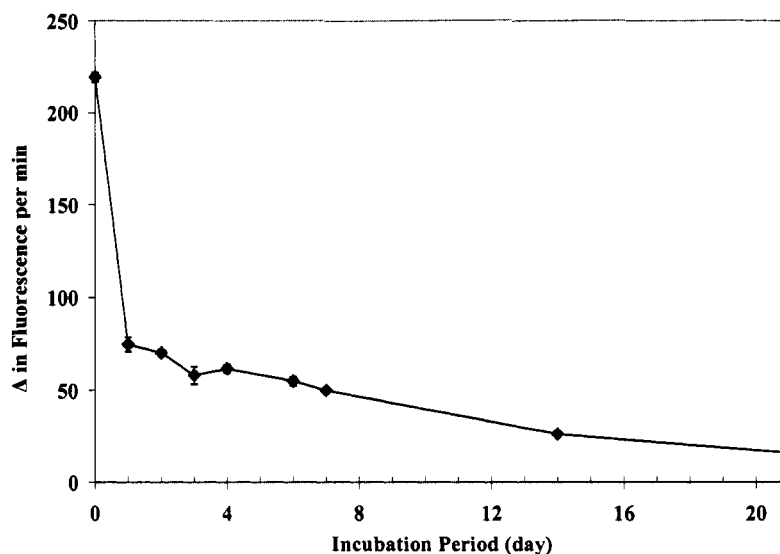
Results

Collagenase Activity in PBS

To accurately model the *in vivo* ability of tissue collagenase to degrade gelatin, it was necessary to maintain sufficient *in vitro* collagenase activity. Accordingly, an activity assay was conducted to measure the change in rate of gelatin digestion by collagenase 1A after various incubation periods at 37°C in PBS. The rate of gelatin

digestion was measured as the increase in fluorescence due to the cleavage of fluorescein conjugated gelatin. As shown in Figure 1, the digestion rate decreased to approximately 34% of its initial value (219.4 ± 2.5 U) after 24 h incubation. However, over the next 3 days, relatively little further loss of enzymatic activity was observed. In fact, collagenase activity remained greater than 25% of its initial value until day 7 when the increase in fluorescence per min was measured to be 49.85 ± 0.22 U, approximately 23% of its initial activity. Accordingly, a 3 to 4 day interval between buffer exchanges in release and degradation experiments was utilized to ensure sufficient enzyme activity throughout the 28 day period. Timepoints generally followed the schedule of previous TGF- β 1 release experiments (134).

Figure IV- 1: Collagenase activity in PBS after various incubation periods at 37°C. Activity values are calculated as the change in fluorescence per min (U) due to cleavage of fluorescein conjugated gelatin. Error bars represent \pm standard deviation with $n=3$ at each time point.



GPC

GPC analysis confirmed the number and weight average molecular weights of the initial PEG to be $9,190 \pm 520$ and $11,180 \pm 490$, respectively. The synthesized OPF was

determined to be of initial number average and weight average molecular weight $21,640 \pm 1,370$ and $144,310 \pm 5,210$, respectively.

In Vitro TGF- β 1 Release and Material Degradation

In general, TGF- β 1 release profiles were seen to follow the same trends exhibited in polymer loss profiles. However, the extent of release and degradation varied greatly, depending on both the buffer and scaffold formulation. To quantify observed trends, release profiles were divided into four phases following the methods of previous investigations (106, 134). In all buffers, a burst release was observed during the initial 24 h (Phase 1) due to equilibrium swelling. While subsequent release at pH 4.0 proceeded at fairly constant rates for all formulations, distinct release rates were observed in buffers of pH 7.4 between days 1-3 (Phase 2) and days 6-21 (Phase 3). Accordingly, TGF- β 1 release rates during these periods were calculated for all treatments. Final cumulative release values were determined to describe the later portion of release curves (Phase 4) in which release was greatly influenced by the extent of swelling and polymer loss.

Release in PBS

As shown in Figure 2a, both formulations of microparticles exhibited similar TGF- β 1 release profiles in standard PBS. Burst release values from 10 and 40 mM microparticles were $46.3 \pm 1.6\%$ and $50.6 \pm 1.4\%$, respectively (Table 1). Relatively little further release was observed over the 28 day period. In fact, final cumulative release values for both formulations were less than 65%. As previously discussed, an ionic complexation of TGF- β 1 with gelatin should persist at pH 7.4. Accordingly, since gelatin is enzymatically degraded, low final release values were expected in the absence of any enzymes.

As shown in Figure 2b, burst release from hydrogels ($43.6 \pm 6.0\%$) was slightly lower than the burst release from non-encapsulated microparticles. Encapsulation of microparticles in an OPF network statistically reduced burst release to $30.6 \pm 0.5\%$ and $26.7 \pm 0.3\%$ with OPF-10 mM and OPF-40 mM composites, respectively. While Phase 2 release rates (Table 2) between hydrogels and composites were not significantly different at pH 7.4, Phase 3 rates for OPF-10 mM ($2.0 \pm 0.4\%$ per day) and OPF-40 mM composites ($2.3 \pm 0.4\%$ per day) were found to be statistically greater than the release rate from hydrogels ($1.0 \pm 0.2\%$ per day). The observance of higher Phase 3 release rates for composites (when compared to hydrogels) agrees with previous experimentation (134) and may be the result of disruption of the polymer network at high microparticle loading. Final cumulative release values for both hydrogels and composites were approximately 80%.

Table IV- 1: Burst release, phase 2 and 3 release rates, and final cumulative TGF- β 1 release from microparticles in buffers of pH 4.0, pH 7.4, and pH 7.4 with collagenase. Statistically greater values ($p < 0.05$) between microparticle formulations in each buffer are indicated by (*).

	Formulation	Buffer		
		pH 7.4	pH 4.0	pH 7.4 with enzyme
Burst Release (%)	10 mM	46.3 ± 1.6	49.0 ± 1.5	36.3 ± 2.2
	40 mM	50.6 ± 1.4 *	56.1 ± 2.8 *	38.8 ± 1.4 *
Phase 2 Release Rates (%/day)	10 mM	5.0 ± 1.0	3.7 ± 0.7	6.8 ± 0.7 *
	40 mM	4.5 ± 1.0	4.7 ± 0.5 *	4.2 ± 0.2
Phase 3 Release Rates (%/day)	10 mM	0.2 ± 0.0	0.6 ± 0.0 *	1.5 ± 0.3
	40 mM	0.2 ± 0.0	0.4 ± 0.0	2.0 ± 0.1 *
Final Cumulative Release (%)	10 mM	61.9 ± 1.1	75.4 ± 1.6	89.7 ± 2.5 *
	40 mM	64.5 ± 1.5 *	76.6 ± 1.1	86.4 ± 0.6

Table IV- 2: Burst release, phase 2 and 3 release rates, and final cumulative TGF- β 1 release from hydrogels and composites in PBS. Composites exhibited significantly lower burst (\wedge , $p < 0.05$) and statistically higher Phase 3 release rates ($*$, $p < 0.05$) than hydrogels.

Delivery System	Burst Release (%)	Phase 2 Rate (%/day)	Phase 3 Rate (%/day)	Cumulative Release (%)
Hydrogel	43.6 ± 6.0	2.9 ± 1.6	1.0 ± 0.2	79.3 ± 9.2
OPF-10 mM Composite	$30.6 \pm 0.5 \wedge$	3.6 ± 0.4	$2.0 \pm 0.4 *$	81.8 ± 8.3
OPF-40 mM Composite	$26.7 \pm 0.3 \wedge$	2.5 ± 0.4	$2.3 \pm 0.4 *$	80.3 ± 6.8

Swelling and Polymer Loss in PBS

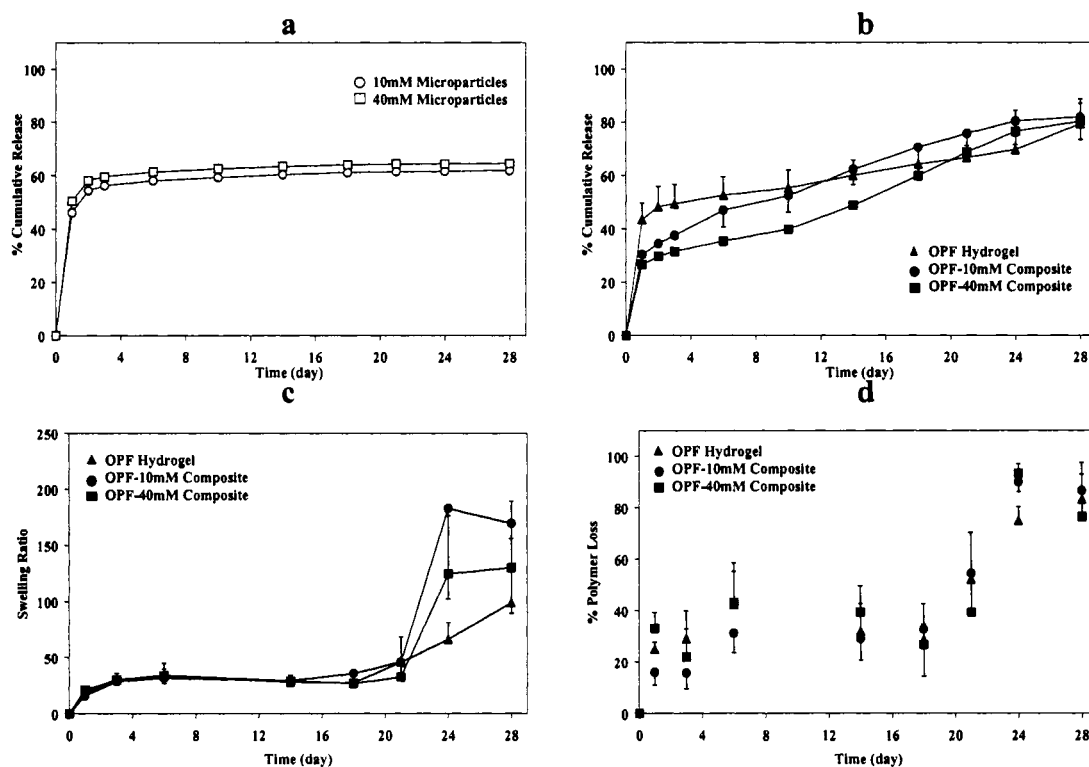
As shown in Figures 2c and 2d, hydrogels and both composite formulations exhibited similar swelling and polymer loss profiles in standard PBS. After the initial 24 hr, equilibrium swelling ratios were approximately 20 fold and polymer loss values were between 15-30%. Over the following 17 to 20 days, the swelling ratios and polymer content of all gels remained fairly constant. However, by the end of Phase 3 (day 21), polymer loss from hydrogels, OPF-10 mM, and OPF-40 mM composites rose to $52.3 \pm 18.2\%$, $54.6 \pm 16.3\%$, and $39.5 \pm 15.2\%$, respectively. Appreciable increases in the swelling ratios followed during Phase 4, and after 28 days incubation in standard PBS, hydrogels, OPF-10 mM, and OPF-40 mM composites became highly swollen networks with respective swelling ratios of 99.2 ± 56.7 , 169.5 ± 79.8 , and 130.1 ± 59.2 . All scaffold formulations exhibited approximately 80% polymer loss by day 28. No significant differences were observed in the final swelling ratios or final polymer loss values between formulations.

Release in an Acidic Environment

Both microparticle formulations exhibited enhanced TGF- β 1 release at pH 4.0 when compared to pH 7.4 (Table 1). Although 40 mM microparticles exhibited a higher burst value ($56.1 \pm 2.8\%$) than 10 mM microparticles ($49.0 \pm 1.5\%$), final cumulative release values between microparticle formulations were not statistically different. In fact,

both formulations exhibited approximately 75% final cumulative release by day 28 (Figure 3a). Since both TGF- β 1 and acidic gelatin have isoelectric points above 4.0, both molecules are positively charged at this pH. Accordingly, the polyionic complexation between gelatin and TGF- β 1 will be disrupted in the acidic environment, leading to enhanced growth factor release.

Figure IV- 2: TGF- β 1 release and material degradation profiles in standard PBS (pH 7.4). Average percent cumulative TGF- β 1 release from gelatin microparticles (a) and OPF scaffolds (b) are shown with $n = 5$ to 6 for all formulations. Average fold swelling ratios (c) and percent polymer loss from scaffolds (d) are shown with $n = 3$ to 4 for all formulations. Error bars represent \pm standard deviation.



However, since enhanced release at pH 4.0 was not observed when microparticles were encapsulated in a network of OPF (Figure 3b), release from composites appears to be diffusionally controlled by the surrounding gel. Furthermore, burst release from OPF-10 mM ($23.6 \pm 8.4\%$) and OPF-40 mM ($22.9 \pm 2.0\%$) composites was significantly less

than burst release from OPF hydrogels ($37.0 \pm 8.5\%$), indicating that encapsulation of TGF- β 1-loaded microparticles in these hydrogels provides a means of minimizing burst release even in conditions that promote dissociation of this growth factor from the gelatin microparticles. Subsequent release from both hydrogels and composites proceeded at a rate of approximately 1.0% per day during both Phase 2 and Phase 3 (Table 3). For all scaffolds at pH 4.0, less than 55% cumulative release was observed at the end of the 28 day period.

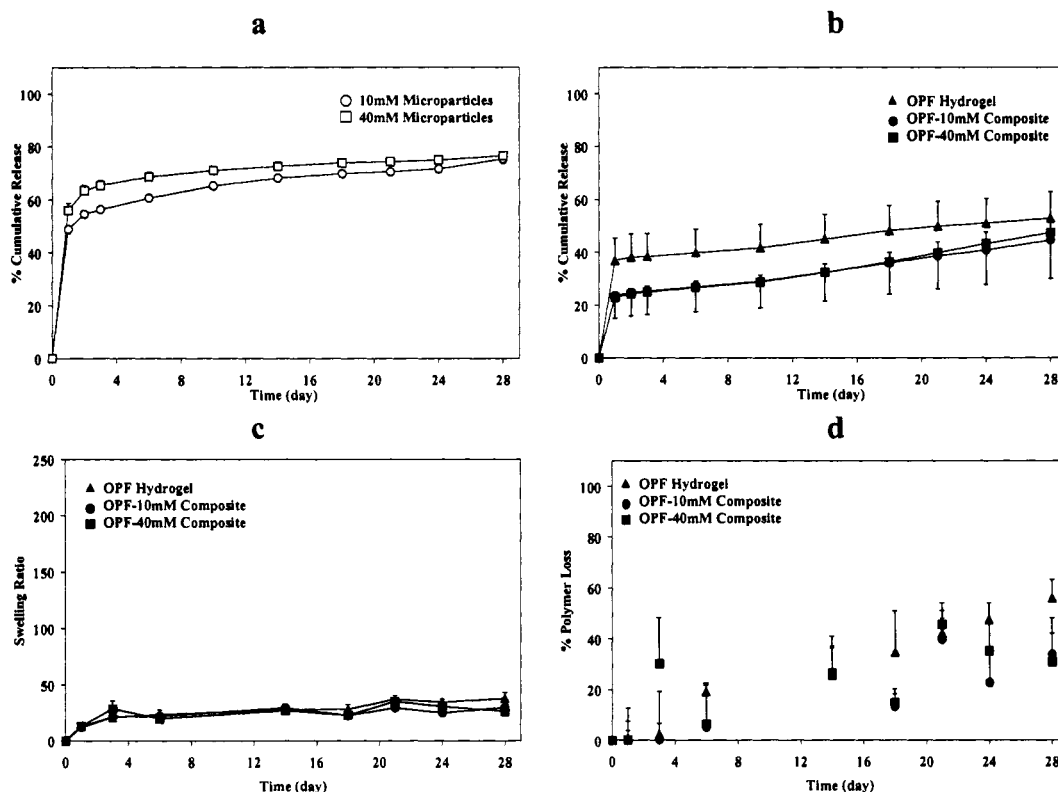
Table IV- 3: Burst release, phase 2 and 3 release rates, and final cumulative TGF- β 1 release from hydrogels and composites in pH 4.0 buffer. OPF-10 mM and OPF-40 mM composites exhibited significantly lower burst release than hydrogels ($^{\wedge}$, $p < 0.05$).

Delivery System	Burst Release (%)	Phase 2 Rate (%/day)	Phase 3 Rate (%/day)	Cumulative Release (%)
Hydrogel	37.0 ± 8.5	0.8 ± 0.2	0.7 ± 0.1	53.0 ± 9.9
OPF-10 mM Composite	$23.6 \pm 8.4^{\wedge}$	0.9 ± 0.3	0.8 ± 0.2	44.7 ± 14.6
OPF-40 mM Composite	$22.9 \pm 2.0^{\wedge}$	1.1 ± 0.1	0.9 ± 0.1	47.4 ± 4.7

Swelling and Polymer Loss in an Acidic Environment

Just as TGF- β 1 release from hydrogels and composites was reduced in the acidic buffer, degradation rates of these scaffolds were greatly diminished at pH 4.0 (Figures 3c and 3d) when compared to observed degradation at pH 7.4. In fact, after the initial 24 hours of incubation in acidic buffer, scaffolds exhibited no measurable loss of polymer. By the end of Phase 2 (day 3), swelling ratios were approximately 20-30 fold, allowing polymer loss to proceed in a slow, linear fashion for all formulations. By day 28, respective polymer loss values of hydrogels, OPF-10 mM, and OPF-40 mM composites were $56.1 \pm 7.3\%$, $33.9 \pm 14.5\%$, and $30.9 \pm 11.3\%$, while swelling ratios were found to be 37.9 ± 5.2 , 29.8 ± 4.4 , and 26.3 ± 4.8 . Both polymer loss and the swelling ratio of hydrogels at day 28 were found to be significantly greater than the swelling ratio of composites.

Figure IV- 3: TGF- β 1 release and material degradation profiles in acidic buffer (pH 4.0). Average percent cumulative TGF- β 1 release from gelatin microparticles (a) and OPF scaffolds (b) are shown with $n = 5$ to 6 for all formulations. Average fold swelling ratios (c) and percent polymer loss from scaffolds (d) are shown with $n = 3$ to 4 for all formulations. Error bars represent \pm standard deviation



Composites were expected to swell less than hydrogels since the 24 hr equilibrium swelling ratio of both 10 mM (8.3 ± 0.4) and 40 mM (5.6 ± 1.3) microparticles was less than the equilibrium swelling ratio of OPF hydrogels (14.5 ± 2.4) at pH 4.0. Accordingly, scaffolds consisting of OPF alone undergo enhanced hydrolysis at pH 4.0 in comparison to scaffolds encapsulating gelatin microparticles.

Release in Collagenase-Containing PBS

Although the microparticle formulation did not influence TGF- β 1 release profiles in the absence of collagenase at pH 7.4 or pH 4.0, release in the presence of collagenase was shown to be dependent on microparticle crosslinking extent (Figure 4a). A statistically higher phase 2 release rate was observed with microparticles crosslinked in

10 mM GA ($6.8 \pm 0.7\%$ per day) when compared to the release rate from more crosslinked (40 mM GA) microparticles ($4.2 \pm 0.2\%$ per day). However, during Phase 3, the reverse trend was observed with 40 mM microparticles exhibiting a statistically higher rate of release than 10 mM microparticles (Table 1). These results suggest that the less crosslinked 10 mM microparticles are rapidly digested by collagenase, while the more crosslinked structure of 40 mM microparticles slows enzymatic degradation. While not quantified, visible disappearance, and thus, digestion of the 10 mM microparticles had begun by day 18. Final cumulative release from 10 mM microparticles ($89.7 \pm 2.5\%$) was statistically greater than release from 40 mM microparticles ($86.4 \pm 0.6\%$).

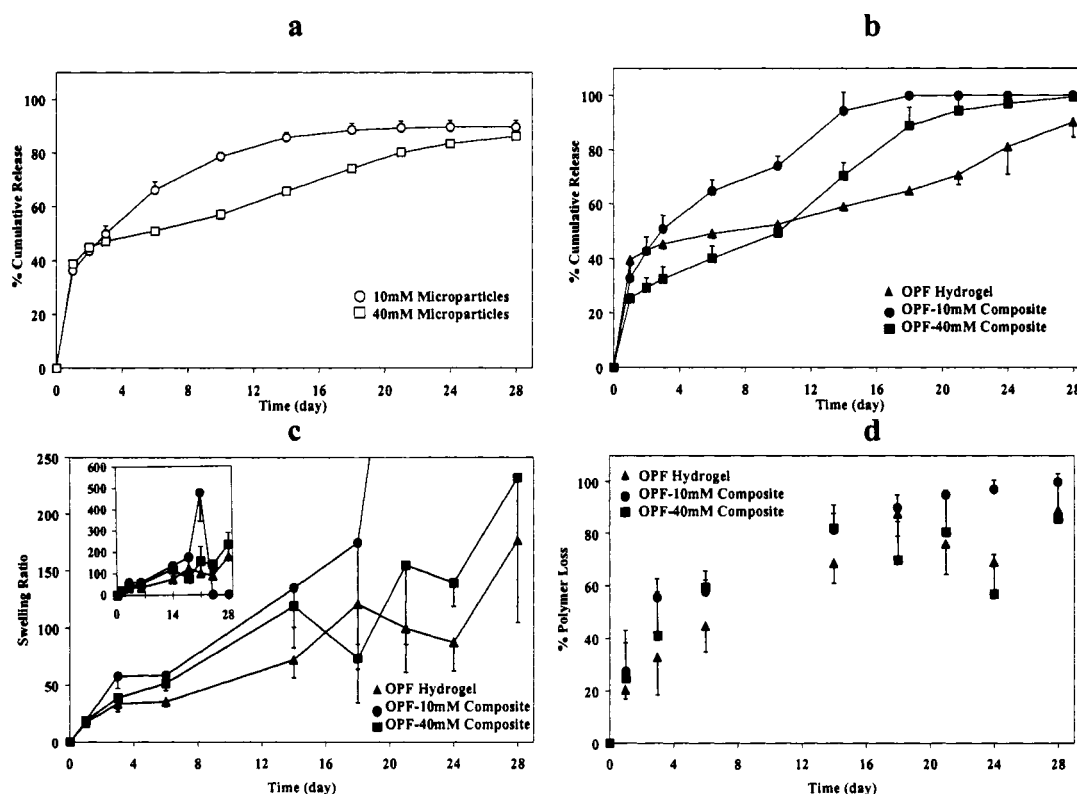
Table IV- 4: Burst release, phase 2 and 3 release rates, and final cumulative TGF- β 1 release from hydrogels and composites in collagenase-containing PBS. Composite values which are statistically ($p < 0.05$) less than or greater than the hydrogel value are indicated by (^) and (*), respectively. Composite values which are statistically ($p < 0.05$) less than or greater than both the hydrogel value and opposing composite value are indicated by (^^) and (**), respectively.

Delivery System	Burst Release (%)	Phase 2 Rate (%/day)	Phase 3 Rate (%/day)	Cumulative Release (%)
Hydrogel	39.5 ± 1.7	2.9 ± 0.1	1.5 ± 0.3	90.3 ± 5.6
OPF-10 mM Composite	32.8 ± 4.8 ^	9.1 ± 0.8 **	2.6 ± 0.3 *	100.0 ± 0.0 *
OPF-40 mM Composite	25.3 ± 1.8 ^^	3.6 ± 1.4	3.9 ± 0.8 **	99.5 ± 1.2 *

The susceptibility of 10 mM microparticles to enzymatic attack was further demonstrated in release studies with scaffolds in collagenase-containing PBS (see Figure 4b and Table 4). As previously mentioned, composite burst release values in standard PBS were shown to be statistically lower than hydrogel burst release. This trend was repeated in the presence of collagenase, with an interesting addition. Burst release from OPF-40 mM composites ($25.3 \pm 1.8\%$) was also significantly less than burst release from OPF-10 mM composites ($32.8 \pm 4.8\%$). Furthermore, the Phase 2 release rate from OPF-10 mM composites was dramatically higher ($9.1 \pm 0.8\%$ per day) than the corresponding

rates for release from hydrogels ($2.9 \pm 0.1\%$ per day) and OPF-40 mM composites ($3.6 \pm 1.4\%$ per day). However, by Phase 3, the highest release rates were observed with OPF-40 mM composites since the encapsulated microparticles of these scaffolds undergo a slower rate of enzymatic digestion. By day 18, OPF-10 mM composites exhibit 100% TGF- β 1 release, becoming completely degraded between days 21-24. In contrast, OPF-40 mM composites did not achieve 100% TGF- β 1 release until day 28. At this time, hydrogels exhibited a statistically lower final cumulative release value of $90.3 \pm 5.6\%$.

Figure IV- 4: TGF- β 1 release and material degradation profiles in collagenase-containing PBS (pH 7.4). Average percent cumulative TGF- β 1 release from gelatin microparticles (a) and OPF scaffolds (b) are shown with $n = 5$ to 6 for all formulations. Average fold swelling ratios (c) and percent polymer loss from scaffolds (d) are shown with $n = 3$ to 4 for all formulations. Error bars represent \pm standard deviation.



Swelling and Polymer Loss in Collagenase-Containing PBS

As shown in Figures 4c and 4d, large swelling ratios and polymer loss values were quickly exhibited with OPF-10 mM composites. In general, values for OPF-40 mM

composites remained below OPF-10 mM values, while the lowest values were observed for hydrogels with no microparticle component. The swelling ratio of OPF-10 mM composites was 57.8 ± 10.6 at the end of Phase 2 (day3) and quickly exceeded 100 fold after 18 days incubation. By the beginning of Phase 4 (day 24), these scaffolds were completely degraded.

OPF-40 mM composites exhibited slower degradation rates. The swelling ratio of these composites persisted near 100 fold for days 18-24. However, by the end of Phase 4 (day 28), 2 of the 4 scaffolds in this treatment were completely degraded, while remaining 2 scaffolds were extremely swollen, loose networks with an average fold swelling ratio of 232 ± 56 . In the presence of collagenase, hydrogels exhibited $89.2 \pm 3.4\%$ polymer loss and a fold swelling ratio of 177 ± 72 at day 28. These values were not statistically different from hydrogel polymer loss and fold swelling values in standard PBS.

Discussion

TGF- β 1 release profiles from microparticles, hydrogels, and composites in standard PBS agreed with previous investigations (134), demonstrating that drug delivery systems with reproducible release kinetics can be easily fabricated. In particular, after approximately 50% burst release, relatively little further release was observed from microparticles as TGF- β 1 remains complexed to acidic gelatin at pH 7.4. As expected, the microparticle crosslinking extent did not influence the kinetics of release from either microparticles or composites at this pH. However, encapsulation of microparticles in an OPF network was again shown to facilitate reduction of TGF- β 1 burst release, indicating that the polymer surrounding these microparticles serves to diffusionally control release.

TGF- β 1 release profiles from hydrogels and composites were seen to directly correlate with swelling and polymer loss profiles in standard PBS. In particular, burst release coincided with equilibrium swelling during the first 24 hours (Phase 1). A moderate rate of release during days 1-3 (Phase 2) paralleled an observed steady loss of polymer during this period. Polymer loss at this early stage may result from hydrolysis of uncrosslinked polymer chains, resulting in increased gel swelling and TGF- β 1 release. Throughout Phase 3 (days 6-21), slightly reduced rates of TGF- β 1 release were observed (when compared to Phase 2). During this period, both composites and hydrogels appeared to undergo minimal further swelling and polymer loss. Accordingly, release during this time is presumably controlled by diffusion rather than hydrolytic degradation of the polymer network. However, by days 24-28 (Phase 4), enhanced swelling and polymer loss resulted in further release.

When hydrogels and composites were incubated in an acidic buffer to model the pH frequently associated with inflammation, dramatically reduced swelling and polymer loss were exhibited throughout the 28 day period. After only 24 hours, equilibrium swelling ratios at pH 4.0 were found to be statistically lower than values at pH 7.4 for all scaffold formulations. This trend persisted for both microparticles formulations, indicating that enhanced TGF- β 1 release from microparticles at pH 4.0 can not be attributed to increased swelling, but, instead, results from disruption of the complexation between TGF- β 1 and gelatin. However, since TGF- β 1 release from scaffolds was greatly reduced at pH 4.0 (when compared to pH 7.4), diffusional control of TGF- β 1 release can still be achieved, despite elimination of electrostatic interactions, by encapsulating loaded microparticles in a network of OPF.

Further evidence of the diffusion barrier provided by the OPF network was seen by comparing scaffold swelling and drug release at pH 7.4 and 4.0. Under normal physiological pH, OPF hydrogels and composites were seen to quickly reach a swelling ratio of approximately 20 fold. However, at acidic conditions, this value was reduced to approximately 13 fold. Accordingly, the mesh size of the OPF network will be greater at pH 7.4, than pH 4.0, allowing for faster diffusion of TGF- β 1. Combined with previous investigations (127, 134) which demonstrate that the mesh size of OPF hydrogels can be systematically controlled by altering the length of the PEG chain in the repeating unit of OPF, these results show that OPF network surrounding encapsulated microparticles can be tailored to achieve the desired swelling extent, and thus, rate of drug diffusion.

Experiments in presence of collagenase demonstrated that systematic control of material degradation and TGF- β 1 delivery could be achieved by altering the microparticle crosslinking extent and loading in OPF hydrogels. The influence of these factors was promptly noted during Phase 1. The equilibrium swelling ratio of 10 mM microparticles in the presence of collagenase (10.9 ± 0.7) after only 24 hours incubation was significantly greater than the swelling ratio in standard PBS (9.9 ± 0.4), suggesting that enhanced swelling in the presence of collagenase results from enzymatic degradation. However, the 24 hr equilibrium swelling ratios of 40 mM microparticles in standard PBS (8.0 ± 0.2) or in collagenase-containing PBS (7.8 ± 0.1) were not statistically different.

Similar trends for swelling ratios were observed with scaffolds after 24 hr incubation in standard PBS or in collagenase-containing PBS. For hydrogels and OPF-40 mM composites no statistical differences were found between equilibrium swelling ratios in the absence or presence of collagenase within each experimental group. However, the

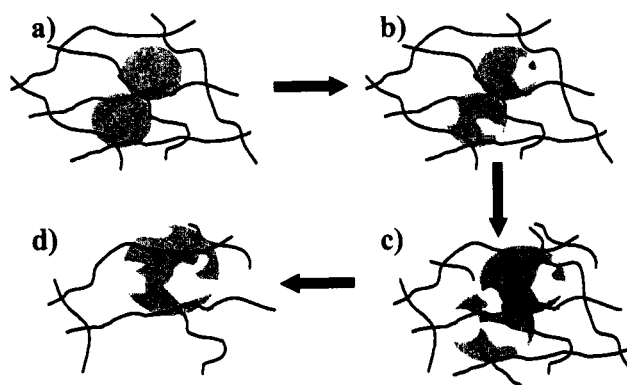
swelling ratio of OPF-10 mM composites in collagenase-containing PBS (19.2 ± 2.7) was significantly greater than the equilibrium swelling ratio in standard PBS (16.0 ± 0.5).

More importantly, microparticle crosslinking extent and loading within hydrogels was shown to affect the final fate of scaffolds. Enzymatic degradation of these microparticles appeared to enhance the swelling and degradation of the synthetic component of scaffolds. Specifically, composites encapsulating less crosslinked microparticles (10 mM) exhibited complete TGF- β 1 release within approximately 18 days and were completely degraded after 24 days. Composite encapsulating more crosslinked microparticles (40 mM) exhibited complete TGF- β 1 release within approximately 28 days. As the gelatin microparticles within composites undergo enzymatic attack, the digestion of gelatin fragments may allow for increased microparticle swelling, exerting mechanical forces on the OPF network and ultimately leading to network disruption (see Figure 5). Additionally, complete digestion of the gelatin microparticles will result in the creation of large pores in these gels, allowing for enhanced hydrolysis of OPF polymer chains. Studies with hydrogels (no microparticle component) clearly demonstrate that OPF is not a substrate for collagenase digestion. For these hydrogels, the final (28 day) values for TGF- β 1 release, polymer loss, and swelling in collagenase-containing PBS were not statistically different from values in standard PBS. Furthermore, hydrogels exhibited only $89.2 \pm 3.4\%$ polymer loss and significantly lower final cumulative release than either composite formulation at 28 days.

Together, the results of both release and degradation experiments with composites and hydrogels show that the inclusion of a digestible porogen will influence the rates of growth factor release and scaffold degradation in the *in vivo* wound healing environment.

This finding is of particular importance since recent cartilage engineering research has demonstrated the importance of scaffold degradability in the quantity (138) and spatial distribution (139) of chondrocytes, proteoglycans, and type II collagen.

Figure IV- 5: Degradation of OPF-gelatin microparticle composites in the presence of collagenase. (a) Gelatin microparticles are initially encapsulated in a network of OPF. (b) Collagenase digests gelatin segments, enhancing microparticle swelling. (c) Increased microparticle swelling disrupts the polymer network. (d) Complete digestion of gelatin microparticles creates pore structures to allow for further hydrolysis of polymer chains.



Conclusions

This research demonstrates that encapsulation of TGF- β 1-loaded gelatin microparticles within a network of the biodegradable polymer OPF provides a means of controlling TGF- β 1 release and material degradability. Specifically, release experiments at normal physiological pH demonstrated that TGF- β 1 burst release from non-encapsulated microparticles is reduced when microparticles are embedded in a network of OPF. Subsequent release at pH 7.4 directly correlates with hydrogel swelling and polymer loss profiles. The ability of the OPF network to diffusionally control TGF- β 1 release was again demonstrated in experiments performed in the acidic environment, typical of inflamed tissue. At these conditions, TGF- β 1 release from non-encapsulated microparticles was accelerated, but when microparticles were encapsulated within a crosslinked structure of OPF, sustained TGF- β 1 release was achieved. Most interestingly,

studies performed in the presence of collagenase demonstrated that complete TGF- β 1 release and material degradation could be achieved within approximately 24 days by the encapsulation of microparticles within an OPF network. Accordingly, these OPF hydrogel release systems offer the novel ability to tailor both TGF- β 1 release and material degradation rates and demonstrate potential for use as tissue scaffolds in articular cartilage repair.

V. OSTEOCHONDRAL REPAIR IN THE RABBIT MODEL UTILIZING BILAYERED, DEGRADABLE OLIGO(POLY(ETHYLENE GLYCOL) FUMARATE) HYDROGEL SCAFFOLDS[†]

Abstract

In this study, hydrogel scaffolds, based on the polymer oligo(poly(ethylene glycol) fumarate) (OPF), were implanted into osteochondral defects in the rabbit model. Scaffolds consisted of two layers – a bottom, bone forming layer and a top, cartilage forming layer. Three scaffold formulations were implanted to assess how material composition and transforming growth factor- β 1 (TGF- β 1) loading affected osteochondral repair. Critical histological evaluation and scoring of the quantity and quality of tissue in the chondral and subchondral regions of defects was performed at 4 and 14 weeks. At both time points, no evidence of prolonged inflammation was observed, and healthy tissue was seen to infiltrate the defect area. The quality of this tissue improved over time with hyaline cartilage filling the chondral region and a mixture of trabecular and compact bone filling the subchondral region at 14 weeks. A promising degree of Safranin O staining and chondrocyte organization was observed in the newly formed surface tissue, while the underlying subchondral bone was completely integrated with the surrounding bone at 14 weeks. Material composition within the bottom, bone forming layer did not appear to affect the rate of scaffold degradation or tissue filling. However, no bone upgrowth into the chondral region was observed with any scaffold formulation. TGF- β 1 loading in the top layer of scaffolds appeared to exert some therapeutic affect on tissue quality, but further studies are necessary for scaffold optimization. Yet, the excellent

[†] This chapter was published as the following article: TA Holland, EWH Bodde, LS Baggett, Y Tabata, AG Mikos, JA Jansen, Osteochondral Repair in the Rabbit Model Utilizing Bilayered, Degradable Oligo(Poly(Ethylene Glycol) Fumarate) Hydrogel Scaffolds, J. Biomed. Materials Res., 75, 156-167 (2005).

tissue filling and integration resulting from osteochondral implantation of these OPF-based scaffolds demonstrates their potential in cartilage repair strategies.

Abbreviations

C⁺/C, scaffolds with an upper OPF layer with loaded microparticles and a bottom OPF layer of blank microparticles; C⁺/H, scaffolds with an upper OPF layer of loaded microparticles and a bottom OPF layer of with no microparticles; C⁻/H, scaffolds with an upper OPF layer of blank microparticles and a bottom OPF layer with no microparticles; H&E, hematoxylin and eosin; MSD, mean score per defect; MSF, mean score per formulation; OPF, oligo(poly(ethylene glycol) fumarate); PBS, phosphate buffered saline; TGF- β 1, transforming growth factor- β 1.

Introduction

Chronic joint pain and arthritis affects approximately one third of adults in the United States (140) and is the leading causes of disabilities among Americans (141). Many of these individuals suffer from lesions to articular cartilage, the thin tissue lining diarthrodial joints which dissipates compressive loads and allows for pain-free movement (3). Lesions, commonly inflicted during improper joint loading, sudden joint rotation, or direct impact to a joint, often fail to heal properly due to the complex structure of this unique tissue (2, 3). In particular, articular cartilage is an avascular tissue with a relatively sparse cell population and a dense, well-ordered extracellular matrix (1, 7). Since articular cartilage exhibits limited intrinsic repair, lesions may lead to further joint degeneration and the onset of osteoarthritis (2, 85, 87).

Treatment options for patients with articular cartilage lesions are currently restricted to surgical procedures aimed at either stimulating a healing response at the injury site or filling the lesion with a tissue graft (87, 142). The former strategy is undertaken by invasive drilling to deepen cartilage lesions to access the bioactive molecules and reparative cells in the underlying bone marrow. The strategy of tissue

grafting requires surgical disruption of healthy tissue to harvest a source of cartilage, periosteal, or perichondrial cells for subsequent transplantation at the lesion site. Thus, both treatment options inflict further tissue destruction before any therapeutic effect can be achieved. Additionally, both surgical strategies have demonstrated very limited long term efficacy. In general, surgical abrasion or drilling appears to produce mainly fibrocartilage or fibrous tissue at the repair site which often deteriorates over time (1, 142, 143). Graft delamination and endochondral ossification are frequently encountered following tissue transplantation (142-144). Accordingly, new treatment options are necessary for the treatment of articular cartilage defects.

Through a series of investigations, our laboratory has developed a novel class of injectable materials for the delivery of bioactive molecules to cartilage lesions to enhance tissue repair (134, 145, 146). These systems are based on oligo(poly(ethylene glycol) fumarate) (OPF), a synthetic polymer which can be used to fabricate biodegradable and biocompatible hydrogels (119, 120). OPF, a water soluble polymer, can be injected into a defect site and crosslinked *in situ* at physiological conditions, thereby eliminating the need for harsh surgeries. Gelatin microparticles, incorporated into these gels at the time of crosslinking, have been shown to act as enzymatically, digestible porogens to speed scaffold degradation (146). Sustained growth factor delivery has been achieved by first loading these microparticles with the desired growth factor and then encapsulating the microparticles within the OPF network (134, 145, 146).

This current work evaluates three different formulations of bilayered OPF hydrogel scaffolds in osteochondral repair. A bilayered scaffold design (Table 1) was employed to spatially control drug loading and scaffold degradability in the approximate

regions where cartilage and bone are found in healthy joints. For all formulations, the upper scaffold layer consisted of an OPF hydrogel in which 0.20 g gelatin microparticles per g polymer were encapsulated. This scaffold composition was utilized since microparticles embedded in the OPF network at this concentration have previously been shown to act as digestible porogens (146). Accordingly, it was hypothesized that this composition would allow for rapid and adequate cell infiltration to the chondral portion of defects from the surrounding cartilage and synovium (60).

Table V- 1: Three formulations of OPF scaffolds implanted into osteochondral defects

	Scaffold Formulations		
	C ⁺ /C	C ⁺ /H	C ⁻ /H
Chondral layer	Composite: Gel encapsulating TGF-β1-loaded microparticles	Composite: Gel encapsulating TGF-β1-loaded microparticles	Composite: Gel encapsulating blank microparticles
Subchondral layer	Composite: Gel encapsulating blank microparticles	Hydrogel with no microparticles or TGF-β1	Hydrogel with no microparticles or TGF-β1

In two scaffold formulations (abbreviated as C⁺/C and C⁺/H), microparticles within this upper composite layer were loaded with transforming growth factor-β1 (TGF-β1), while microparticles in the third scaffold formulation (abbreviated as C⁻/H) were loaded with PBS. TGF-β1 is an excellent candidate for cartilage drug delivery strategies as this growth factor has been shown to enhance chondrocyte proliferation (36, 37) to promote the chondrogenic differentiation of progenitor cells (10, 28, 29), and to increase cartilage extracellular matrix synthesis (32, 34, 35). The bottom layer of all scaffolds was unloaded (TGF-β1-free) since TGF-β1 delivery to the osseous tissue of osteochondral defects has resulted in bone upgrowth into the cartilaginous region of defects (105). In

two scaffold formulations (C^+/H and C^-/H), the bottom layer was composed solely of an OPF hydrogel without any porogen. This material composition was chosen to act as a structural barrier to further prevent bone upgrowth, since OPF hydrogels have been shown to degrade slower than OPF-gelatin microparticle composite gels (146).

Histological evaluation of the quantity and quality of tissue repair in the upper and lower portion of defects treated with these three scaffold formulations was performed at both 4 and 14 weeks to assess the following questions:

1. Do these novel, hydrogel scaffolds support cartilage and bone growth in the rabbit osteochondral defect model?
2. How does the quality and quantity of tissue repair compare over time?
3. Does the rate of material degradation in the lower, bone forming portion of scaffolds affect tissue formation?
4. How does TGF- β 1 delivery to the upper portion of osteochondral defects affect cartilage repair?

Experimental Methods

Gelatin Microparticle Fabrication and Loading

Gelatin microparticles were fabricated from acidic gelatin (Nitta Gelatin Inc., Osaka, Japan) and crosslinked in 10 mM glutaraldehyde (Sigma, St. Louis, MO) according to previously established methods (122). After drying, the microparticles were sieved to obtain particles 50-100 μ m in size and then sterilized by exposure to ethylene oxide gas (123).

Sterile microparticles were then loaded with TGF- β 1 by swelling in an aqueous solution of TGF- β 1 at pH 7.4 according to previous methods (134, 146). At this pH, TGF- β 1 (with an isoelectric point of 9.5) is positively charged, and therefore, forms a polyionic complexation with negatively charged acidic gelatin (isoelectric point of 5.0) (122, 123). A TGF- β 1 loading solution concentration of 1.2 μ g TGF- β 1/ml PBS was utilized to achieve an overall growth factor loading of approximately 200 ng TGF- β 1/ml

in the top crosslinked, layer of scaffolds. This concentration of TGF- β 1 has previously been shown to be therapeutic in the treatment of full and partial thickness rabbit and porcine defects (105, 114). Blank microparticles were loaded with PBS in a similar fashion.

OPF Synthesis

OPF with an initial number average molecular weight of $12,300 \pm 100$ and weight average molecular weight of $51,300 \pm 6,700$ was synthesized according to a method developed in our laboratory (125). Molecular weight determination was likewise conducted using established procedures for gel permeation chromatography with samples run in triplicate (146). The resulting OPF was sterilized by exposure to UV light for 3 h following an established technique (147).

Scaffold Fabrication

Table 1 displays the three different scaffold formulations fabricated for this study. All scaffolds consisted of two layers: a top, cartilage forming layer and a bottom, bone forming layer with respective thicknesses of 1 mm and 2 mm. Although the thickness of articular cartilage was expected to vary amongst animals, these dimensions were chosen as a means of tailoring scaffold composition and drug loading to the upper or lower portion of defects, rather than as a model of exact anatomy. Since the animals utilized in this study were already undergoing bilateral joint surgery for creation of the osteochondral defects, scaffolds were implanted, rather than injected, at the defect site.

As noted in Table 1, the scaffold formulations have been assigned abbreviations based on the material compositions within each layer – either an OPF hydrogel layer (H) or a composite gel layer (C) in which gelatin microparticles were encapsulated in the

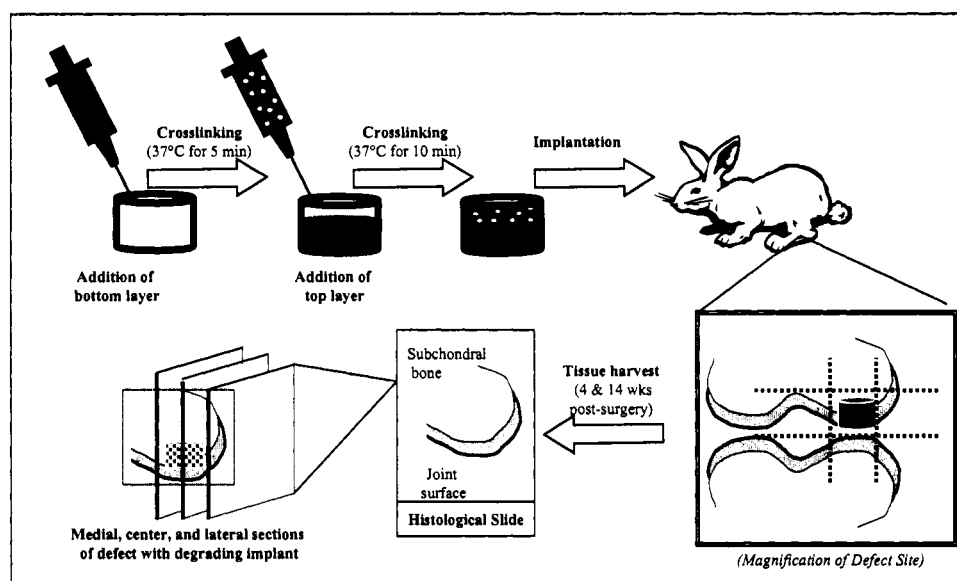
OPF network. The first letter of each abbreviation corresponds to the material composition of the upper, cartilage forming layer. Subscripts “-” or “+” respectively refer to upper layers containing microparticles loaded with PBS or loaded with TGF- β 1. No growth factors were added to the bottom, bone forming layer of any scaffold formulation.

All scaffolds were fabricated using a two step crosslinking procedure (Figure 1) in which an OPF solution with the desired bottom layer composition was first injected into a mold and partially crosslinked prior to the injection and crosslinking of the upper layer. More specifically, 0.15 g OPF was dissolved in 395 μ l of PBS containing 14 mg N,N'-methylene bisacrylamide (Sigma, St. Louis, MO) as a crosslinking agent. Then, the appropriate amount of microparticles (32 mg or 0 mg) was added to the polymer solution with an additional 118 μ l PBS. The resulting mixture was thoroughly vortexed. Finally, 51 μ l of 0.3 M tetramethylethylenediamine (in PBS) (Sigma, St. Louis, MO) and 51 μ l of 0.3 M ammonium persulfate (in PBS) (Sigma, St. Louis, MO) were added to initiate crosslinking. After vortexing, the suspension was injected into a cylindrical Teflon mold (3 mm in diameter) to a height of 2 mm and incubated at 37°C to achieve crosslinking. The cytocompatibility of this tetramethylethylenediamine/ammonium persulfate initiating system has previously been demonstrated by the successful encapsulation of rat marrow stromal cells in OPF hydrogels during the time of crosslinking (147, 148).

After 5 minutes incubation, this formulation of OPF forms a partially crosslinked hydrogel, enabling lamination to a second layer (134, 146). Accordingly, at this time, a second solution of OPF-gelatin microparticles was injected into the Teflon mold to form the upper scaffold layer (1 mm in height). Prior to injection, this solution was mixed as previously described. The mold was then incubated at 37°C for 10 min to achieve

complete crosslinking of both layers. It should be noted that all PBS, initiator, and bisacrylamide solutions were sterilized prior to use by filtration through a cellulose acetate membrane filter (0.2 μm pore diameter) according to an established procedure (147). The final dimensions of all scaffolds matched the dimensions of osteochondral defects in the rabbit model (3 mm in diameter x 3 mm in depth) (149-151). Scaffolds were fabricated 2 to 4 hours prior to implantation.

Figure V-1: Overview of the methods utilized for scaffold fabrication and implantation, as well as subsequent retrieval and processing of tissue



Animal Surgery

Seventeen, 4-month old New Zealand white rabbits were utilized in this study. All surgical procedures followed protocols approved by the University of Nijmegen's Animal Care and Use Committee and were based on a well-established bilateral, rabbit, osteochondral defect model (149-151). Eight of the seventeen rabbits were used to examine tissue repair at 4 weeks with the remaining nine rabbits utilized to examine repair at 14 weeks.

Prior to surgery, anesthesia was induced by an intravenous injection of Hypnorm® (0.32 mg/ml fentanyl citrate and 10 mg/ml fluanisone) and atropine. General inhalation anesthesia was then maintained by a mixture of nitrous oxide, isoflurane, and oxygen administered through a constant volume ventilator. To reduce peri-operative infection risk and to minimize post-operative discomfort, antibiotic prophylaxis (Baytril 2.5%, Enrofloxacin, 5-10 mg/kg) and Fynadyne® were preoperatively administered to the rabbits.

After administration of anesthesia, rabbits were immobilized on their back. Hair from both legs of each animal was shaved, and the legs disinfected with povidine-iodine. Both knee joints were then exposed through a medial parapatellar longitudinal incision. The capsule was incised, and the medial femoral condyle exposed after lateral luxation of the patella. With the knee maximally flexed, a full-thickness defect (3 mm in diameter and 3 mm in depth) was created in the center of the condyle using a dental drill (KAVO, Intrasept 905, KAVO Nederland BV, Vianen, The Netherlands). A 2 mm drill bit was first used to establish a 2 mm diameter defect. This defect was then irrigated and gradually enlarged using drill bits with a diameter of 2.8 mm and then 3.0 mm. All bits were fashioned with a 3 mm stop to ensure a defect of precisely 3 mm in depth was created. All debris was removed from the defect with a curette and the edge carefully cleaned with a scalpel blade.

A scaffold was then placed into the defect. Subsequently, the patella was repositioned, and the capsule and muscle closed with a continuous 4-0 Vicryl suture. Finally, the skin was closed with single intracutaneous 4-0 Vicryl sutures. This procedure was repeated for both knees of each rabbit with different scaffold formulations implanted

into the right and left knees of each rabbit. More specifically, five rabbits received one C⁺/H scaffold and one C⁺/C scaffold, while an additional six rabbits received one C⁻/H scaffold and one C⁺/H scaffold. Finally, the last six rabbits received one C⁺/C and one C⁻/H scaffold.

To minimize post-operative discomfort, Fynadyne® was administered for two days postoperatively. The animals were housed in conventional rabbit cages which allowed for unrestricted weight-bearing activity and were observed for signs of pain, infection and proper activity.

Tissue Processing

At four and fourteen weeks post-surgery, rabbits were euthanized by intravenous administration of Nembutal (pentobarbital). The tissue surrounding the medial femoral condyle was retrieved en bloc. Specimens were fixed in 10% buffered formalin (pH 7.4) for 1 week, decalcified in Formical2000 (Decal Corporation, Congers, NY, USA) for 2 weeks, dehydrated through graded ethanols, and embedded in paraffin. Using a microtome (Leica RM 2165, Leica Microsystems, Nussloch, Germany), longitudinal sections of 6 µm in thickness were taken throughout the defect. Sections from the defects' center and lateral and medial edges were then stained with hematoxylin and eosin (H&E). Likewise, center, lateral, and medial sections were separately stained with Safranin O/light green and Masson's trichrome. This methodical processing of the sections allowed for subsequent evaluation of tissue repair at the defect edges and center.

In addition to standard H&E, the two additional staining methods enabled identification of key attributes of the newly formed tissue – in particular, glycoasminoglycan and collagen content. Safranin O is routinely used in cartilage

histology since this stain colors basophilic structures, like the negatively charged glycoasminoglycans of articular cartilage, with shades of red. Light green is a neutral stain utilized as a counter stain in Safranin O-stained sections. Masson's trichrome staining is also a well established histological technique for evaluating connective tissue. This technique identifies collagen fibers with a green color, while cell nuclei and cytoplasm are respectively stained black and red (152).

Histological Scoring

Histological sections were blindly and independently scored by two evaluators (TH and EB) using a modified graded system based on the five histological characteristics examined in the original O'Driscoll method for examining tissue graft performance: graft integration and integrity, and cartilage morphology, regularity, and thickness (153). However, since the present study examined the performance of degradable implants, rather than tissue grafts, this system was amended to examine neo-tissue ingrowth and integration, rather than graft integrity and integration (Table 2). Additionally, since the material composition of the bottom, subchondral layer of these implants was varied to examine how the rate of implant degradation affected tissue formation, parameters were also included to separately examine neo-tissue in-growth and morphology in this region. Overall implant degradation was also scored.

Finally, following well established modifications to the original O'Driscoll system, additional parameters examined potential chondrocyte clustering within the newly formed cartilaginous tissue (154-156), as well as the cellularity and GAG content (assessed by Safranin O staining) within the neo-tissue and in the cartilage immediately adjacent to the defect (151, 154, 156). Similarly, apparent total collagen content in the

neo-tissue was assessed by Masson's trichrome staining. These parameters were scored relative to the respective characteristics of uninjured cartilage far removed from the defect site. Thus, the histological scoring system shown in Table 2 facilitated a thorough, systematic means of evaluating tissue quality and quantity in the overall 3 x 3 mm defect, as well as in the subchondral (the bottom 2 mm) and chondral (the upper 1 mm) regions of defects. Furthermore, this comprehensive system allowed for assessment of possible degenerative changes in the tissue adjacent to defects.

Statistical analysis

Ordered logistic regression of histological scores was performed using SAS Version 8.2 statistical software (SAS, Cary, NC, USA). This statistical method provides a means of assessing potential factors affecting outcomes with discrete, ordinal values (157). For each histological parameter, ordered logistic regression was performed to analyze the potential single factor affects of time, scaffold formulation, and location within the defect (edge vs. center sections). The Wald Chi Square test statistic with a significance level of 0.05 was first used to confirm the validity of each regression. An analysis of effects was then performed with a significance level of 0.05. Potential two and three factor interactions amongst time, scaffold formulation, and location were also evaluated for each histological parameter.

Calculation of Average Histological Scores

Ordered logistic regression revealed that section location (edge vs. center) within defects was not a significant factor affecting any of the twelve histological parameters. Thus, for each parameter, the medial, lateral, and center scores for a particular defect were averaged. Then, at each time point, the mean score and corresponding standard

deviation amongst these averages was calculated for each treatment group. These values are reported in Tables 3 and 4 as mean scores per formulation (MSF) \pm standard deviation.

Table V- 2: Histological scoring system for evaluation of overall tissue filling (a), subchondral bone repair (b), and cartilage repair (c)

(a) Overall tissue filling

<i>Overall defect evaluation (throughout the entire defect depth)</i>	<i>Score</i>
1. Percent filling with neo-formed tissue	
100%	3
>50%	2
<50%	1
0%	0
2. Percent degradation of the implant	
100%	3
>50%	2
<50%	1
0%	0

(b) Subchondral bone repair

<i>Subchondral bone evaluation (within the bottom 2 mm of defect)</i>	<i>Score</i>
3. Percent filling with neo-formed tissue	
100%	3
>50%	2
<50%	1
0%	0
4. Subchondral bone morphology	
Normal, trabecular bone	4
Trabecular, with some compact bone	3
Compact bone	2
Compact bone and fibrous tissue	1
Only fibrous tissue or no tissue	0
5. Extent of neo-tissue bonding with adjacent bone	
Complete on both edges	3
Complete on one edges	2
Partial on both edges	1
Without continuity on either edge	0

(c) Cartilage repair

<i>Cartilage evaluation (within the upper 1 mm of defect)</i>	Score
6. Morphology of neo-formed surface tissue	
Exclusively articular cartilage	4
Mainly hyaline cartilage	3
Fibrocartilage	2
Only fibrous tissue or bone	1
No tissue	0
7. Thickness of neo-formed cartilage	
Greater than surrounding cartilage	3
Similar to the surrounding cartilage	2
Less than the surrounding cartilage	1
No cartilage	0
8. Joint surface regularity	
Smooth, intact surface	3
Surface fissures (<25% neo-surface thickness)	2
Deep fissures (25-99% neo-surface thickness)	1
Complete disruption of the neo-surface	0
9. Chondrocyte clustering	
None at all	3
< 25% chondrocytes	2
25-100% chondrocytes	1
No chondrocytes present (no cartilage)	0
10. Cell and glycoasminoglycan (GAG) content of neo-formed cartilage	
Normal cellularity with normal Safranin O staining	3
Normal cellularity with moderate Safranin O staining	2
Clearly less cells with poor Safranin O staining	1
Few cells with no or little Safranin O staining or no cartilage	0
11. Collagen content	
Normal	3
Moderately reduced	2
Severely reduced	1
Absent or no cartilage	0
12. Cell and glycoasminoglycan (GAG) content of adjacent cartilage	
Normal cellularity with normal GAG content	3
Normal cellularity with moderate GAG content	2
Clearly less cells with poor GAG content	1
Few cells with no or little GAGs or no cartilage	0

It should be noted that for all parameters, except parameter 7, scores of maximum value correspond to the characteristics of healthy, uninjured tissue. For parameter 7 (neo-

cartilage thickness), a score of 2, rather than the maximum value of 3, corresponds to normal cartilage thickness. Although neo-cartilage thickness was commonly observed to be thinner than the surrounding cartilage, only one instance of overfilling was noted. Thus, average scores for this parameter accurately represent relative tissue thickness.

Results Animal Health & Macroscopic Joint Appearance at Recovery

Animals appeared to recover quickly from the bilateral surgical procedure and were observed to regain full movement within less than one week. The rabbits continued to exhibit no physical limitations, with normal behavior and movement observed throughout the 14 week period. It should be noted that complications during the surgical creation of one defect led to exclusion of that specimen from the study. With all other defects, no signs of inflammation, infection, or swelling were noticed upon visible inspection of the joint surfaces at the time of tissue retrieval.

Histological Appearance

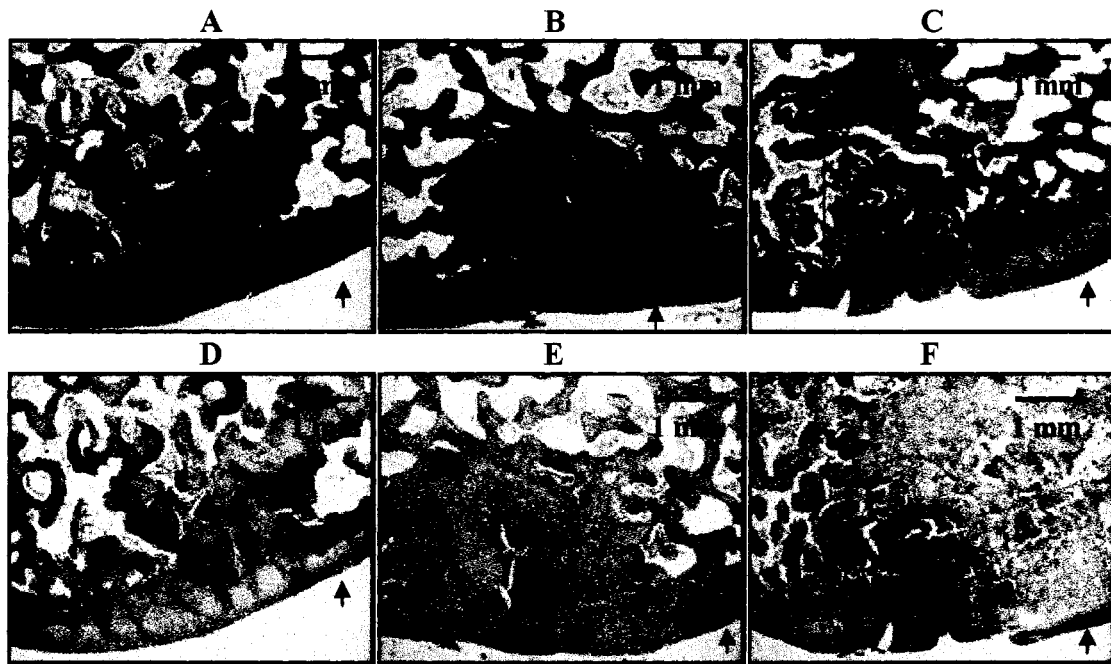
Tissue Repair at 4 Weeks

No evidence of a persistent inflammatory response was observed at 4 weeks despite the significant extent of implant degradation which was observed at this early time point. Immature tissue was seen to fill greater than 50% of the defect area in histological sections of joints treated with all scaffold formulations. The overall percentage of tissue filling and scaffold degradation appeared to vary amongst all defects, regardless of scaffold type. Compact bone and a small amount of fibrous tissue generally filled the subchondral portion of defects (the bottom 2 mm). However, in many specimens, especially those with little scaffold material remaining, some trabecular bone

was already present at this early time point. Overall, this osseous tissue was well integrated with the surrounding bone.

Likewise, the newly formed tissue in the chondral region of defects (the upper 1 mm) displayed continuity with both the adjacent cartilage and underlying subchondral tissue. This neo-surface had the appearance of fibrocartilage or fibrous tissue and was generally thinner than the surrounding, uninjured cartilage. Elongated, thin cells and sparse Safranin O staining were observed at 4 weeks (Figure 2). Some fissures in the neo-surface were present, but these generally did not extend to the underlying bone. Both the subchondral and chondral tissue adjacent to the defect site maintained a healthy appearance.

Figure V- 2: Sections showing representative 4-week tissue repair in three defects after osteochondral implantation of C⁺/C (A and D), C⁺/H (B and E), and C⁺/H (C and F) scaffolds. Figures A-C show H&E stained tissue sections, while Figures D-F show sections stained with Safranin O/light green. Original magnification of all sections is 2.5x. Arrows point towards the joint surface, while surface fissures are respectively indicated by FI.

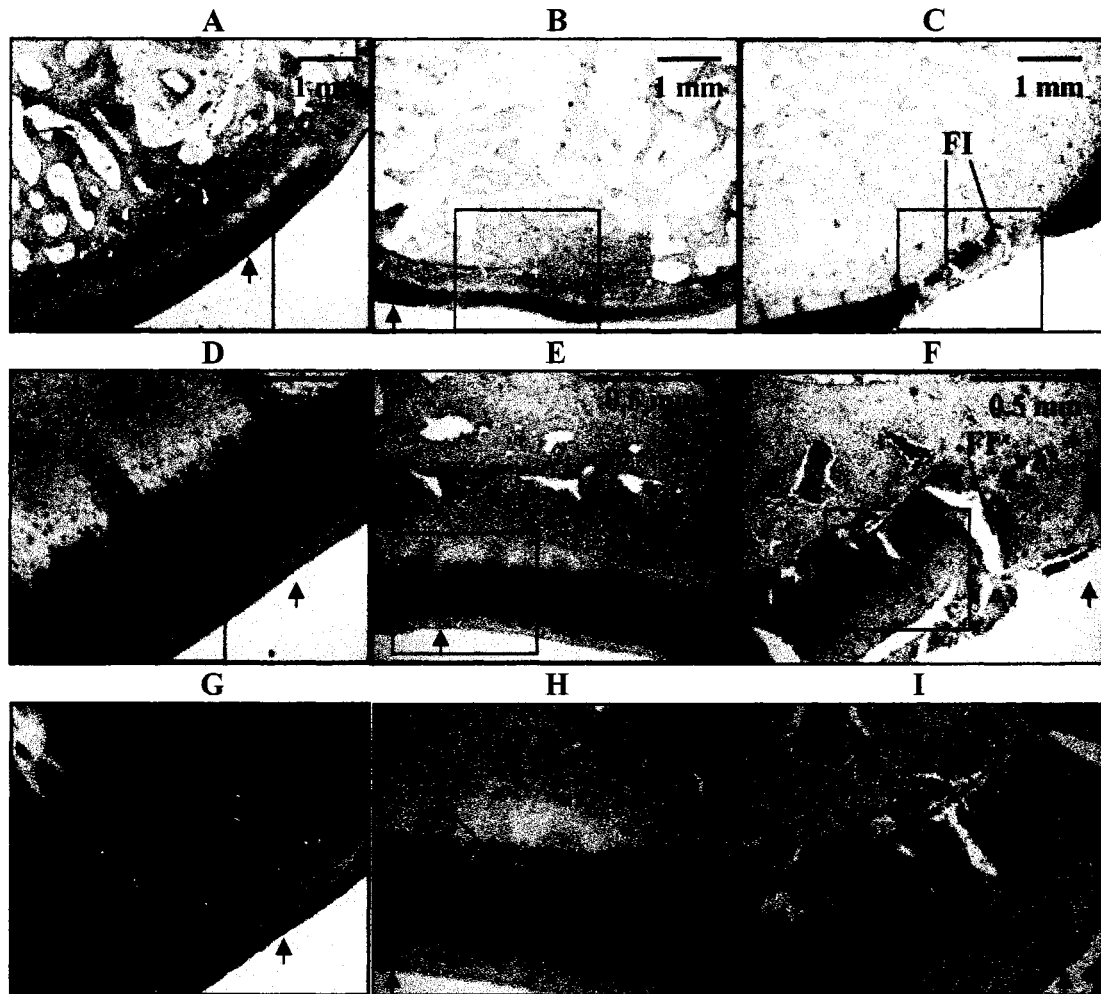


Tissue Repair at 14 Weeks

In general, by 14 weeks, defects were completely filled with tissue, and scaffolds were completely degraded. With all treatment groups, the neo-formed subchondral and chondral tissue had undergone considerable remodeling between 4 and 14 weeks, as apparent in the morphology of the newly formed tissue at this later time point (Figure 3). In some sections, the only visible marker of the former defect area was a slightly thinner cartilage layer with less intense Safranin O staining than the surrounding joint surface. Trabecular bone, and sometimes a small amount of remaining compact bone, filled the subchondral region. In all cases, this bone was completely integrated with the adjacent bone.

The new joint surface was also well-integrated with the surrounding cartilage at 14 weeks, but was occasionally dotted with fissures as shown in Figure 3i. With all treatment groups, chondrocytes now populated the former defect area but were reduced in number when compared to the uninjured cartilage. These chondrocytes were often arranged in a zonal organization resembling healthy articular cartilage. As shown in the magnifications of Figures 3g and 3h, chondrocytes near the joint surface were slightly elongated. Below these cells, more rounded chondrocytes were seen to form columns and to stain more intensely for GAG, as expected for cells in the intermediate zone of articular cartilage (3, 4). Cartilage surrounding this neo-formed surface maintained a healthy appearance and thickness (Figure 3a-c).

Figure V- 3: Sections (stained with Safranin O/light green) showing representative 14-week tissue repair in three defects after osteochondral implantation of C^+/C (A, D, and G), C^+/H (B, E, and H), and C^-/H (C, F, and I) scaffolds. The boxed regions in A-C (2.5x magnification) are shown at higher magnifications in D-F (10x), and G-I (20x). Arrows point towards the joint surface, while columnar arrangements of chondrocytes, cell clusters, and cartilage fissures are respectively indicated by CO, CL, and FI.



Histological Scores at 4 Weeks

As previously discussed, some variability in tissue filling and scaffold degradation was observed in 4 week sections. Again, scaffold type was not seen to influence the degree of tissue filling or scaffold degradation. Mean histological scores for subchondral bone morphology were between 2.0 and 1.0 (Table 3), indicating the predominance of remodeling compact bone with some remaining fibrous tissue in this

portion of defects at 4 weeks. Contrary to expectations, the material composition of the bottom layer of scaffolds did not influence bone filling, morphology, or integration. However, no bone upgrowth into the chondral region was observed with any of the treatment groups.

Table V- 3: Mean histological scores per scaffold formulation (MSF) at 4 weeks. Values are shown as mean \pm standard deviation.

Histological Parameter	Mean Score Per Formulation		
	C ⁺ /C (n=4)	C ⁺ /H (n=6)	C ⁻ /H (n=5)
<i>Overall defect evaluation</i>			
1. Percent filling with neo-formed tissue	2.2 \pm 0.8	2.7 \pm 0.4	2.3 \pm 0.7
2. Percent degradation of the implant	2.7 \pm 0.5	2.7 \pm 0.4	2.3 \pm 0.7
<i>Subchondral bone evaluation</i>			
3. Percent filling with neo-formed tissue	2.0 \pm 0.7	2.1 \pm 1.1	2.1 \pm 0.8
4. Subchondral bone morphology	1.5 \pm 1.1	1.5 \pm 1.0	1.7 \pm 0.7
5. Extent of neo-tissue bonding with adjacent bone	2.0 \pm 1.0	2.1 \pm 1.3	3.0 \pm 0.0
<i>Cartilage evaluation</i>			
6. Morphology of neo-formed surface tissue	1.8 \pm 0.6	1.6 \pm 0.5	1.6 \pm 0.5
7. Thickness of neo-formed cartilage	1.3 \pm 1.0	0.7 \pm 0.4	0.8 \pm 0.8
8. Joint surface regularity	2.6 \pm 0.5	2.0 \pm 0.6	1.7 \pm 0.8
9. Chondrocyte clustering	1.6 \pm 1.1	1.2 \pm 1.0	0.9 \pm 0.9
10. Cell and GAG content of neo-formed cartilage	1.1 \pm 0.8	0.7 \pm 0.8	0.8 \pm 0.8
11. Collagen content	1.7 \pm 1.2	1.2 \pm 0.9	1.3 \pm 1.3
12. Cell and GAG content of adjacent cartilage	2.3 \pm 0.3	1.8 \pm 0.3	2.6 \pm 0.4

Histological evaluation revealed that TGF- β 1 delivery had little effect on early cartilage repair. Regardless of treatment group, the neo-surface at 4 weeks scored between 1.0 and 2.0 for surface tissue morphology, reflecting the fibrous nature of this new surface. Critical histological scoring revealed that this tissue was thinner and contained lower cell, GAG, and collagen content than the surrounding uninjured cartilage (See Table 3). Very limited degenerative changes were observed in the cartilage adjacent to defects. As shown in Table 3, mean scores for cell and GAG content in the surrounding cartilage tissue (Parameter 12) were at or near 2.0 for all formulations,

indicating normal cellularity with moderately reduced GAG content. Again, these findings further confirm the biocompatibility of these OPF composites and their degradation products. By 14 weeks, the surrounding cartilage, as well as the neo-formed surface, displayed overall improvements in tissue quality as reflected in the higher histological scores at this later time point.

Histological Scores at 14 Weeks

In general, scaffolds were completely degraded at 14 week. Tissue filling was seen to statistically improve by 14 weeks. However, perhaps the most striking improvements between 4 and 14 weeks were observed in the morphology of both the subchondral and chondral regions of the former defect areas. While the 4 week mean scores for subchondral bone morphology were below 2.0 for all treatments, by 14 weeks these scores had risen to 3.0 ± 0.7 , 2.7 ± 0.6 , 3.1 ± 0.9 , for defects treated with C⁺/C, C⁺/H, and C⁻/H, respectively. Thus, the compact bone and fibrous tissue present at 4 weeks and undergone significant remodeling to form trabecular bone at 14 weeks. As shown in Figure 3, this bone was completely integrated with the surrounding bone. In fact, maximum scores of 3.0, indicating complete bonding on both defect edges, were awarded to all tissue sections evaluated at 14 weeks.

Tissue quality in the chondral portion of the former defect area had also improved considerably by week 14 (See Figure 3). In fact, scores for tissue morphology, thickness, chondrocyte clustering, and cell, GAG, and collagen content were statistically higher at 14 weeks than at 4 weeks. For example, scores for cell and GAG content, which had been at or below 1.0 at 4 weeks, now approached 2.0 at 14 weeks, indicating an increase in both cellularity and GAG content. Likewise, scores for total collagen content were also

seen to improve between 4 and 14 weeks. Perhaps most indicative of the overall improvement in tissue quality were the elevated 14 week mean scores for surface tissue morphology (2.9 ± 0.6 , 2.7 ± 0.5 , 2.6 ± 0.8 for C⁺/C, C⁺/H, and C⁻/H treatment groups, respectively). These scores reflected the high frequency of hyaline cartilage filling the chondral region and the zonal arrangement of chondrocytes at 14 weeks. It should be noted that this cartilage was still thinner than the surrounding cartilage, but its thickness had statistically improved between 4 and 14 weeks. While Safranin O staining in cartilage immediately adjacent to the former defect was slightly reduced (when compared to cartilage far from the defect site), normal chondrocyte density and arrangement perpetuated this tissue indicating that no severe, adverse effects were inflicted by these OPF-based scaffolds.

Table V- 4: Mean histological scores per scaffold formulation (MSF) at 14 weeks. Values are shown as mean \pm standard deviation. Asterisks (*) indicate those parameters which were shown to statistically improve over time from 4 week values.

Histological Parameter	Mean Score Per Formulation		
	C ⁺ /C (n=4)	C ⁺ /H (n=6)	C ⁻ /H (n=5)
<i>Overall defect evaluation</i>			
1. Percent filling with neo-formed tissue *	2.8 \pm 0.3	2.6 \pm 0.2	2.9 \pm 0.2
2. Percent degradation of the implant	2.8 \pm 0.3	2.6 \pm 0.2	2.9 \pm 0.2
<i>Subchondral bone evaluation</i>			
3. Percent filling with neo-formed tissue*	2.8 \pm 0.3	2.7 \pm 0.3	2.9 \pm 0.2
4. Subchondral bone morphology*	3.0 \pm 0.7	2.7 \pm 0.6	3.1 \pm 0.9
5. Extent of neo-tissue bonding with adjacent bone	3.0 \pm 0.0	3.0 \pm 0.0	3.0 \pm 0.0
<i>Cartilage evaluation</i>			
6. Morphology of neo-formed surface tissue*	2.9 \pm 0.6	2.7 \pm 0.5	2.6 \pm 0.8
7. Thickness of neo-formed cartilage*	1.7 \pm 0.4	1.7 \pm 0.2	1.5 \pm 0.6
8. Joint surface regularity	2.6 \pm 0.5	2.4 \pm 0.4	2.2 \pm 0.3
9. Chondrocyte clustering*	2.1 \pm 0.7	1.7 \pm 0.4	1.9 \pm 0.7
10. Cell and GAG content of neo-formed cartilage*	1.9 \pm 0.6	1.7 \pm 0.5	1.7 \pm 0.6
11. Collagen content*	2.3 \pm 0.7	2.2 \pm 0.6	2.4 \pm 1.0
12. Cell and GAG content of adjacent cartilage*	2.8 \pm 0.3	2.7 \pm 0.3	2.6 \pm 0.4

Discussion

The rigorous histological analysis undertaken in this study allowed for critical evaluation of tissue repair in osteochondral defects treated with three different formulations of OPF hydrogel scaffolds. More specifically, the twelve-parameter system shown in Table 2 permitted individual assessment of the neo-formed tissue in both the subchondral and chondral regions of defects. At either time point and in either region of the defect, no evidence of persistent inflammation was observed. Overall, at 4 weeks, scaffolds were largely degraded with immature tissue filling defects. Although mainly compact bone with some fibrous tissue filled the subchondral region at 4 weeks, this tissue had been remodeled to contain predominantly trabecular bone at 14 weeks. Likewise, the fibrocartilage filling the subchondral region of defects at 4 weeks had been remodeled to contain mainly hyaline cartilage at 14 weeks.

This observed improvement in bone and cartilage morphology indicate the biocompatibility of these OPF-based scaffolds and their degradation products. In previous *in vitro* studies, designed to model the low pH environment typical of prolonged inflammation, OPF-gelatin microparticle composites and OPF hydrogels were seen to degrade at a relatively slow rate at decreased pH. In fact, less than 60% polymer loss was observed at pH 4.0 after 4 weeks (146). In the present study, scaffold degradation *in vivo* generally exceeded 60% at 4 weeks. Thus, this observation indicates that low pH, and thus an inflammatory environment, did not persist around the defect site. Furthermore, since neither inflammatory cells nor joint swelling were observed at either 4 or 14 weeks, the biocompatibility of the byproducts from these degrading OPF scaffolds is clearly confirmed.

In this study, the observed rate of implant degradation conformed to the expected degradation kinetics for scaffold layers consisting of an OPF-gelatin microparticle composite at normal, physiological conditions (146). However, layers containing OPF gels with no microparticles were expected to degrade at a slower rate, as complete degradation at pH 7.4 within 4 weeks was not observed in prior *in vitro* studies (146). Compressive loading during normal, joint movement may explain this enhanced rate of gel degradation. Scaffold type, and thus composition, did not appear to greatly affect the extent of repair. However, bone upgrowth into the chondral region was not observed with either material composition, demonstrating that both compositions have degradation rates which support controlled osteochondral repair. The similar *in vivo* degradation profiles of these scaffolds may account for the similar healing responses observed amongst scaffold formulations.

Like scaffold degradation, bone integration was not observed to significantly change between 4 and 14 weeks. While partial integration was occasionally observed at the early time point, 4 week scores for this parameter were not found to be statistically different from the complete integration observed at 14 weeks. Often, when grafts (87) or degradable scaffolds (150, 151) are utilized in cartilage repair, incomplete integration with the surrounding tissue is observed upon long term evaluation. This may lead to displacement of the implant and inflict further joint pain (87). Thus, the excellent tissue integration exhibited with these novel scaffolds demonstrates their potential in advancing the treatment of cartilage lesions.

Likewise, the lack of statistical changes in joint surface regularity scores reflects the utility of these scaffolds in cartilage engineering. At both 4 and 14 weeks, disruptions

in the joint surface were generally limited to surface fissures, as indicated by the histological scores in Table 3 and 4. It should be noted that scaffold type was seen to affect this marker of cartilage repair. In particular, higher scores corresponded with TGF- β 1-loaded scaffolds. While these results suggest some therapeutic effect of the TGF- β 1 released from these scaffolds, further research is necessary to investigate why growth factor delivery did not affect additional markers of tissue repair. Since other researchers have also encountered a lack of significant differences between treatment groups upon histological evaluation of osteochondral scaffolds (100, 151), this issue may be related to the complexity of articular cartilage repair and/or the use of relatively young animals with higher regenerative potential. Although numerous other studies have also utilized the current animal model (150, 151), future studies will investigate these scaffolds in the osteochondral repair in older animals.

However, the excellent tissue filling and integration resulting from osteochondral implantation of these novel OPF-based scaffolds demonstrates their potential for improving cartilage repair. As shown in Figure 3, hyaline cartilage with well-organized chondrocytes and intense GAG staining was seen to fill the chondral portion of defects at 14 weeks. Trabecular bone with some remodeling compact bone was seen to fill the subchondral region. Untreated rabbit osteochondral defects have been shown to be filled with highly fibrillar, fibrous tissue or fibrocartilage in the chondral region with bone up to or beyond the tidemark (150). Accordingly, the quality of repair achieved with these scaffolds reveals their promise in advancing cartilage repair and compels further *in vivo* investigations with these materials.

Conclusions

Through osteochondral implantation of OPF-based hydrogels, the potential of this novel class of degradable scaffolds has been demonstrated in the field of cartilage tissue engineering. Specifically, this research illustrates that OPF-based hydrogel scaffolds undergo biocompatible degradation and support healthy tissue growth in rabbit, osteochondral defects. Tissue quality was seen to improve over time with mostly hyaline cartilage filling the chondral region and a mixture of trabecular and compact bone filling the subchondral region at 14 weeks. Although scaffold material composition was not seen to affect scaffold degradation or tissue filling, no bone upgrowth into the chondral region was observed, and new bone tissue was completely integrated with the surrounding bone at 14 weeks. Although further studies are necessary to optimize these scaffolds, TGF- β 1 loading in the top layer of scaffolds appeared to exert some affect on cartilage quality in the defect area. Accordingly, this research demonstrates the exciting potential of these OPF-based hydrogels as carriers of bioactive agents for cartilage repair.

VI. DUAL GROWTH FACTOR DELIVERY FROM DEGRADABLE OLIGO(POLY(ETHYLENE GLYCOL) FUMARATE) HYDROGEL SCAFFOLDS FOR CARTILAGE TISSUE ENGINEERING[†]

Abstract

This work describes the development of a non-invasive means of simultaneously delivering insulin-like growth factor-1 (IGF-1) and transforming growth factor- β 1 (TGF- β 1) to injured cartilage tissue in a controlled manner. This novel delivery technology employs the water-soluble polymer, oligo(poly(ethylene glycol) fumarate) (OPF) in the fabrication of biodegradable hydrogels which encapsulate gelatin microparticles. Release studies first examined the effect of gelatin IEP and crosslinking extent on IGF-1 release from these microparticles. In the presence of collagenase, highly crosslinked, acidic gelatin (IEP = 5.0) provided sustained release of IGF-1, $95.2 \pm 2.9\%$ cumulative release at day 28, while less crosslinked microparticles and microparticles of alternate IEP exhibited similar release values after only 6 days. Encapsulation of these highly crosslinked microparticles in a network of OPF provided a means to further control release, reducing final cumulative release to $70.2 \pm 4.7\%$ in collagenase-containing PBS. Final release values from OPF-gelatin microparticle composites could be altered by incorporating less crosslinked, non-loaded microparticles within these constructs. Finally, this technology was extended to the dual delivery of IGF-1 and TGF- β 1 by loading these growth factors into either the OPF hydrogel phase or gelatin microparticle phase of composites. Release profiles were successfully manipulated by altering the phase of growth factor loading and microparticle crosslinking extent. For instance, by loading TGF- β 1 into the gelatin microparticle phase, a burst release of $10.8 \pm 0.7\%$ was achieved,

[†] This chapter was published as the following article TA Holland and AG Mikos, Dual Growth Factor Delivery From Degradable Oligo(Poly(Ethylene Glycol) Fumarate Hydrogel Scaffolds for Cartilage Tissue Engineering, *J. Control. Release*, 101, 111-125 (2005).

while loading this growth factor into the OPF hydrogel phase resulted in a burst release of $25.2 \pm 1.5\%$. With either system, simultaneous, slow release of IGF-1 over a 4 week period was accomplished by selectively loading this protein into highly crosslinked, encapsulated microparticles. These results demonstrate the utility of these systems in future studies to assess the interplay and time course of multiple growth factors in cartilage repair.

Abbreviations

CC-PBS, collagenase-containing phosphate buffered saline; GA, glutaraldehyde; H, oligo(poly(ethylene glycol) fumarate) hydrogel phase of composites; IEP, isoelectric point; IGF-1, insulin-like growth factor-1; MPs, microparticles; OPF, oligo(poly(ethylene glycol) fumarate); PBS, phosphate buffered saline; TGF- β 1, transforming growth factor- β 1; 10, composite phase consisting of acidic gelatin microparticles crosslinked in 10 mM GA; 40, composite phase consisting of acidic gelatin microparticles crosslinked in 40 mM GA; Subscripts: b, IGF, TGF, IGF*, TGF*, respective loadings with PBS, non-radioactive solutions of IGF-1 or TGF- β 1, or solutions containing trace I^{125} labeled IGF-1 or trace I^{125} labeled-TGF- β 1.

Introduction

Severe cartilage degeneration afflicts an estimated 20.7 million Americans with joint pain and, in some cases, lifelong debilitation (158). Degeneration may often be initiated by lesions to articular cartilage during sports activities, accidents, or improper joint loading, making this tissue more susceptible to additional injuries (2, 3). This tendency toward repeated injury, coupled with the tissue's low cellularity and isolation from the vascular network's rich supply of bioactive molecules, severely limit intrinsic cartilage repair (7, 115). Accordingly, surgical strategies for repair have focused on accessing the regenerative signaling molecules and cells within the subchondral bone marrow. Unfortunately, these techniques require invasive drilling or abrasion through the overlying articular cartilage and into the marrow, and thus, inflict further tissue damage

before any therapeutic effect is achieved. Furthermore, the biomechanical and biochemical properties of the resulting tissue generally fail to match that of uninjured cartilage (1, 2).

As an alternative to these harsh surgical techniques, our laboratory has developed a class of novel, injectable materials for the delivery of bioactive molecules to cartilage lesions to enhance tissue repair. These systems are based on oligo(poly(ethylene glycol) fumarate) (OPF), a synthetic polymer which can be used to fabricate biodegradable and biocompatible hydrogels (119, 120). OPF, a water soluble polymer, can be injected into a defect site and crosslinked *in situ* at physiological conditions, thereby eliminating the need for invasive implantation and retrieval surgeries. Furthermore, we have shown that gelatin microparticles may be incorporated to these gels at the time of crosslinking to act as enzymatically, digestible porogens to speed scaffold degradation (146). More specifically, the rate of scaffold degradation may be controlled by altering the crosslinking extent of these microparticles and their loading within the OPF network. Additional research has demonstrated the utility of gelatin microparticles as simultaneous carriers of growth factors within these synthetic hydrogel scaffolds (134, 146). In particular, controlled drug release can be achieved by altering either the microparticle composition or hydrogel mesh size of these delivery systems.

Thus far, these novel release systems have focused on the delivery of transforming growth factor- β 1 (TGF- β 1), a 25 kDa protein which has been shown to promote the chondrogenic differentiation of progenitor cells (10, 28, 29), to increase cartilage extracellular matrix synthesis (32, 34, 35), and to enhance chondrocyte proliferation (36, 37). However, numerous other bioactive molecules are involved in the

maintenance and repair of articular cartilage. In particular, insulin-like growth factor-1 (IGF-1) has been shown to act primarily in an anabolic fashion to increase proteoglycan and type II collagen synthesis (33, 38, 52, 53, 159). In fact, IGF-1, also known as somatomedin C, was initially discovered as a result of its ability to promote sulfate incorporation into proteoglycans (33, 52). Maintenance of the proper level and distribution of proteoglycan networks and collagen fibers in articular cartilage is of utmost importance, since these extracellular matrix components, respectively, impart cartilage tissue with its compressive and tensile strength (3, 7, 8). Thus, sustained delivery of IGF-1 provides a potential means to stimulate proteoglycan and collagen synthesis in injured cartilage, enhancing the biomechanical and biochemical properties of repaired tissue.

Accordingly, the following work investigates the delivery of IGF-1 from gelatin microparticles, OPF hydrogels, and OPF-gelatin microparticle composites. In particular, initial studies were performed to identify how gelatin isoelectric point (IEP) and crosslinking extent affect IGF-1 release from microparticles in standard phosphate buffered saline (PBS) and collagenase-containing PBS (CC-PBS). Upon identification of the appropriate microparticle carrier for IGF-1, further release studies were performed to assess release from microparticles encapsulated in a network of OPF. To examine IGF-1 diffusion through the OPF network alone, IGF-1 release from OPF hydrogels (with no encapsulated microparticles) was also examined. Additionally, the effect of co-encapsulation of non-loaded microparticles with IGF-1-loaded microparticles in composites was also assessed.

Finally, this technology for the release of IGF-1 was extended towards the development of systems for dual release of TGF- β 1 and IGF-1. Since IGF-1 has been shown to function mainly as a progression factor (33, 38, 52, 53, 159), effectively stimulating *in vitro* matrix synthesis when continuously delivered to chondrocyte cultures for six weeks (159), dual release systems were designed to provide sustained delivery of IGF-1 over the course at least four weeks. In contrast, since TGF- β 1 has been shown to act effectively as a chemotractant (60, 105), morphogen (10, 28, 30), and progression factor (32, 34, 35), the carrier of TGF- β 1 in these composites was manipulated between the hydrogel or microparticle phase, to achieve varied TGF- β 1 release profiles. In addition to assessing how carrier of TGF- β 1 affected the release kinetics of this growth factor, further studies were conducted to assess how TGF- β 1 release affected IGF-1 release from these systems.

Experimental Methods

Gelatin Microparticle Fabrication

Basic and acidic gelatin (Nitta Gelatin Inc., Osaka, Japan) with respective isoelectric points of 9.0 and 5.0 were used separately to fabricate basic or acidic microparticles according to an established method (122). Briefly, 5 g gelatin was dissolved in 45 ml distilled, deionized water (ddH₂O) by mixing and heating (60°C). This aqueous gelatin solution was added dropwise to 250 ml olive oil while stirring at 500 rpm. The temperature of the emulsion was then decreased to approximately 15°C with constant stirring. After 30 min, 100 ml chilled acetone (4°C) was added to the emulsion. After 1 hour, the resulting microspheres were collected by filtration and washed with acetone to remove residual olive oil.

Microspheres were crosslinked in a 0.1 wt% solution of Tween 80 (Sigma, St. Louis, MO) containing either 10 mM or 40 mM glutaraldehyde (GA) (Sigma, St. Louis, MO) for 15 h at 15°C. By altering the GA concentration in this reaction, the crosslinking extent of the resulting microparticles may be systematically controlled (134). Crosslinked microparticles were collected by filtration, washed with ddH₂O, and then agitated in a 25 mM glycine solution to block residual aldehyde groups of unreacted GA. After 1 hour, microparticles were again collected by filtration, washed with ddH₂O, and then vacuum dried overnight. After drying, the microparticles were sieved to obtain particles 50-100 μ m in size.

Microparticle Loading

Acidic microparticles crosslinked with 10 mM GA were diffusionally loaded with TGF- β 1 following previously established methods (122, 134). In particular, microparticles were partially swollen in aqueous TGF- β 1 solutions at pH 7.4. At this pH, the TGF- β 1-gelatin binding is enhanced by an ionic complexation between positively charged TGF- β 1 (IEP of 9.5) and negatively charged acidic gelatin (IEP of 5.0) (124, 146). However, at physiological pH, a significant charge density is not expected to be associated with IGF-1 (IEP of 7.5). Therefore, both basic and acidic gelatin microparticles, were loaded with this growth factor and utilized in release studies to examine their potential as a carrier of IGF-1.

Growth factor loading solutions were composed of trace I¹²⁵ labeled-growth factor (Perkin Elmer Life Sciences, Boston, MA) and unlabeled-growth factor (R&D Systems, Minneapolis, MN) to allow for detection of drug release. Microparticle loading was achieved by adding 5 μ l of the growth factor solution per mg dried microparticles. This

solution volume is below the microparticles' theoretical, equilibrium swelling volume to allow for complete drug absorption. The resulting mixture was vortexed and incubated at 4°C for 15h. A loading solution of 2.38 ng TGF- β 1/ μ l PBS was applied to load microparticles with this growth factor. The loading solution for IGF-1-loaded microparticles was composed of 1.19 ng IGF-1/ μ l PBS. These growth factor concentrations were chosen to provide a total, initial loading of approximately 200 ng TGF- β 1/g gel and 100 ng IGF-1/g gel in composites fabricated for dual growth factor delivery. These growth concentrations are within the range of those shown to be therapeutic in the treatment of full and partial thickness rabbit and porcine articular cartilage defects (105, 114). For consistency, these respective solutions were applied to all TGF- β 1- and IGF-1-loaded microparticles. Accordingly, the total growth factor loading in some formulations varied from that of the total loading in composites for dual growth factor release. Loadings are shown in Tables 1 and 2. Systems with blank microparticles were loaded with PBS (5 μ l PBS/mg dried microparticle).

Table VI- 1: Composition and loading of systems for IGF-1 release

Formulation	Gel Composition					Total IGF-1 Loading
	(H) Hydrogel	(10) MPs crosslinked with 10mM GA		(40) MPs crosslinked with 40mM GA		
	Loading Solution	g MPs per g polymer	Loading Solution	g MPs per g polymer	Loading Solution	(ng IGF-1 per g gel)
H _{IGF} *	IGF*	-----	-----	-----	-----	100
H _b 40 _{IGF} *	PBS	-----	-----	0.20	IGF*	200
H _b 10 _b 40 _{IGF} *	PBS	0.10	PBS	0.10	IGF*	100

In Vitro Growth Factor Release from Gelatin Microparticles

IGF-1 release from acidic and basic gelatin microparticles, each crosslinked with 10 mM GA, was assessed in standard PBS or collagenase-containing PBS (CC-PBS). TGF- β 1 release from acidic gelatin microparticles was also examined under the same

conditions. This enabled comparison of the extent of the IGF-1-gelatin complexation to the TGF- β 1-gelatin complexation, which has been shown to persist in standard PBS for at least 4 weeks (134). The effect of microparticle crosslinking extent on IGF-1 release from microparticles was also assessed.

Table VI- 2: Composition and loading of systems for IGF-1 and TGF- β 1 release

Formulation	Gel Composition					Protein Loading	
	(H) Hydrogel	(10) MPs crosslinked with 10mM GA		(40) MPs crosslinked with 40mM GA		TGF- β 1 (ng TGF- β 1 per g gel)	IGF-1 (ng IGF-1 per g gel)
	Loading Solution	g MPs per g polymer	Loading Solution	g MPs per g polymer	Loading Solution		
H _b 10 _{TGF*} 40 _{IGF}	PBS	0.10	TGF*	0.10	IGF	200	100
H _b 10 _{TGF} 40 _{IGF*}	PBS	0.10	TGF	0.10	IGF*	200	100
H _{TGF*} 10 _b 40 _{IGF}	TGF*	0.10	PBS	0.10	IGF	200	100
H _{TGF} 10 _b 40 _{IGF*}	TGF	0.10	PBS	0.10	IGF*	200	100

After the 15 h incubation period, loaded microparticles of the indicated composition were then placed into vials with 3 ml of PBS or 3 ml PBS containing 373 ng bacterial collagenase 1A (E.C. 3.4.24.3, Sigma, St. Louis, MO) per ml. This collagenase concentration was chosen to model tissue collagenase concentrations in the synovial fluid of patients with osteoarthritis (136). All specimens were agitated on a shaker table (70 rpm) at 37°C. The supernatant of each specimen was collected and replaced by fresh buffer following a schedule designed to maintain an enzyme activity at least 25% of initial enzymatic activity throughout the study (146).

At each time point, the supernatant of each specimen was analyzed for radioactivity using a gamma counter (Cobra II Autogamma, Packard, Meridian, CT). The amount of growth factor in the supernatant was determined by correlation to a standard curve. Cumulative release was determined by normalizing the total growth factor released at each time point with the sum of the total growth factor released over the course of 28

days and the growth factor remaining in the specimens at day 28. Release rates were determined by taking the slope of the percent cumulative release curve for each sample over the stated range and averaging the resultant slopes for each formulation. Accordingly, rates are stated in terms of the change in the percent cumulative release per day. For all treatments, n was 4 to 6.

OPF Synthesis and Characterization

OPF with an initial number average molecular weight of $21,600 \pm 1,400$ and weight average molecular weight of $144,300 \pm 5,200$ was synthesized according to a method developed in our laboratory (125). Molecular weight determination was likewise conducted using established procedures for gel permeation chromatography (146) with samples run in triplicate.

Hydrogel and Composite Fabrication

The OPF hydrogel and composite formulations assessed during the course of this work are shown in Tables 1 and 2. As indicated, these systems were comprised of at least one of three phases: the OPF hydrogel phase (H), acidic microparticles crosslinked with 10 mM GA (10), and acidic microparticle crosslinked with 40 mM GA (40). Abbreviations of each phase in a given formulation are followed by the subscripts b, TGF, or IGF, and respectively, refer to phases which were blank (loaded with PBS), loaded with TGF- β 1, or loaded with IGF-1. Asterisks indicate the use of trace I^{125} labeled-growth factor to detect growth factor release.

All gel formulations were fabricated by first dissolving 0.15 g OPF in 395 μ l of PBS containing 14 mg N,N'-methylene bisacrylamide (Sigma, St. Louis, MO) as a crosslinking agent. Although crosslinking may proceed solely through the OPF double

bonds, methylene bisacrylamide is added to accelerate the reaction. For composite fabrication, 0.2 g gelatin microparticles per g OPF were then added to the polymer solution, and the mixture thoroughly vortexed. For hydrogels with no microparticle component, microparticles were omitted. Finally, for both composites and hydrogels, 118 μ l PBS, 51 μ l of 0.3 M tetramethylethylenediamine (in PBS) (Sigma, St. Louis, MO), and 51 μ l of 0.3 M ammonium persulfate (in PBS) (Sigma, St. Louis, MO) were added to initiate crosslinking.

The cytocompatibility of this tetramethylethylenediamine/ammonium persulfate initiating system has previously been demonstrated by the successful encapsulation of rat marrow stromal cells in OPF hydrogels during the time of crosslinking (147, 148). For systems designed with growth factor loading in the OPF hydrogel phase (H), the PBS aliquot in this step contained the appropriate concentration of the desired protein to achieve the loading indicated in Table 1. After vortexing, the suspension was injected into a Teflon mold and incubated at 37°C. After 10 minutes incubation, this formulation of OPF forms crosslinked hydrogels or composites (134). After completion of crosslinking, gels were removed from their mold, and a cork bore used to cut discs of approximately 3 mm in diameter and 1 mm in thickness.

Single and Dual Growth Factor Release from Hydrogels and Composites in Vitro

Initial release studies examined IGF-1 release alone from hydrogels and two composite formulations (Table 1). The first composite formulation, abbreviated H_b40_{IGF*}, was composed of two phases: 0.20 g IGF-1-loaded microparticles (crosslinked with 40 mM GA) per g polymer and the surrounding OPF hydrogel phase. This formulation allowed for examination of the effect of microparticle encapsulation on release kinetics.

The second composite formulation, abbreviated $H_b10_b40_{IGF^*}$, was composed of three phases: unloaded 10 mM microparticles, IGF-1-loaded 40 mM microparticles, and the surrounding OPF hydrogel phase. For these constructs the microparticle density was again 0.20 g microparticles per g polymer, with a 1:1 mass ratio between the two microparticle types. IGF-1 release from this composite formulation was examined since dual release systems utilized the same material composition. Accordingly, comparing the release profiles of $H_b10_b40_{IGF^*}$ and $H_b40_{IGF^*}$ constructs allowed for assessment of the effect of co-encapsulating a population of non-loaded gelatin microparticles on IGF-1 release. Additionally, the IGF-1 release profiles of $H_b10_b40_{IGF^*}$ constructs were later compared to IGF-1 release profiles in dual release systems to assess the effect of co-loaded TGF- β 1 on IGF-1 release.

As shown in Table 1, dual release systems were based on the three phase composition discussed above, with IGF-1 delivery from encapsulated 40 mM microparticles. TGF- β 1 was delivered from either the encapsulated 10 mM microparticles ($H_b10_{TGF}40_{IGF}$) or from the surrounding OPF hydrogel ($H_{TGF}10_b40_{IGF}$). For each dual release formulation, two sets of gels were fabricated to separately follow TGF- β 1 and IGF-1 release, as noted with an asterisk in abbreviations. For the first set, the loading procedure was performed with an IGF-1 solution containing trace I^{125} labeled-IGF-1, while loading of the second set was performed with a TGF- β 1 solution containing trace I^{125} labeled-TGF- β 1. All specimens (for both single and dual release studies) were placed in 3 ml of PBS or CC-PBS and maintained according to the methods described above for release studies with non-encapsulated microparticles. For all formulations, n was 4 to 6.

Statistical analysis

The F test and Tukey's multiple comparison test ($p < 0.05$) was used to statistically compare the cumulative release values and release rates exhibited by the three treatments of non-encapsulated, IGF-1-loaded microparticles (132). Likewise, these tests were used to compare measured release values and rates in OPF systems for IGF-1 delivery. For dual delivery systems, the F test ($p < 0.05$) was used to assess potential statistical differences in IGF-1 release values and rates obtained between the two composite formulations. Potential statistical differences in TGF- β 1 release values and rates were assessed in the same manner. For all statistical comparisons, treatments in each buffer were separately compared. Additional statistical analysis was performed as discussed below.

Results

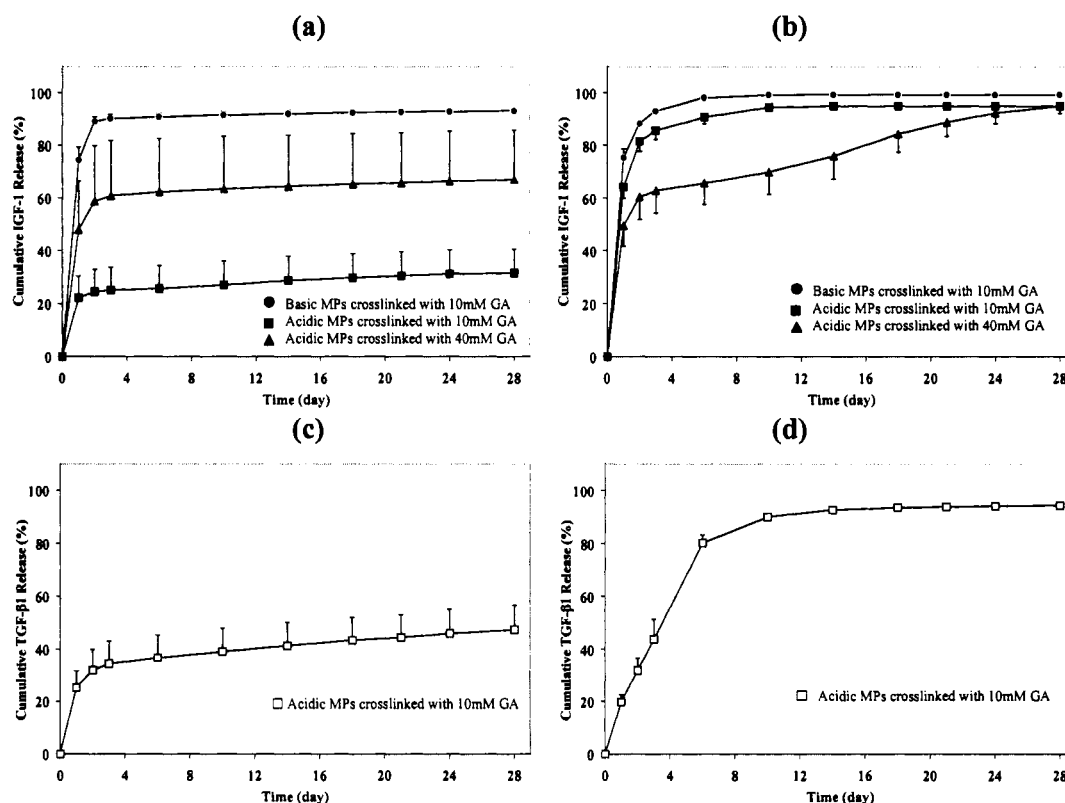
To quantify observed trends, release profiles were divided into four phases following the methods of previous investigations (106, 134, 146). Phase 1 was clearly defined by a 24 h burst release from non-encapsulated microparticles, hydrogels, and composites. Distinct release rates were then noted between days 1-3 (Phase 2) and days 6-21 (Phase 3), especially for composites and microparticles in the presence of collagenase. Final cumulative release values were determined to describe the later portion of the observation period (Phase 4) and appeared to correlate well with the extent of visible gel or microparticle degradation.

In Vitro Growth Factor Release from Gelatin Microparticles

IGF-1 release profiles from basic (IEP = 9.0) and acidic (IEP = 5.0) gelatin microparticles crosslinked with the indicated GA concentration are shown in Figures 1a (PBS) and 1b (CC-PBS). Release studies performed in standard PBS allowed for the

evaluation of the extent of the gelatin-IGF-1 complexation. TGF- β 1 release from acidic gelatin microparticles (crosslinked with 10 mM GA) was performed as a control since this growth factor is known to have a persistent complexation with acidic gelatin (Figures 1c). Parallel studies, conducted in CC-PBS, examined the effect of microparticle crosslinking on gelatin digestion and growth factor release.

Figure VI-1: Effect of gelatin microparticle IEP and crosslinking extent on growth factor release: Average percent cumulative IGF-1 release from microparticles in PBS and in CC-PBS is shown in Figures (a) and (b), respectively, and compared to average percent cumulative TGF- β 1 release from microparticles in PBS (c) and in CC-PBS (d). Error bars represent \pm standard deviation with $n = 4$ to 6 for each formulation.



Release in Standard PBS

As shown in Figure 1a, after only 24 h, basic microparticles crosslinked with 10 mM GA demonstrated a very high burst release ($74.4 \pm 5.1\%$). The remaining IGF-1 in these microparticles appeared to diffuse over the next few days, with $90.3 \pm 1.4\%$ release by day 3 and $93.3 \pm 1.1\%$ by day 28. On the contrary, when acidic gelatin was employed

in the fabrication of gelatin microparticles, significantly lower burst release and final cumulative release values were obtained (Table 3a). In fact, the IGF-1 release profile from acidic gelatin microparticles crosslinked with 10 mM GA appeared to correlate well with the observed TGF- β 1 release profile (Figure 1c) from this same microparticle formulation. These results confirmed expectations that gelatin of an IEP below physiological pH would act as a more effective complexation agent due to the slight positive charge character associated with IGF-1 (IEP = 7.5) in PBS. It should be noted that microparticle crosslinking extent appeared to affect the extent of complexation as IGF-1 burst release from microparticles crosslinked with 10 mM GA ($22.2 \pm 8.2\%$) was statistically lower than burst release from microparticles crosslinked with 40 mM GA ($48.0 \pm 18.4\%$). Likewise, final cumulative release in PBS was statistically lower for microparticles crosslinked with 10 mM GA ($31.6 \pm 9.1\%$) rather than 40 mM GA ($67.1 \pm 18.7\%$).

Release in CC-PBS

However, in the presence of collagenase, the more tightly crosslinked structure of microparticles crosslinked with 40 mM GA appeared to slow enzymatic gelatin digestion and subsequent IGF-1 release when compared to release from less crosslinked 10 mM microparticles. As shown in Figure 1b and Table 3b, the highest IGF-1 burst ($75.5 \pm 3.1\%$) and final cumulative ($99.5 \pm 0.1\%$) release values were observed with basic microparticles, presumably due to their low crosslinking density and poor ability to complex with IGF. Statistically lower burst ($64.3 \pm 4.3\%$) and final cumulative ($95.0 \pm 0.6\%$) release values were obtained with acidic microparticles crosslinked with 10 mM GA. However, acidic gelatin microparticles crosslinked with 40 mM GA demonstrated

the lowest burst release ($49.6 \pm 7.8\%$) among all formulations since their tight network structure resists degradation by collagenase.

Trends in Phase 2 and 3 release rates further demonstrated that release and degradation kinetics may be controlled by altering the crosslinking extent of these microparticles. As shown in Table 3b, the Phase 2 release rate ($10.7 \pm 0.7\%$ per day) for acidic microparticles crosslinked with 10 mM GA was statistically higher than the corresponding rate ($6.7 \pm 0.5\%$ per day) for microparticles crosslinked with 40 mM GA. However, by the beginning of Phase 3 (day 6), release from the less crosslinked microparticles had risen to approximately 91%, and accordingly, IGF-1 release during this period fell to $0.2 \pm 0.1\%$ per day. In contrast, the more crosslinked microparticles exhibited only 66% release by day 6, and thus, demonstrated a Phase 3 release rate of almost ten fold higher ($1.6 \pm 0.2\%$ per day). Moreover, both TGF- β 1 and IGF-1 release (Figures 1b and 1d) from acidic microparticles crosslinked with 10 mM GA proceeded with very similar release kinetics in CC-PBS.

Table VI- 3: Burst release, phase 2 and 3 release rates, and final cumulative IGF-1 release from various microparticle formulations in PBS (a) and in CC-PBS (b). For each measurement, the highest and lowest values ($p < 0.05$) amongst formulations are indicated by (#) and (^), respectively.

(a) Release in PBS

Microparticle Formulation		Burst Release (%)	Phase 2 Rate (%/day)	Phase 3 Rate (%/day)	Cumulative Release (%)
IEP	GA Concentration				
9	10 mM	$74.4 \pm 5.1^{\#}$	8.0 ± 2.0	$0.1 \pm 0.0^{\wedge}$	$93.3 \pm 1.1^{\#}$
5	10 mM	$22.2 \pm 8.2^{\wedge}$	$1.4 \pm 0.3^{\wedge}$	$0.3 \pm 0.1^{\#}$	$31.6 \pm 9.1^{\wedge}$
5	40 mM	48.0 ± 18.4	6.4 ± 1.3	0.2 ± 0.1	67.1 ± 18.7

(b) Release in CC-PBS

Microparticle Formulation		Burst Release (%)	Phase 2 Rate (%/day)	Phase 3 Rate (%/day)	Cumulative Release (%)
IEP	GA Concentration				
9	10 mM	$75.5 \pm 3.1^{\#}$	8.8 ± 1.3	0.1 ± 0.0	$99.5 \pm 0.1^{\#}$
5	10 mM	64.3 ± 4.3	$10.7 \pm 0.7^{\#}$	0.2 ± 0.1	95.0 ± 0.6
5	40 mM	$49.6 \pm 7.8^{\wedge}$	$6.7 \pm 0.5^{\wedge}$	$1.6 \pm 0.2^{\#}$	95.2 ± 2.9

IGF-1 Release from Hydrogels and Composites in Vitro

Release in Standard PBS

Since acidic microparticles crosslinked with 40 mM GA provided sustained release of IGF-1 for 28 days in CC-PBS, this microparticle formulation was utilized in preparing OPF-gelatin microparticle composites. Figure 2a provides IGF-1 release profiles from two formulations of composites (H_{b40IGF^*} and $H_{b10b40IGF^*}$) in standard PBS, as well as the IGF-1 release profile from OPF hydrogels (H_{IGF^*}) with no microparticle component. By comparing Figures 1a and 2a, the dramatic reduction in burst release, obtained by encapsulating these microparticles in a network of OPF, is seen. More specifically, burst release in standard PBS was reduced from approximately 48% with non-encapsulated microparticles to approximately 14% with both formulations of composites. As shown in Table 4a, both composite formulations also exhibited burst release values statistically lower than the burst release from OPF hydrogels ($47.0 \pm 3.9\%$). Likewise, the final cumulative release from both composite formulations ($44.6 \pm 1.4\%$ for H_{b40IGF^*} and $48.3 \pm 1.7\%$ for $H_{b10b40IGF^*}$) was statistically lower than the final cumulative release from OPF hydrogels ($79.2 \pm 3.3\%$) in PBS, indicating that the use of a gelatin carrier for IGF-1 within these networks provides a means to tightly control release. It should also be noted that the final cumulative release values exhibited with composites were below the value exhibited by non-encapsulated microparticles, indicating that the OPF crosslinking procedure does not disrupt the IGF-gelatin complexation and binding.

As previously mentioned, two composite formulations were examined to assess the effect of a population of co-encapsulated, non-loaded microparticles on IGF-1 release kinetics. As shown in Figure 2a, initially the non-loaded, 10 mM microparticles appeared to have no effect on IGF-1 release from the 40 mM microparticles as no significant

differences in either the burst release values or Phase 2 release rates were observed between composite formulations in PBS (Table 4a). However, composites encapsulating microparticles crosslinked with both 10 and 40 mM GA ($H_{b10b40IGF^*}$) eventually yielded statistically higher Phase 3 release rates and cumulative release values than constructs encapsulating only the more crosslinked microparticles (H_{b40IGF^*}). As later discussed, this trend appeared to be more pronounced in release studies conducted in CC-PBS.

Table VI- 4: Burst release, phase 2 and 3 release rates, and final cumulative IGF-1 release from OPF hydrogels (H_{IGF^*}) and two formulations of OPF-gelatin microparticle composites (H_{b40IGF^*} and $H_{b10b40IGF^*}$) in PBS (a) and in CC-PBS (b). For each measurement, the highest and lowest values ($p < 0.05$) amongst formulations are indicated by (#) and (^), respectively.

(a) Release in PBS

Gel Formulation	Burst Release (%)	Phase 2 Rate (%/day)	Phase 3 Rate (%/day)	Cumulative Release (%)
H_{IGF^*}	$47.0 \pm 3.9^{\#}$	$8.0 \pm 0.9^{\#}$	0.6 ± 0.0	$79.2 \pm 3.3^{\#}$
H_{b40IGF^*}	14.2 ± 0.4	6.0 ± 0.3	0.8 ± 0.1	$44.6 \pm 1.4^{\wedge}$
$H_{b10b40IGF^*}$	13.5 ± 0.4	5.5 ± 0.2	$1.0 \pm 0.1^{\#}$	48.3 ± 1.7

(b) Release in CC-PBS

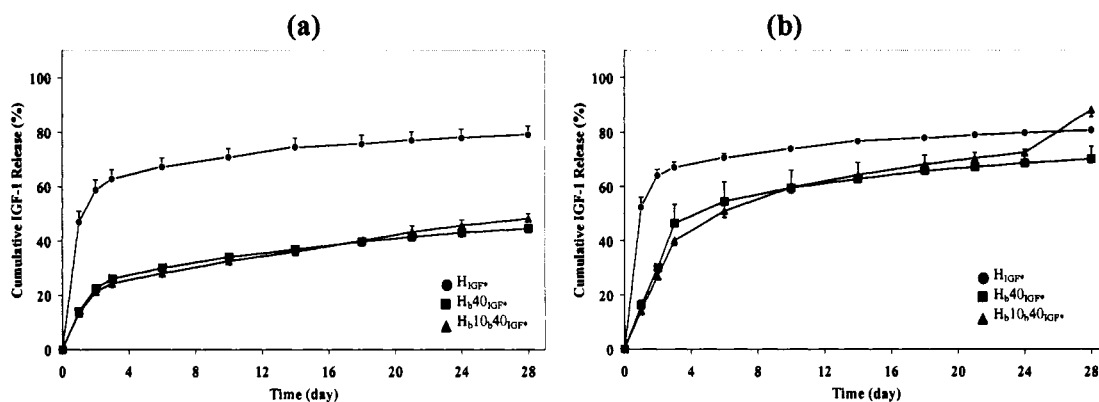
Gel Formulation	Burst Release (%)	Phase 2 Rate (%/day)	Phase 3 Rate (%/day)	Cumulative Release (%)
H_{IGF^*}	$52.5 \pm 3.7^{\#}$	$7.4 \pm 1.0^{\wedge}$	$0.5 \pm 0.1^{\wedge}$	80.9 ± 0.6
H_{b40IGF^*}	16.3 ± 1.7	15.1 ± 2.9	0.8 ± 0.2	$70.2 \pm 4.7^{\wedge}$
$H_{b10b40IGF^*}$	14.3 ± 1.6	12.9 ± 0.4	$1.3 \pm 0.1^{\#}$	$88.3 \pm 2.6^{\#}$

Release in CC-PBS

In the presence of collagenase, reduced microparticle burst release was still achieved by encapsulation in a network of OPF. Likewise, composite burst release values ($16.3 \pm 1.7\%$ for H_{b40IGF^*} and $14.3 \pm 1.6\%$ for $H_{b10b40IGF^*}$) were dramatically lower than the burst release value from hydrogels ($52.5 \pm 3.7\%$) in CC-PBS (Figure 2b). However, as encapsulated microparticles were enzymatically digested by collagenase, the rate of IGF-1 release from composites began to exceed the rate of release from hydrogels. In fact, both Phase 2 and Phase 3 composite release rates were statistically higher the

corresponding rates obtained with hydrogels. And by day 28, final cumulative release from $H_b10_b40_{IGF^*}$ composites ($88.3 \pm 2.6\%$) exceeded final cumulative release from hydrogels ($80.9 \pm 0.6\%$).

Figure VI- 2: OPF systems for IGF-1 delivery: Average percent cumulative IGF-1 release from both OPF hydrogels (H_{IGF^*}) and two formulations of OPF-gelatin microparticles composites ($H_b40_{IGF^*}$ and $H_b10_b40_{IGF^*}$) are shown in PBS (a) and in CC-PBS (b). Error bars represent \pm standard deviation with $n = 4$ to 6 for each formulation.



More interestingly, gels encapsulating a population of less crosslinked microparticles exhibited statistically higher Phase 3 and final cumulative release values than gels only encapsulating the more crosslinked (40 mM) microparticles (see Table 4b). Specifically, the final cumulative release from $H_b40_{IGF^*}$ composites ($70.2 \pm 4.7\%$) was intermediate to those values mentioned for hydrogels and $H_b10_b40_{IGF^*}$ composites. By day 28, only fragments of $H_b10_b40_{IGF^*}$ composites remained in CC-PBS, while $H_b40_{IGF^*}$ composites were in tact, yet highly swollen networks. Accordingly, the less crosslinked, non-loaded microparticles in $H_b10_b40_{IGF^*}$ constructs appear to accelerate degradation and IGF-1 release, when compared to $H_b40_{IGF^*}$ and H_{IGF^*} gels, by acting a digestible porogen which is quickly degraded by collagenase. A faster rate of enzymatic digestion of microparticles crosslinked with 10 mM GA (vs microparticles crosslinked with 40 mM GA) was also observed in studies with non-encapsulated microparticles.

Dual IGF-1 and TGF- β 1 Release from Hydrogels and Composites in Vitro

Two different formulations of three phase composites ($H_b10_{TGF40_{IGF}}$ or $H_{TGF10_b40_{IGF}}$) were utilized to simultaneously deliver IGF-1 and TGF- β 1. The method of IGF-1 delivery was kept constant between formulations to provide a means of sustained delivery of this growth factor for approximately 4 weeks. IGF-1 release profiles from both formulations are shown in Figure 3a (PBS) and Figure 3b (CC-PBS). Since TGF- β 1 plays a number of different regulatory roles in cartilage tissue, the method of TGF- β 1 delivery was altered to achieve different release profiles. TGF- β 1 release profiles from both formulations are shown in Figure 3c (PBS) and Figure 3d (CC-PBS).

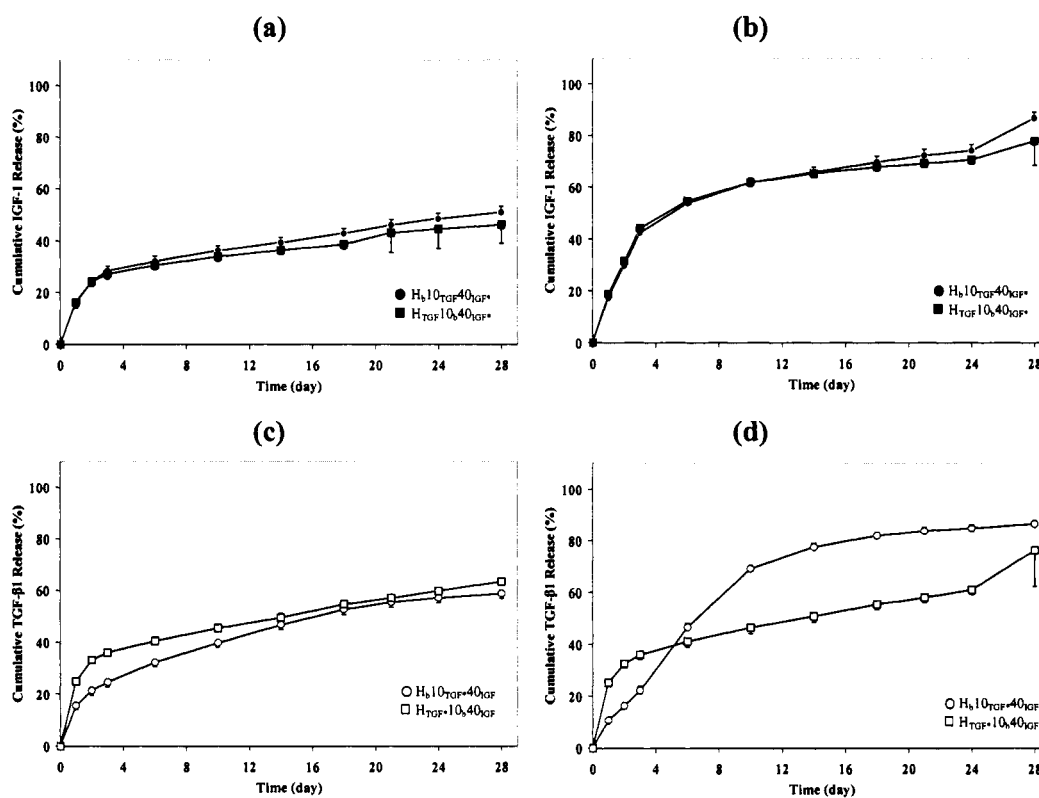
Release in Standard PBS

As shown in Figure 3a and Table 5a, IGF-1 release proceeded in an almost identical fashion from both composite formulations in standard PBS. A burst release of approximately 16% was exhibited after 24 hrs, followed by Phase 2 and 3 release rates of 5-6% per day and 1% per day, respectively. Final cumulative release from both formulations was approximately 50% in PBS. In fact, no statistical differences between composite formulations were present in any of these measured parameters.

IGF-1 burst release, Phase 2 and 3 rates, as well as final cumulative release in these dual release systems ($H_b10_{TGF40_{IGF}}$ and $H_{TGF10_b40_{IGF}}$) were also statistically compared to respective values obtained from constructs formulated with the same material composition but loaded only with IGF-1 ($H_b10_b40_{IGF}$). No statistical differences were seen among Phase 2 rates, Phase 3 rates, or final cumulative burst release values. However, the burst release ($13.5 \pm 0.4\%$) from composites only loaded with IGF-1 ($H_b10_b40_{IGF}$) was statistically lower than burst release from composites loaded with both TGF- β 1 and IGF-1 ($16.6 \pm 1.1\%$ for $H_b10_{TGF40_{IGF}}$ and $16.3 \pm 2.1\%$ for $H_{TGF10_b40_{IGF}}$),

indicating that TGF- β 1 loading in these composites may slightly accelerate initial IGF-1 release. A similar trend among IGF-1 burst release values was noted in CC-PBS and is discussed below.

Figure VI- 3: OPF systems for IGF-1 and TGF- β 1 delivery: Figures (a) and (c) respectively show simultaneous release of IGF-1 and TGF- β 1 from two formulations of OPF-gelatin microparticle composites ($H_b10_{TGF}40_{IGF}$ and $H_{TGF}10_b40_{IGF}$) in PBS. Figures (b) and (d) respectively display IGF-1 and TGF- β 1 release from these composites in CC-PBS. Error bars represent \pm standard deviation of average percent cumulative release values with $n = 4$ to 6 for each formulation.



The rate of TGF- β 1 release in standard PBS (Figure 3b) was altered by loading this growth factor within either the OPF hydrogel phase or within encapsulated 10 mM microparticles. As shown in Table 5a, when TGF- β 1 was delivered from the hydrogel phase faster overall delivery of this growth factor was achieved. In fact, burst release values, Phase 2 rates, and final cumulative TGF- β 1 release values were statistically

higher for $H_{TGF} \cdot 10_b 40_{IGF}$ composites. Since the use of a gelatin carrier for IGF-1 was shown to greatly slow release in the absence of gelatin digesting enzymes, these results were expected for TGF- β 1 and agree with previous findings (134, 146).

Table VI- 5: Burst release, phase 2 and 3 release rates, and final cumulative IGF-1 and TGF- β 1 release from dual release systems ($H_b 10_{TGF} 40_{IGF}$ and $H_{TGF} 10_b 40_{IGF}$) in PBS (a) and in CC-PBS (b). IGF-1 release values from composites are statistically compared ($p < 0.05$) and higher values indicated by (#). The same statistical evaluation is provided for TGF- β 1 release values from composites.

(a) Release in PBS

Gel Formulation	Burst Release (%)	Phase 2 Rate (%/day)	Phase 3 Rate (%/day)	Cumulative Release (%)
IGF-1 Release				
$H_b 10_{TGF} 40_{IGF}^*$	16.6 ± 1.1	5.9 ± 0.5	0.9 ± 0.0	50.9 ± 2.3
$H_{TGF} 10_b 40_{IGF}^*$	16.3 ± 2.1	5.4 ± 0.7	0.8 ± 0.3	46.1 ± 7.1
TGF- β 1 Release				
$H_b 10_{TGF} \cdot 40_{IGF}$	15.5 ± 1.4	4.5 ± 0.5	$1.6 \pm 0.1^{\#}$	58.8 ± 1.8
$H_{TGF} \cdot 10_b 40_{IGF}$	$24.8 \pm 0.5^{\#}$	$5.7 \pm 0.6^{\#}$	1.1 ± 0.0	$63.4 \pm 0.6^{\#}$

(b) Release in CC-PBS

Gel Formulation	Burst Release (%)	Phase 2 Rate (%/day)	Phase 3 Rate (%/day)	Cumulative Release (%)
IGF-1 Release				
$H_b 10_{TGF} 40_{IGF}^*$	17.4 ± 1.3	12.5 ± 0.5	$1.2 \pm 0.1^{\#}$	86.6 ± 2.2
$H_{TGF} 10_b 40_{IGF}^*$	18.8 ± 2.2	12.7 ± 0.5	0.9 ± 0.0	77.9 ± 9.4
TGF- β 1 Release				
$H_b 10_{TGF} \cdot 40_{IGF}$	10.8 ± 0.7	5.7 ± 0.7	$2.3 \pm 0.1^{\#}$	86.6 ± 1.2
$H_{TGF} \cdot 10_b 40_{IGF}$	$25.2 \pm 1.5^{\#}$	5.4 ± 0.5	1.1 ± 0.1	76.3 ± 14.1

Release in CC-PBS

Since these delivery systems will ultimately be used *in vivo* in the presence of tissue collagenase and other matrix metalloproteinases, release studies in CC-PBS may more accurately model expected release trends. Under these conditions, very similar IGF-1 release profiles (Figure 3b) were again observed when comparing composite formulations. However, release values were higher than observed in standard PBS. Initial burst release values from both formulations were approximately 18%, with subsequent

Phase 2 release rates of approximately 13% per day (Table 5b). However, Phase 3 rates were found to be statistically different between formulations ($1.2 \pm 0.1\%$ per day for $H_b10_{TGF40_{IGF^*}}$ and $0.9 \pm 0.0\%$ per day for $H_{TGF10_b40_{IGF^*}}$). Final cumulative release from $H_b10_{TGF40_{IGF^*}}$ composites ($86.6 \pm 2.2\%$) was higher, though not statistically, than cumulative release from $H_{TGF10_b40_{IGF^*}}$ constructs ($77.9 \pm 9.4\%$). Accordingly, these results may suggest that free TGF- β 1 in the OPF hydrogel phase of composites may migrate and help to eventually stabilize the IGF-gelatin interactions.

Statistical comparison of IGF-1 release profiles from composites loaded only with IGF-1 ($H_b10_b40_{IGF^*}$) with dually loaded composites provides further evidence that TGF- β 1 may interact with IGF-1 to slightly alter release kinetics. More specifically, IGF-1 burst release values from composites loaded with both IGF-1 and TGF- β 1 ($17.4 \pm 1.3\%$ for $H_b10_{TGF40_{IGF^*}}$ and $18.8 \pm 2.2\%$ for $H_{TGF10_b40_{IGF^*}}$) were statistically higher than the burst release from composites loaded with only IGF-1 ($14.3 \pm 1.6\%$). This trend was also seen in standard PBS. Thus, initially, free TGF- β 1 (TGF- β 1 in the OPF hydrogel phase or TGF- β 1 which is not tightly complexed to gelatin) may accelerate IGF-1 release. However, in the later stages of release experiments (Phases 3 and 4), IGF-1 release from $H_{TGF10_b40_{IGF^*}}$ composites was seen to be slower than release from either $H_b10_{TGF40_{IGF^*}}$ or $H_b10_b40_{IGF^*}$ composites. For instance, final cumulative IGF-1 release from $H_{TGF10_b40_{IGF^*}}$ composites ($77.9 \pm 9.4\%$) was statistically lower than release from $H_b10_{TGF40_{IGF^*}}$ ($86.6 \pm 2.2\%$) or $H_b10_b40_{IGF^*}$ ($88.3 \pm 2.6\%$) composites. This later trend may indicate the free TGF- β 1 in the OPF hydrogel phase ultimately migrates to the gelatin phase to stabilize IGF-1-gelatin interactions. In $H_b10_{TGF40_{IGF^*}}$ constructs, tightly

complexed TGF- β 1 may be unable to dissociate from its gelatin carrier and serve the same role.

TGF- β 1 release profiles from these dual release systems are shown in Figure 3d. Initially, significantly higher burst release was observed when TGF- β 1 was loaded into the hydrogel phase of composites. As shown in Table 5b, release after 24 hrs was $25.2 \pm 1.5\%$ from $H_{TGF*10b40IGF}$ composites but only $10.8 \pm 0.7\%$ from $H_b10_{TGF*40IGF}$ composites. However by the beginning of Phase 3 (day 6), enzymatic digestion of gelatin allowed TGF- β 1 release from $H_b10_{TGF*40IGF}$ composites to exceed release from $H_{TGF*10b40IGF}$ composites. In fact, the Phase 3 TGF- β 1 release rate for composites with TGF- β 1 loading in the microparticle phase ($2.3 \pm 0.1\%$ per day) was statistically greater than the rate for composites with TGF- β 1 loading in the hydrogel phase ($1.1 \pm 0.1\%$ per day). Final cumulative TGF- β 1 release from $H_b10_{TGF*40IGF}$ composites rose to approximately 87%, while the corresponding value in $H_{TGF*10b40IGF}$ composites was only 76%. Accordingly, these results indicate that TGF- β 1 release rates in the presence of collagenase may be systematically adjusted by altering the material phase of TGF- β 1 loading.

Discussion

Since IGF-1 has been shown to function primarily as a progression factor, stimulating the synthesis of collagen and proteoglycans in cartilage tissue, a series of *in vitro* release experiments were conducted to determine an effective means of providing sustained IGF-1 release over the course of several weeks. Because gelatin has been shown to form an effective ionic complexation with a number of growth factors, allowing for controlled drug delivery (124), gelatin microparticles were explored as a possible

IGF-1 carrier. Initial release experiments were assessed the effect of gelatin microparticle IEP and crosslinking extent on IGF-1 release. Since gelatin is primarily degraded by enzymatic digestion, growth factors which effectively complex or bind to these microparticles will generally display release profiles with two prominent features in standard, enzyme-free PBS (134). First, any non-complexed or poorly bound growth will be released during the first 24 hrs as these microparticles reach equilibrium swelling. However, unlike diffusion controlled release systems, relatively little subsequent release will be observed due to the growth factor-gelatin complexation.

As shown in Figure 1a and Table 3a, IGF-1 did not appear to effectively complex with basic gelatin microparticles (IEP of 9.0). However, acidic gelatin microparticles crosslinked with 10 mM GA retained approximately 68% of their loaded IGF-1 over the course of 28 days in standard PBS. Similar retention values were observed when this microparticle formulation was loaded with TGF- β 1, a growth factor which has been shown to form an effective ionic complexation with acidic gelatin (124), indicating that acidic gelatin was a promising IGF-1 carrier. However, lower retention of IGF-1 in PBS was observed with acidic microparticles crosslinked with 40 mM GA. Since TGF- β 1 retention in gelatin microparticles in standard PBS is not affected by their crosslinking extent (134, 146), these results may suggest that the lysine and hydroxylysine amino acid residues in gelatin, which react with the aldehyde groups of GA, are also utilized in IGF-gelatin binding. Alternatively, the more tightly crosslinked network of these gelatin microparticles may prevent efficient diffusional loading of IGF-1. Yet, since decreased growth factor retention in these highly crosslinked microparticles is not observed with TGF- β 1, a protein with a substantially higher molecular weight (25 kDa) than IGF-1 (7.5

kDa), it is unlikely that this behavior is due to diffusional limitations during IGF-1 loading.

However, since gelatin is enzymatically degraded, release studies in CC-PBS more accurately model expected *in vivo* release profiles. As shown in Figure 1b, both basic and acidic microparticles crosslinked with 10 mM GA were rapidly digested by collagenase, releasing 90% of their IGF-1 as early as day 6. Only the more crosslinked (40 mM) acidic microparticles provided a means of sustained IGF-1 delivery over the course of 28 days in CC-PBS. Accordingly, this microparticle formulation was utilized in subsequent studies aimed at optimizing IGF-1 delivery.

More specifically, further experiments examined IGF-1 release when these microparticles were encapsulated in a network of OPF. The encapsulation procedure provides a means of maintaining microparticles within a defect site to localize growth factor delivery. Additionally, as shown in Figure 2, encapsulated IGF-1-loaded microparticles exhibited much lower burst release values than both non-encapsulated microparticles and OPF hydrogels (with no microparticle component) in PBS and CC-PBS, allowing for sustained IGF-1 release over the course of 4 weeks.

While release profiles from the two composite formulations were very similar, the final extent of IGF-1 release from these systems in CC-PBS was shown to be dependent on microparticle crosslinking. $H_b10_b40_{IGF^*}$ composites, which encapsulated both IGF-1-loaded 40 mM microparticles and non-loaded 10 mM microparticles, exhibited statistically higher release ($88.3 \pm 2.6\%$) than $H_b40_{IGF^*}$ composites ($70.2 \pm 4.7\%$), which encapsulated only IGF-1-loaded 40 mM microparticles. Accordingly, the non-loaded, less crosslinked microparticles appear to speed release by acting as a porogen which is readily

digested in the presence of collagenase. Furthermore, since higher final release from $H_{b10b40IGF^*}$ composites was also observed in standard PBS, these results indicate that non-loaded microparticles do not act as a significant reservoir for IGF-1. Accordingly, by adjusting the amount and crosslinking extent of encapsulated microparticles, release kinetics may be systematically tailored.

A final set of release experiments examined dual delivery of IGF-1 and TGF- β 1 from three phase composites. IGF-1 was again loaded into the 40 mM microparticle phase to allow for sustained release. However, TGF- β 1 loading was varied between the 10 mM microparticle phase ($H_{b10TGF40IGF}$) and the OPF hydrogel phase ($H_{TGF10b40IGF}$). As expected, very similar IGF-1 release profiles were observed with both composite formulations since IGF-1 was delivered from the same phase in each formulation. As discussed above, statistical comparison of IGF-1 release values from $H_{b10TGF40IGF^*}$ and $H_{TGF10b40IGF^*}$ composites with values from composites loaded only with IGF-1 ($H_{b10b40IGF^*}$) indicated that the presence of co-loaded TGF- β 1 slightly alters IGF-1 release. In particular, as shown in Figure 3b, when TGF- β 1 was loaded into the OPF hydrogel phase, lower final IGF-1 release was observed, indicating that free TGF- β 1 may eventually diffuse to sites of IGF-1-gelatin interactions and help to stabilize this complex. While further experiments are needed to explore this phenomenon, these release systems proved successful in providing sustained release of IGF-1 with very similar release profiles. As designed, these dual release systems exhibited less than 90% final cumulative IGF-1 release in CC-PBS over a 4 week period.

As shown in Figure 3d, altering the phase of TGF- β 1 loading proved to be a successful means of altering TGF- β 1 release kinetics. Significantly lower burst release

($10.8 \pm 0.7\%$) was observed when this growth factor was released from the 10mM microparticle phase, rather than the hydrogel phase ($25.2 \pm 1.5\%$). Gradual release of TGF- β 1 from H_b10_{TGF}*40_{IGF} composites then continued as encapsulated microparticles were digested by collagenase. However, TGF- β 1 release from H_{TGF}*10_b40_{IGF} proceeded in a diffusion-controlled manner, defined a high burst release with a steady subsequent release rate. Final cumulative release values for both systems were not statistically different at day 28. Accordingly, since the total amount of TGF- β 1 released from these systems over a 4 week period was approximately equal, yet delivered via unique release profiles, implementation of these two systems *in vivo* would allow a means of assessing how TGF- β 1 release kinetics affect tissue repair.

Conclusions

This research details the development of a non-invasive means of simultaneously delivering both IGF-1 and TGF- β 1 to damaged articular cartilage through the use of an injectable, biodegradable scaffold comprised of the polymer OPF and gelatin microparticles. More specifically, a series of release studies assessed the effects of gelatin IEP and crosslinking extent on IGF-1 release from gelatin microparticles and demonstrated that highly crosslinked, acidic microparticles (IEP = 5.0) serve as an effective carrier of IGF-1, providing sustained delivery of this progression factor over the course of 4 weeks. Furthermore, encapsulation of these IGF-1-loaded microparticles in a network of the biodegradable polymer OPF, provided a means to further control and localize release. Using these OPF-gelatin microparticle composites, dual release of TGF- β 1 and IGF-1 was achieved with growth factor loading in either the microparticle phase or OPF phase of gels. Parameters such as microparticle crosslinking extent and density

within these gel networks, as well as the phase of growth factor loading, provided an effective means of controlling the release profiles of these growth factors. Accordingly, this ability provides a powerful tool by which researchers can now assess the release kinetics of one or more growth factors on tissue repair.

VII. DEGRADABLE HYDROGEL SCAFFOLDS FOR *IN VIVO* EVALUATION OF GROWTH FACTOR INTERACTIONS IN CARTILAGE REPAIR

Abstract

As our population ages, treatment for joint pain associated with articular cartilage damage is becoming a prevalent challenge. Accordingly, this work investigates local delivery of two regulatory proteins - transforming growth factor- β 1 (TGF- β 1) and insulin-like growth factor-1 (IGF-1) – to cartilage defects from degradable scaffolds as a potential strategy for improving cartilage repair. The effects of TGF- β 1 and/or IGF-1 delivery on osteochondral repair in adult rabbits were examined through histomorphometric analysis of 11 markers of osteochondral repair. Complete scaffold degradation occurred allowing for assessment of the healing response at 12 weeks post-surgery. When compared to untreated defects, higher scores were observed with IGF-1-treated defects for the 6 markers of neo-surface repair: neo-surface morphology, cartilage thickness, surface regularity, chondrocyte clustering, and the chondrocyte and glycoasminoglycan content of the neo-surface and the cartilage surrounding the defect. Surprisingly, the benefits of IGF-1 delivery were not maintained when this growth factor (GF) was co-delivered with TGF- β 1, despite numerous *in vitro* reports of the combinatory actions of these growth factors. While localized delivery of IGF-1 may be a promising repair strategy, further *in vivo* assessment is necessary, since fibrous tissue was commonly observed in the neo-surface of all treatment groups. More importantly, this study highlights the need to rigorously examine GF interactions in the wound healing environment and demonstrates that *in vitro* observations do not directly translate to the *in vivo* setting.

Abbreviations

CC-PBS, collagenase-containing PBS; ECM, extracellular matrix; IGF-1, insulin-like growth factor-1; GAGs, glycoasminoglycans; GF, growth factor; mesenchymal stem cells, MSCs; MPs, microparticles; OPF, oligo(poly(ethylene glycol) fumarate); PBS, phosphate buffered saline; TGF- β 1, transforming growth factor- β 1.

Introduction

The prevalence of joint pain among adults is projected to steadily increase throughout the next 25 years. In fact, by 2030, an estimated 65 million adult Americans will be diagnosed with arthritis (160). Accordingly, clinicians, biologists, and biomedical engineers are working to develop new cartilage repair strategies by investigating how various bioactive factors participate in the regulation of healthy articular cartilage (115, 161). Numerous signaling molecules have been isolated from articular cartilage (115). However, research efforts to understand how multiple factors interact have primarily been limited to *in vitro* studies (61, 80, 159, 162-167). Given the inherent difficulties associated with maintaining *in vitro* cultured chondrocytes in their differentiated state (168), *in vivo* methods for studying GF interactions in the wound healing environment are necessary.

While a few carriers have been developed for dual GF delivery to calcified and vascular tissues (169-171), cartilage research has yet to employ synthetic carriers for controlled dual drug delivery *in vivo*. Fibrin clots have been utilized for GF localization in chondral defects (114), but in order to investigate how the kinetics of release affect healing, synthetic carriers which allow for precise tailoring of drug release rates and material properties are desired. Towards this goal, our laboratory has developed a novel class of hydrogels to deliver multiple GFs (145, 172). These systems are based on oligo(poly(ethylene glycol) fumarate) (OPF), a water soluble polymer that crosslinked to

form biodegradable and biocompatible hydrogels (172). Gelatin microparticles (MPs), incorporated into these gels at the time of crosslinking, have been shown to act as enzymatically digestible porogens to speed *in vitro* scaffold degradation (146). Sustained GF delivery has been achieved by first loading MPs with the desired GF(s) and then encapsulating these MPs within the OPF network (134, 145, 146). Alternatively, GFs can be entrapped within the OPF phase of composites for accelerated release (145).

Co-encapsulation of bovine chondrocytes with GF-loaded MPs in these gels has demonstrated the stimulatory action of incorporated TGF- β 1. In particular, OPF scaffolds co-encapsulating TGF- β 1-loaded MPs and bovine chondrocytes were seen to have statistically higher cellularity than constructs co-encapsulating chondrocytes and blank MPs after 21 and 28 days of *in vitro* culture (173). Most recently, OPF scaffolds were seen to undergo biocompatible degradation and support healthy tissue in-growth in osteochondral defects in 4-month-old, New Zealand White rabbits (172).

The present work employs these OPF scaffolds to investigate the potential roles of TGF- β 1 and IGF-1 in osteochondral repair in adult rabbits, since these growth factors are among those most widely investigated for articular cartilage repair (115, 161). In particular, TGF- β 1, a 25 kDa protein, has been shown to promote the chondrogenic differentiation of progenitor cells (10, 28, 29) and to enhance chondrocyte proliferation (36, 37, 173). IGF-1, a 7.5 kDa protein, appears to primarily act in an anabolic fashion to increase proteoglycan and type II collagen synthesis (33, 38, 52, 53, 159). Accordingly, scaffolds were designed to provide fast, initial release of TGF- β 1 as a chemotractant and morphogen (10, 28, 60) and/or sustained release of IGF-1 as a stimulator of ECM synthesis (52, 53, 65, 98). GF loadings were based on concentrations shown to be

therapeutic in the treatment of full and partial thickness rabbit and porcine defects (105, 114).

To investigate the role of TGF- β 1 and IGF-1 in cartilage repair, three different formulations of bilayered OPF hydrogels were fabricated and implanted in rabbit osteochondral defects to spatially localize GF delivery to the approximate region where cartilage is found in a healthy joint. The first two scaffold formulations (Table 1) were loaded with either TGF- β 1 or IGF-1 to separately examine the effects of these factors on cartilage repair. A third group of scaffolds was loaded with both TGF- β 1 and IGF-1 to examine the combinatory role of these molecules. After 12 weeks, tissue repair in untreated defects and in defects treated by scaffold implantation was examined by histomorphometric analysis. Additionally, to estimate growth factor release from these scaffolds, a 28-day *in vitro* release study was conducted.

Table VII- 1: In vivo study design

Scaffold Type	Protein Loading (ng/ g gel)		Repetitions/ Treatment
	TGF- β 1	IGF-1	
TGF- β 1	200	0	11
IGF-1	0	200	10
Dual (TGF- β 1&IGF-1)	200	200	11
No scaffold	-----	-----	11

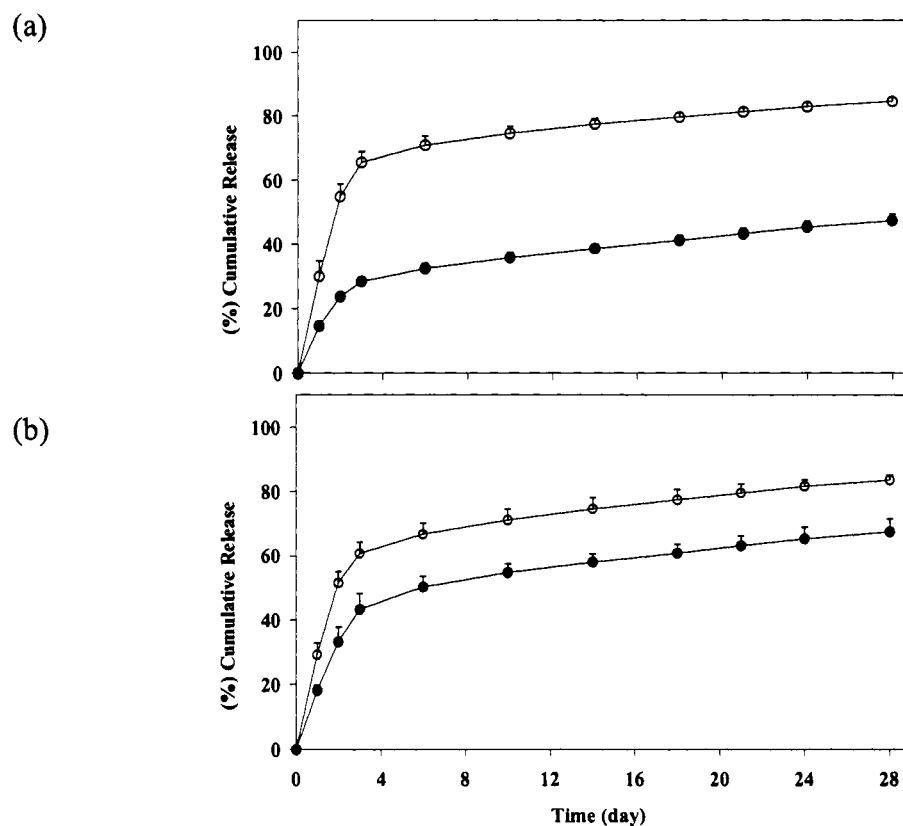
Results

In Vitro Growth Factor Release

TGF- β 1 and IGF-1 release experiments estimated protein release kinetics from OPF scaffolds (Figure 1) in standard phosphate buffered saline (PBS) and in collagenase-containing PBS (CC-PBS). The later buffer was utilized since gelatin MPs degrade primarily by enzymatic hydrolysis (146). High TGF- β 1 burst release occurred within the first 3 days ($65.5 \pm 3.3\%$ in PBS and $60.8 \pm 3.4\%$ in CC-PBS) as expected for proteins

released from the OPF phase of scaffolds. More specifically, GFs are released by diffusion as OPF scaffolds swell, and burst release is greatly influenced by hydrogel mesh size (134, 145). Lower burst release was expected for IGF-1 since gelatin MPs were utilized as an intermediate carrier, making drug release dependent on enzymatic degradation of the gelatin network and diffusion through the scaffold (145, 146). Indeed, IGF-1 burst release was only $28.4 \pm 1.4\%$ in PBS and $43.3 \pm 4.9\%$ in CC-PBS, statistically lower than the corresponding values for TGF- β 1 release. Likewise, 28-day cumulative IGF-1 release in PBS ($47.3 \pm 2.0\%$) and in CC-PBS ($67.4 \pm 4.0\%$) was significantly lower than the corresponding TGF- β 1 release values ($84.6 \pm 1.1\%$ in PBS and $83.6 \pm 1.5\%$ in CC-PBS).

Figure VII- 1: *In vitro* IGF-1 (●) and TGF- β 1 (○) release from OPF scaffolds in PBS (a) and in CC-PBS (b). Data is shown as average cumulative release with error bars representing \pm standard deviation (n = 6).



Animal Health & Macroscopic Joint Appearance at Recovery

Animals regained full movement within approximately one week with normal behavior and movement observed throughout the 12-week period. It should be noted that 5 specimens were removed from the study due to complications common to adult rabbits but unrelated to the surgeries (obstructed digestive tract and pre-existing bacterial skin infection). Accordingly, each treatment group included 10 to 11 specimens. With these joints, no signs of inflammation, infection, or swelling were noticed upon visible inspection of the joint surfaces at 12 weeks.

Histological Appearance

Three histological sections per defect were observed by light microscopy, allowing for assessment of the healing response at the defect edges and center (See Materials & Methods). The subchondral regions of untreated defects contained a majority of osseous tissue. However, in 8 of 11 defects, cartilaginous tissue regions occupied up to 30% of the subchondral region. These regions were generally covered by a fibrous surface and primarily existed at the subchondral/chondral interface. However, in some cases, this un-remodeled tissue penetrated as far as 2 mm from the joint surface. The neo-surface of untreated defects was mainly composed of fibrous tissue and often extended into the joint space (Figure 2). In general, the neo-surface of control specimens was highly disrupted by fissures.

In all sections of specimens treated with OPF scaffolds, no remaining hydrogel material or MPs were observed and degradation appeared to be complete at 12 weeks (Figures 3-6). The subchondral regions of these defects were generally filled with a majority of trabecular bone. However, like untreated defects, regions of hypertrophic

cartilage were also visible at the subchondral/chondral interface in some specimens within each treatment group. The frequency of these hyaline subchondral regions (# defects per treatment) was 45%, 27%, and 18% in TGF- β 1-, TGF- β 1&IGF-1-, and IGF-1-treated defects, respectively. Figure 3 shows the most striking example of cartilaginous tissue remaining in the subchondral region. However, it should be noted that in all other defects, these regions were confined to less than 30% of the subchondral zone. In fact, complete subchondral restoration with trabecular bone and complete integration with the surrounding osseous tissue was frequently observed (Figure 6).

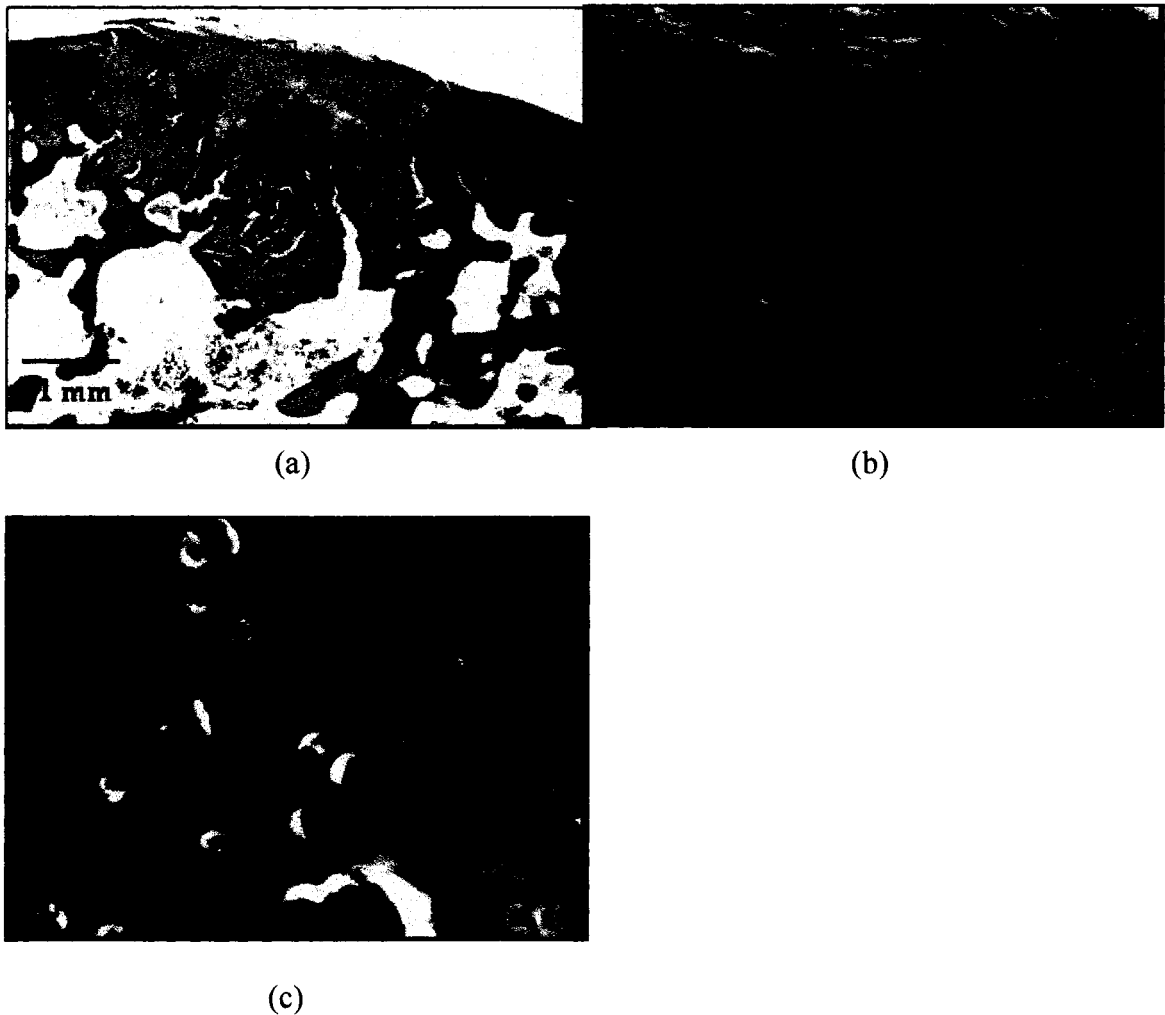
The neo-formed surface morphology of defects treated with scaffolds was primarily composed of fibrous tissue of variable thickness, but fibrocartilage was observed in several specimens within each group. Likewise, regions of cartilage-like cells were often visible near the defect margins (Figure 4), but true articular cartilage repair with a zonal organization of cells was only observed once in an IGF-1-treated defect. Very thin fibrous tissue was sometimes observed with all experiment treatments and tended to accompany complete or near complete subchondral restoration, as exemplified by Figures 4 and 6. In other specimens, thick surface tissue with fissures was observed, especially when subchondral remodeling was incomplete (Figure 5).

Histomorphometric Analysis

Quantitative scoring of 11 markers of osteochondral repair (Table 2) (172) examined the potential effects of GF delivery and location within the defect (edge vs. center). Section location within the former defect did not significantly impact any of the 11 markers of osteochondral repair, indicating that the observed tissue response was generally uniform throughout the defect. However, it should be noted that regions of un-

remodeled subchondral tissue were often located towards the middle of the subchondral zone on lateral, medial, and center sections. New bone and chondrocytes appeared to infiltrate the subchondral and chondral regions from the defect margins.

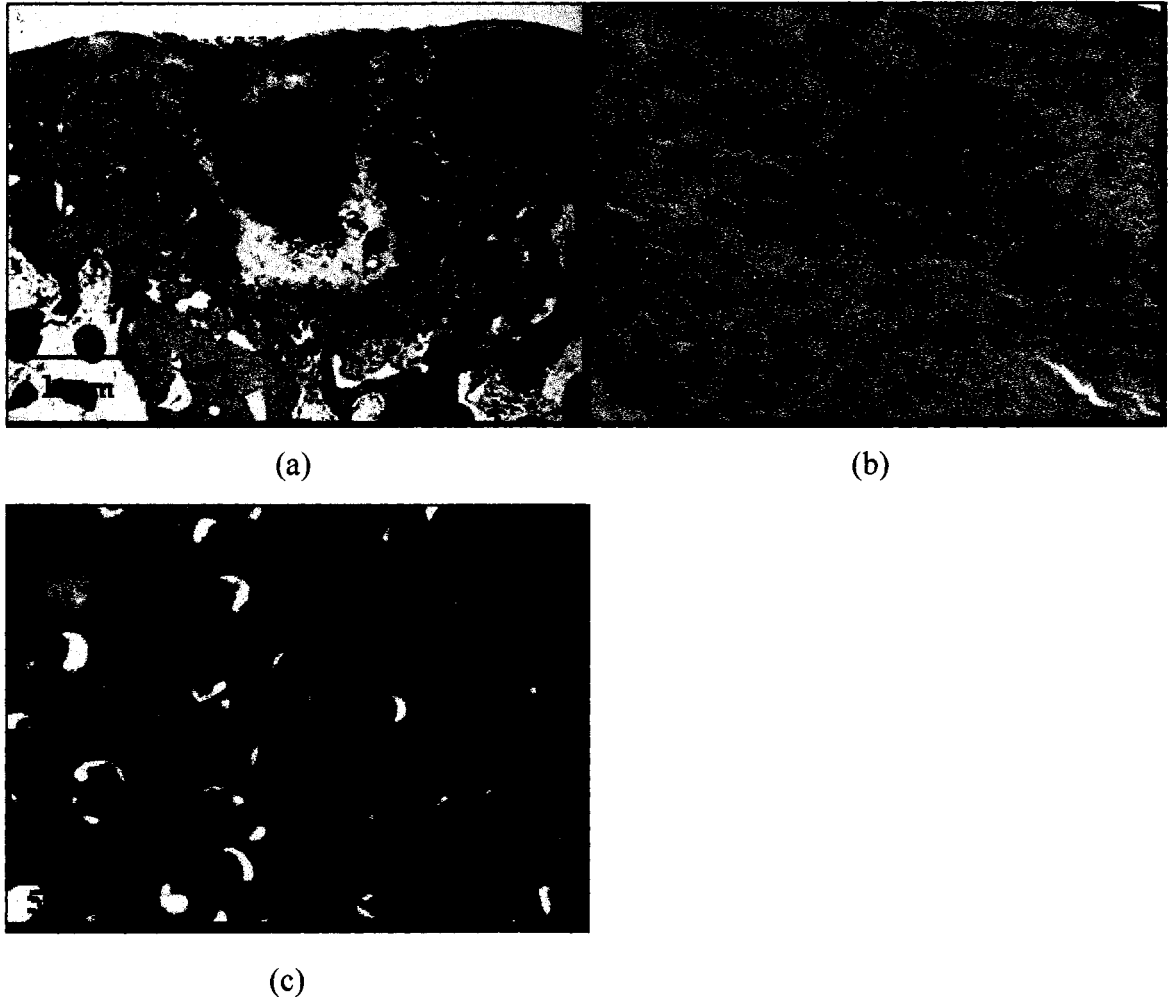
Figure VII- 2: Histological section displaying the thick fibrous tissue commonly observed at the neo-surface and that often accompanied un-remodeled cartilaginous regions in the subchondral zone. The boxed regions in (a) (2X magnification) are shown at 20X magnification to illustrate the cell morphology observed in portions of the chondral (b) and subchondral (c) regions. This defect was untreated.



No significant differences in overall tissue filling and implant degradation were observed among the four treatment groups (Figure 3a). All sections received maximal scores for scaffold degradation, and scores for overall tissue filling approached but did

not equal the maximal score. This difference was due to the very thin neo-surface tissue often observed amongst specimens from all treatment groups.

Figure VII- 3: Histological section displaying the most striking example of cartilaginous tissue remaining in the subchondral defect area. The boxed regions in (a) (2X magnification) are shown at 20X magnification to illustrate the fibrous tissue and hypertrophic cartilage observed in portions of the chondral (b) and subchondral (c) regions, respectively. This defect was treated by IGF-1 delivery.



Likewise, average scores for bone filling and bone morphology were below their maximal scores (Figure 3b) since un-remodeled regions were observed in all treatment groups. However, the high average scores for bone integration reflect the complete integration commonly observed with all treatments. Although the frequency of inadequate bone filling was highest amongst untreated defects, scaffold implantation was

not observed to significantly influence subchondral bone repair. However, improved bone healing with scaffold implantation was not expected since growth delivery was confined to the upper portion of osteochondral defects, and repeated research has demonstrated that scaffolds alone often serve as insufficient templates to guide tissue regeneration (174-179). Since the goal of this study was to examine the GF interactions in cartilage repair, GFs were not delivered to the subchondral bone.

Figure VII- 4: Histological section displaying fibrocartilage in-growth near the chondral defect margins and significant subchondral restoration. The boxed regions in (a) (2X magnification) are shown at 20X magnification to illustrate the spherical shape of cartilage cells in the neo-surface (b) and small regions of remodeling tissue in subchondral region (c). This defect was treated by IGF-1 delivery.

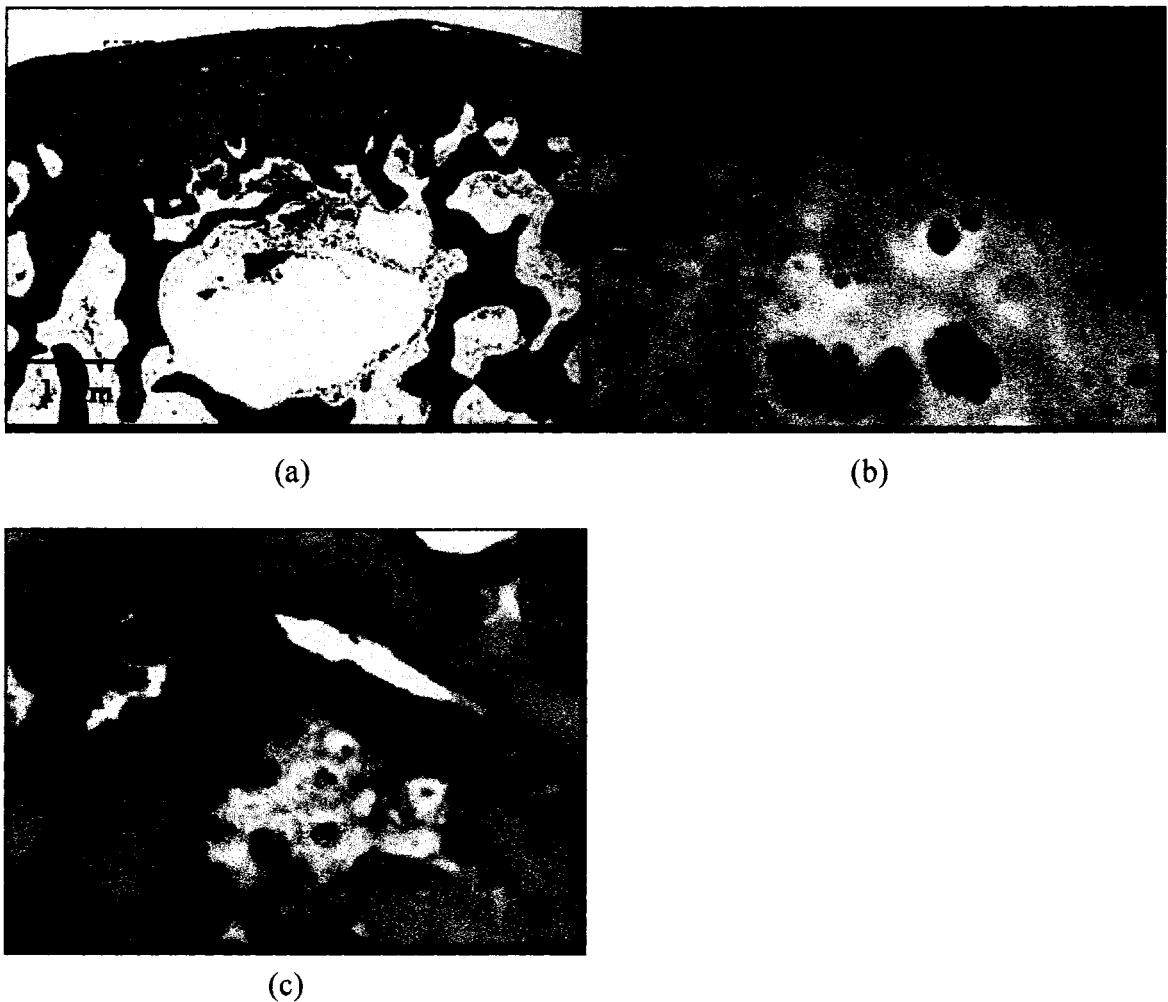
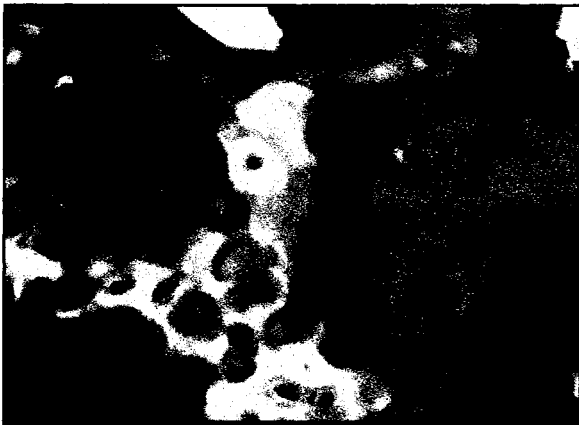


Figure VII- 5: Histological section displaying excessive fibrous tissue growth into the joint space and significant subchondral restoration. The boxed regions in (a) (2X magnification) are shown at 20X magnification to illustrate the spindle-like cells in the neo-surface (b) and small regions of remodeling tissue in subchondral region (c). This defect was treated by TGF- β 1 delivery.



(a)

(b)



(c)

As shown in Figure 7c, the neo-surface of defects treated by IGF-1 delivery had significantly higher scores for 5 indicators of neo-surface repair when compared to untreated defects and defects treated by TGF- β 1 delivery. These results suggest the potential of IGF-1 delivery strategies in chondral repair. However, since a large variation in tissue quality was observed within this treatment group, these findings should be interpreted cautiously. True articular cartilage with a zonal arrangement of chondrocytes was only observed in one IGF-1 treated defect, leading to higher average scores and

standard deviations for this treatment group. As reflected by the average scores in Figure 7c, fibrous tissue was generally observed in the neo-surface of all treatments. Only 30-40% of IGF-1, TGF- β 1, and TGF- β 1&IGF-1-treated defects, and 20% of untreated defects, had sufficient “cartilage-like” cells to meet the criterion for classification as non-fibrous (Table 2c).

Table VII- 2: Histological scoring system for the overall defect (a), subchondral region (b), and chondral region (c)

(a) Overall tissue filling

<i>Overall defect evaluation (throughout the entire defect depth)</i>	Score
1. Percent filling with neo-formed tissue	
100%	3
>50%	2
<50%	1
0%	0
2. Percent degradation of the implant	
100%	3
>50%	2
<50%	1
0%	0

(b) Subchondral region

<i>Subchondral bone evaluation</i>	Score
3. Percent filling with neo-formed tissue	
100%	3
>50%	2
<50%	1
0%	0
4. Subchondral bone morphology	
Normal, trabecular bone	4
Trabecular, with some compact bone	3
Compact bone	2
Compact bone and fibrous tissue	1
Only fibrous tissue or no tissue	0
5. Extent of neo-tissue bonding with adjacent bone	
Complete on both edges	3
Complete on one edges	2
Partial on both edges	1
Without continuity on either edge	0

(b) Chondral region

<i>Cartilage evaluation</i>	<i>Score</i>
6. Morphology of neo-formed surface tissue	
Exclusively articular cartilage	4
Mainly hyaline cartilage	3
Fibrocartilage (spherical morphology observed with $\geq 75\%$ of cells)	2
Only fibrous tissue (spherical morphology observed with $< 75\%$ of cells)	1
No tissue	0
7. Thickness of neo-formed cartilage	
Similar to the surrounding cartilage	3
Greater than surrounding cartilage	2
Less than the surrounding cartilage	1
No cartilage	0
8. Joint surface regularity	
Smooth, intact surface	3
Surface fissures ($< 25\%$ neo-surface thickness)	2
Deep fissures (25-99% neo-surface thickness)	1
Complete disruption of the neo-surface	0
9. Chondrocyte clustering	
None at all	3
$< 25\%$ chondrocytes	2
25-100% chondrocytes	1
No chondrocytes present (no cartilage)	0
10. Chondrocyte and glycoasminoglycan (GAG) content of neo-formed cartilage	
Normal cellularity with normal Safranin O staining	3
Normal cellularity with moderate Safranin O staining	2
Clearly less cells with poor Safranin O staining	1
Few cells with no or little Safranin O staining or no cartilage	0
11. Chondrocyte and glycoasminoglycan (GAG) content of adjacent cartilage	
Normal cellularity with normal GAG content	3
Normal cellularity with moderate GAG content	2
Clearly less cells with poor GAG content	1
Few cells with no or little GAGs or no cartilage	0

One of the most interesting findings of this study centered upon the apparent lack of TGF- β 1 and IGF-1 synergy when simultaneously delivered to osteochondral defects. Compared to untreated defects, treatment with both GFs only improved scores for only two parameters: the regularity of the neo-surface and the chondrocyte/GAG content of the adjacent surface. However, all experimental treatments were observed to have significantly higher scores for the adjacent cartilage's chondrocyte/GAG content when

compared to untreated defects. This finding suggests that scaffold implantation reduces degenerative changes to the surrounding cartilage.

Figure VII- 6: Histological section displaying thin fibrous tissue growth along the surface of a joint with complete subchondral restoration. The boxed regions in (a) (2X magnification) are shown at 20X magnification to illustrate the morphology of the fibrous neo-surface (b) and the mature bone in the subchondral region (c). This defect was treated by TGF- β 1&IGF-1 delivery.



(a)

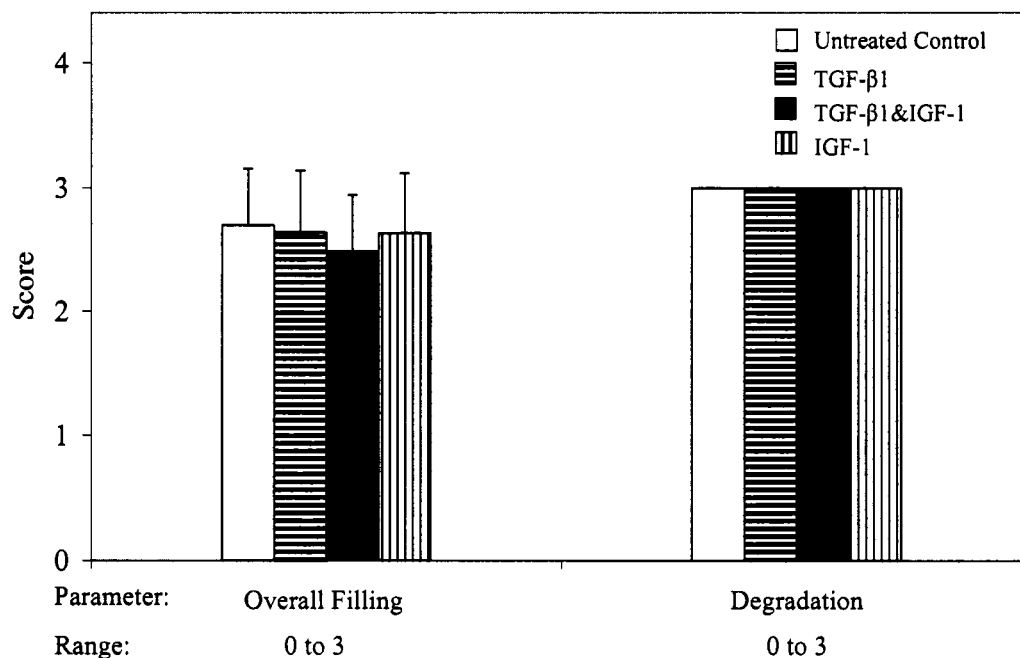
(b)



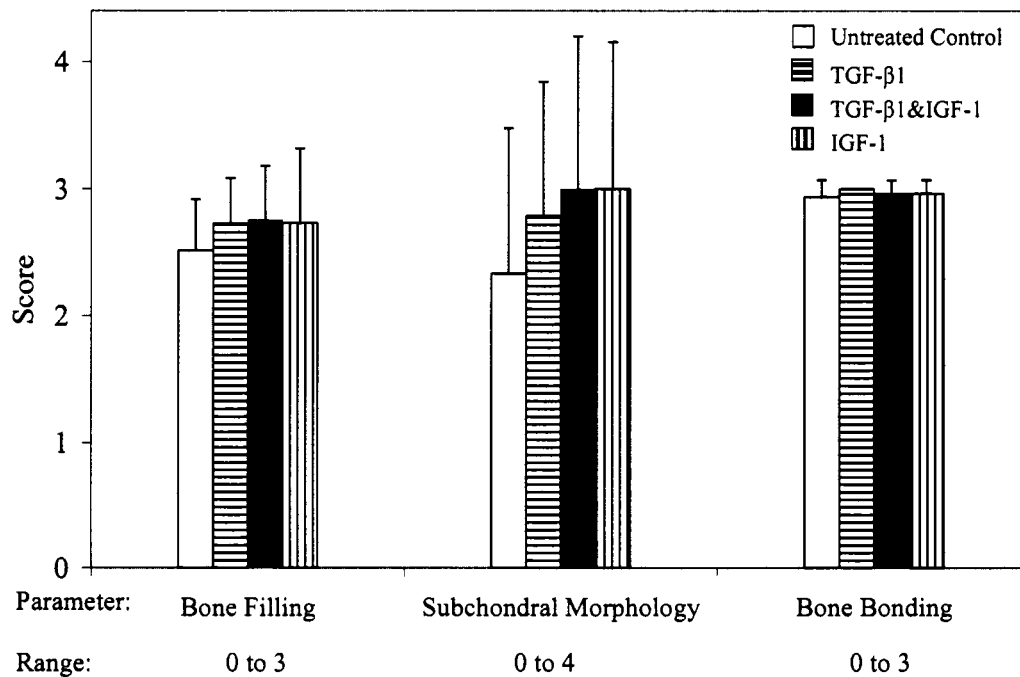
(c)

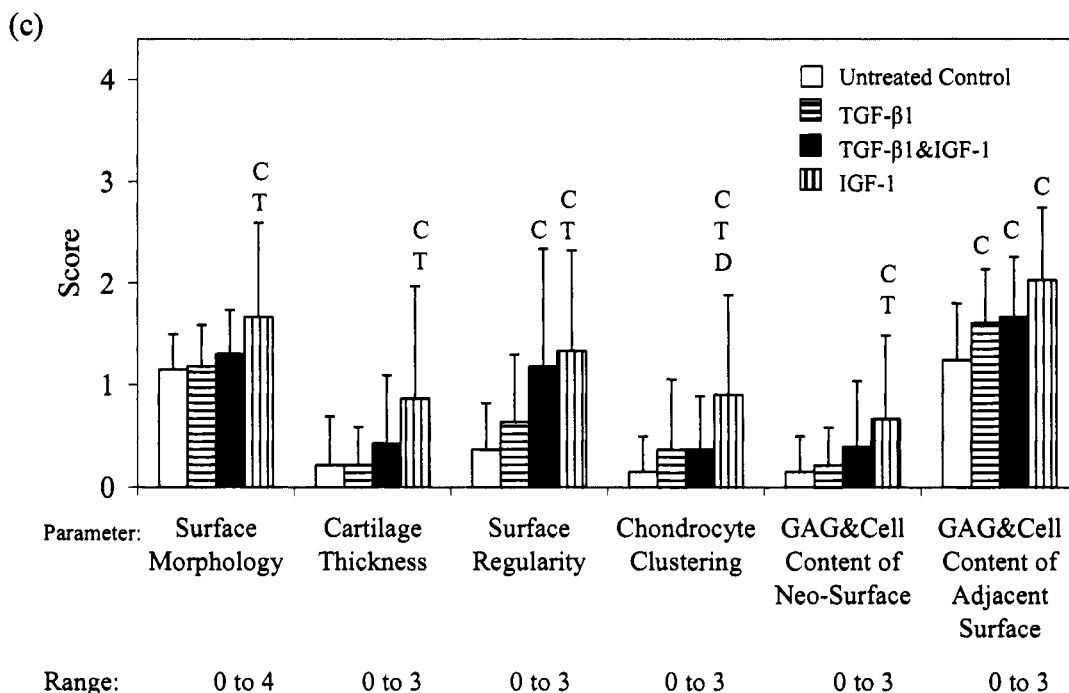
Figure VII- 7: Comparison of results following histomorphometric analysis of the overall defect (a), subchondral region (b), and chondral region (c). Data is shown as average scores with error bars representing \pm standard deviation (n = 10 to 11 defects per treatment). Scores with significant differences ($p < 0.05$) compared to untreated defects (control), defects treated by TGF- β 1-loaded scaffolds, or defects treated by dual TGF- β 1&IGF-1-loaded scaffolds are respectively indicated by C, T, and D.

(a)



(b)





Discussion

Numerous scaffolds have been investigated for cartilage drug delivery (115), but as of yet, these scaffolds have not been employed to examine the *in vivo* effects of multiple GFs. OPF scaffolds have numerous material parameters which can be manipulated to achieve desired drug release rates (134, 145, 146) and to study delivery of multiple GFs. Here, we examine *in vivo* delivery of two proteins, TGF- β 1 and IGF-1, whose single and combined effects have been the focus of numerous *in vitro* investigations.

TGF- β 1 has been shown to promote *in vitro* chondrogenic differentiation of mesenchymal stem cells (MSCs) and chondrocyte proliferation, (10, 27-29, 31, 173). However, stimulation of GAG synthesis and mRNA expression for type II collagen, important markers of the chondrogenic phenotype, frequently do not accompany TGF- β 1-stimulated proliferation (61, 80, 173). However, several studies have demonstrated that together TGF- β 1 and IGF-1 can synergistically promote proliferation, GAG

synthesis, and collagen II expression *in vitro* (61, 163, 165, 166). These results are not surprising since IGF-1 was initially identified for its ability to promote GAG incorporation into proteoglycans and has been shown to regulate cartilage matrix synthesis (33, 52, 98). Due to these reports, scaffolds for *in vivo* analysis of possible TGF- β 1/IGF-1 synergy were designed to provide fast, initial release of TGF- β 1 (Figure 1) as a morphogen in the earlier stages of healing (10, 28) and sustained release of IGF-1 as a progression factor (52, 53, 65, 98).

Surprisingly, when these scaffolds were used in the repair of osteochondral defects in adult rabbits, combinatory delivery of TGF- β 1 and IGF-1 did not result in widespread improvement to the quality of the neo-surface when compared to untreated defects. Dual delivery of TGF- β 1 and IGF-1 only appeared to improve neo-surface regularity (vs. untreated defects), indicating that findings of *in vitro* TGF- β 1 and IGF-1 synergy do not directly correlate with *in vivo* observations. These inconsistencies may be due to the complex *in vivo* environment and the numerous cell types involved in the healing response.

For example, previous studies have demonstrated TGF- β 1's pluripotent stimulation of chemotaxis and proliferation of inflammatory cells, fibroblasts, chondrocytes, and other cells (20, 21, 60, 105). And although TGF- β 1 is known to promote chondrogenesis (115, 161), high dosages of exogenous TGF- β 1 (42, 180-182), have frequently been associated with *in vivo* formation of osseous or chondroid outgrowths in joints. Lower doses of TGF- β 1 (200-600 ng/ml) have been reported to be therapeutic, but these studies have been almost exclusively limited to chondral defects (60, 114). In the present study, numerous instances of excessive tissue growth at the neo-

surface were observed in defects treated by TGF- β 1 and TGF- β 1&IGF-1 delivery, as well as in untreated defects. Accordingly, IGF-1 may be a more promising candidate than TGF- β 1 for delivery strategies, especially since this GF appears to act primarily as a progression factor (98).

Here, individual delivery of IGF-1 resulted in consistently higher scores than untreated defects and defects treated with only TGF- β 1 (Figure 3c). However, given the large variation in healing responses in IGF-1-treated defects, these results do not conclusively confirm the therapeutic ability of this GF. Instead, these results and the apparent lack of TGF- β 1&IGF-1 synergy demonstrate the necessity for *in vivo* studies to more accurately examine the role of GFs in healing.

Additionally, the present study's thorough histological analysis led to several other interesting observations. Our findings of hyaline cartilaginous regions in the subchondral zone agree with previous reports (183) and the suggestion that the post-injury response involves a rapid influx of mesenchymal cells into the defect area and the fabrication of embryonic-like cartilage tissue throughout the defect (Figure 3) and sometimes into the joint space (183, 184). As shown in Figure 2, this cartilage appears to become hypertrophic in the subchondral zone as vascularization initiates bone formation at the defect margins and progressively inward. These observations support previous suggestions that vascularization controls the rate at which the cartilaginous tissue disappears (184). However, the cartilage repair tissue near the chondral surface, initially isolated from vascularization, appears to undergo a simultaneous, but separate remodeling as illustrated by the fibrous tissue along the neo-surface in Figures 2, 3 and 5. Since spherical chondrocyte-like cells and GAG staining were primarily observed near

the chondral defect margins (Figure 4), cells near the joint surface appear to play a major role in this process (60, 114).

Understanding the role of GF interactions in chondrogenesis will undoubtedly prove beneficial, since very thin surface tissue commonly accompanied complete subchondral restoration in this study (Figure 6) and in other investigations (185) (183). GF delivery via scaffolds remains a logical strategy for articular cartilage repair, but this study highlights the need for the caution when interpreting the implications of *in vitro* studies. As evident by this research, the *in vitro* effects of GFs, including the synergistic actions of multiple factors, may not always translate to the wound healing environment. Thus, thorough *in vivo* analysis of GF interactions in tissue repair is necessary. The flexible design properties of OPF hydrogels allow these scaffolds to be used as powerful tools to explore the effectiveness of various GF delivery regimes in the cartilage wound healing environment and in other many other tissue defects. Accordingly, these systems will help scientists to unravel the vital interactions and signaling cascades of these complex molecules in tissue repair.

Materials and Methods

Gelatin Microparticle Fabrication and Loading

Gelatin MPs (50-100 μm) were fabricated from acidic gelatin (Nitta Gelatin Inc., Osaka, Japan), crosslinked in 40 mM glutaraldehyde (Sigma, St. Louis, MO), and then sterilized by exposure to ethylene oxide gas using established methods (134, 172). Sterile MPs were then loaded with IGF-1 (R&D Systems, Minneapolis, MN) by swelling in an aqueous solution of IGF-1 (1.19 μg IGF-1/ml PBS) to achieve an overall GF loading of approximately 200 ng IGF-1/ml in the top crosslinked, layer of scaffolds (145). Blank MPs were loaded with PBS.

OPF Synthesis

High molecular weight poly(ethylene glycol) PEG) (Polysciences, Warrington, PA) with a number average molecular weight (M_n) of $25,400 \pm 500$ and weight average molecular weight (M_w) of $41,900 \pm 300$, was utilized to synthesize OPF ($M_n = 32,500 \pm 1400$, $M_w = 74,900 \pm 10,000$) according to established methods (134). The molecular weights of the parent PEG and resulting OPF were determined by gel permeation chromatography ($n=3$) (146). OPF was sterilized by exposure to UV light for 3 h following an established technique (172).

Scaffold Fabrication

All implanted scaffolds consisted of 2 layers: a top, cartilage forming layer and a bottom, bone forming layer with respective thicknesses of 1 and 2 mm. These dimensions were chosen as a means of restricting drug loading to the upper portion of defects, rather than as a model of exact anatomy. No GFs or MPs were added to the bone forming layer of any scaffold formulation. This basic scaffold design was modeled after a design previously shown to undergo degradation in a timeframe sufficient to support osteochondral tissue repair (172).

Approximately 4 hrs prior to implantation, scaffolds were fabricated using a 2 step crosslinking procedure (172). To form the bottom layer, 0.15 g OPF was dissolved in 395 μ l of PBS containing 14 mg N,N'-methylene bisacrylamide (Sigma, St. Louis, MO) as a crosslinking agent. Then, 118 μ l PBS, 51 μ l of 0.3 M tetramethylethylenediamine (in PBS) (Sigma, St. Louis, MO) and 51 μ l of 0.3 M ammonium persulfate (in PBS) (Sigma, St. Louis, MO) were added to initiate crosslinking. After vortexing, the suspension was injected into a cylindrical Teflon mold to a height of 2 mm and incubated at 37°C for 5 min to achieve partial crosslinking, enabling lamination to a second layer (134, 172).

During this time, the polymer solution for the top scaffold layer was prepared as outline above, except that 32 mg IGF-1-loaded or PBS-loaded MPs were added to the polymer solution. For scaffolds loaded with TGF- β 1, the PBS addition contained 1.65 ng TGF- β 1/ μ l (R&D Systems, Minneapolis, MN). The final mixture was injected into the mold to form the upper scaffold layer and incubated at 37°C for 10 min for complete scaffold crosslinking.

All PBS, initiator, and bisacrylamide solutions were sterilized prior to use by filtration according to an established procedure (172). Furthermore, the cytocompatibility of this initiating system has been demonstrated by cellular successful encapsulation of bovine chondrocytes (173) in OPF hydrogels during crosslinking. The final dimensions of all scaffolds matched the dimensions of osteochondral defects in the rabbit model (3 mm in diameter x 3 mm in depth) (151) with the top, scaffold layer containing 200 ng of the indicated GF(s) per g crosslinked gel (Table 1).

Quantification of In Vitro Growth Factor Release

To approximate the expected *in vivo* release profiles of TGF- β 1 and IGF-1, dual release of these GFs from OPF-gelatin microparticle composites was assessed *in vitro* in standard PBS or PBS containing 370 ng bacterial collagenase 1A (Sigma, St. Louis, MO) per ml. Since gelatin is degraded primarily by enzymatic hydrolysis, this collagenase concentration was chosen to model tissue collagenase concentrations in the synovial fluid of patients with osteoarthritis (136). Single layer scaffolds (3 mm in diameter and 1 mm in thickness) were crosslinked according to the method described above with the exception that one of the two GF solutions contained a trace amount of I¹²⁵ labeled-GF (Perkin Elmer Life Sciences, Boston, MA) to allow for detection of drug release. Thus,

two sets of scaffolds were fabricated to separately detect TGF- β 1 and IGF-1 release from scaffolds. Previously, GF release profiles from these scaffolds have been shown to be controlled by scaffold composition, rather than protein interactions (145). Accordingly, the individual release of TGF- β 1 and IGF-1 from scaffolds incorporating only one of these GFs was not assessed.

After crosslinking, scaffolds (n=6) were placed in 3 ml of the indicated buffer and were agitated on a shaker table (70 rpm) at 37°C. The supernatant of each specimen was collected and replaced by fresh buffer following an established schedule (145, 146). GF release was determined by correlation of measured radioactivity (Cobra II Autogamma, Packard, Meridian, CT) to a standard curve.

Animal Surgery

Twenty-four, 6-month old New Zealand White rabbits were utilized in this study. Adult rabbits were utilized since the capacity for articular cartilage repair decreases with age (186). All surgical procedures were based on an established bilateral, rabbit, osteochondral defect model (151, 172) and were approved by the Animal Care and Use Committees of Radboud University Nijmegen and Rice University. Prior to surgery, anesthesia was induced by an intravenous injection of Hypnorm® (0.32 mg/ml fentanyl citrate and 10 mg/ml fluanisone) and atropine. General anesthesia was then maintained by a mixture of nitrous oxide, isoflurane, and oxygen administered through a ventilator. To minimize peri-operative infection risk and post-operative discomfort, antibiotic prophylaxis (Baytril 2.5%, Enrofloxacin, 5-10 mg/kg) and Fynadyne® was preoperatively administered.

Following anesthesia, rabbits were immobilized on their back. Both legs were then shaved and disinfected with povidine-iodine. The left knee was then exposed through a medial parapatellar longitudinal incision. After lateral luxation of the patella, the medial femoral condyle was exposed. With the knee maximally flexed, a full-thickness defect (3 mm in diameter x 3 mm in depth) was created in the center of the condyle using a dental drill (KAVO, Intrasept 905, KAVO Nederland BV, Vianen, The Netherlands). A 2 mm drill bit was first used to establish a 2 mm diameter defect and then gradually enlarged using drill bits with diameters of 2.8 and 3.0 mm. All bits were fashioned with a 3 mm stop to ensure a defect depth of precisely 3 mm. Debris was removed from the defect with a curette and the edge carefully cleaned with a scalpel blade.

For rabbits belonging to one of the three experimental treatment groups, an appropriate scaffold was then placed into the defect, while untreated defects remained empty. Subsequently, the patella was repositioned, and the capsule and muscle closed with a continuous 4-0 Vicryl suture. Finally, the skin was closed with single intracutaneous 4-0 Vicryl sutures. This same procedure was repeated for the right knee but with this knee receiving a different treatment from that of the left knee. Thus, each treatment group utilized twelve rabbits (n=12). To minimize post-operative discomfort, Fynadyne® was administered for two days postoperatively. The animals were then housed in conventional rabbit cages, which allowed for unrestricted weight-bearing activity and were observed for signs of pain, infection, and proper activity.

Tissue Processing

At 12 weeks post-surgery, rabbits were euthanized by intravenous administration of Nembutal (pentobarbital). The tissue surrounding the medial femoral condyle was retrieved en bloc, fixed in 10% buffered formalin (pH 7.4) for 1 week, decalcified in 5% formic acid for 14 days, dehydrated through graded ethanols, and embedded in paraffin. Using a microtome (Leica RM 2265, Leica Microsystems, Bannockburn, IL), longitudinal sections of 6 μm in thickness were taken from the defects' center and lateral and medial edges and then stained with Safranin O to identify the glycoasminoglycans of articular cartilage with shades of red and light green as a counter stain.

Histomorphometric Analysis

Histological sections (n=3) were blindly and independently scored by two evaluators (TH and VJ) using a previously established graded system (172). This histological scoring method was based on the original O'Driscoll system (153) and examines the extent of neo-tissue in-growth and implant degradation, as well as detailed evaluations of the subchondral and chondral regions (Table 2). It should be noted that the scale for thickness of the neo-formed cartilage was modified from its original form (172). Previously, neo-cartilage thickness was scored from 0 to 3, with scores of 3 and 2 respectively indicating cartilage of "increased thickness" or "similar thickness" to normal articular cartilage. However, for the present study, this scale was revised so that maximum scores represent the desired healing response for all parameters. Additionally, the criterion for classifying chondral tissue morphology was further specified to clearly distinguish between fibrocartilage and fibrous tissue. In particular, a neo-surface was designated as "fibrous" if less than 75% of its cell population was observed to have a spherical, chondrocyte-like morphology (Table 2).

Statistical analysis

A significance level of 0.05 was utilized for all statistical analysis. The F test was used for the comparisons of *in vitro* TGF- β 1 and IGF-1 release values. Following previous methods, ordered logistic regression of histological scores was performed using SAS Version 8.2 statistical software (SAS, Cary, NC, USA) to analyze the potential single factor affects of treatment group and location within the defect (edge vs. center sections) (157, 172). Figures display average values \pm standard deviation of the measured variable.

VIII. SUMMARY

The engineering goals of this research centered upon the development and characterization of hydrogel systems for controlled growth factor delivery and the utilization of these systems in examining the potential effects of growth factors in articular cartilage repair. Initial studies demonstrated that oligo(poly(ethylene glycol) fumarate) (OPF) hydrogels could be successfully fabricated for the controlled release of transforming growth factor- β 1 (TGF- β 1). Hydrogel mesh size was seen to affect the material properties of these gels as well as the release kinetics of TGF- β 1. Additional investigations demonstrated that TGF- β 1 release rates could be further controlled by releasing this protein from gelatin microparticles encapsulated in OPF hydrogels.

Since gelatin degrades primarily by enzymatic digestion, further *in vitro* studies characterized these release systems in the presence of collagenase to more accurately model the cartilage wound healing environment. These investigations revealed that microparticle crosslinking extent and loading within the OPF network influence material degradation and TGF- β 1 release under these conditions. Specifically, microparticles appeared to act as digestible porogens to speed the rate of scaffold degradation.

Next, bilayered OPF hydrogel scaffolds were successfully fabricated to spatially control protein loading to the cartilage region of osteochondral defects in 4 month old rabbits. These scaffolds were seen to undergo biocompatible degradation and support healthy tissue growth in young rabbits. Histomorphometric analysis confirmed that tissue quality in both the chondral and subchondral regions of defects improved between 4 and 14 weeks post-surgery. However, TGF- β 1 delivery did not appear to greatly influence cartilage repair.

Accordingly, further investigations examined these hydrogel systems as carriers of TGF- β 1 and/or insulin-like growth factor (IGF-1) since these growth factors have been shown to synergistically promote chondrocyte proliferation and cartilage extracellular matrix synthesis *in vitro*. Highly crosslinked microparticles were seen to function as an effective carrier of IGF-1, enabling sustained delivery of this progression factor over the course of 4 weeks. Furthermore, the phase of growth factor loading was observed to provide an effective means of controlling the release profiles of these growth factors.

Scaffolds were successfully fabricated for a large initial release of TGF- β 1 from the hydrogel phase and/or sustained release of IGF-1 from the microparticle phase. When implanted into osteochondral defects in 6 month old rabbits, complete scaffold degradation was observed at 12 weeks post-surgery. Histomorphometric analysis revealed that growth factor delivery had no effect on subchondral repair. Individual delivery of IGF-1 delivery appeared to improve neo-surface repair, although articular cartilage was rarely observed. Surprisingly, the apparent benefits of IGF-1 delivery were not maintained when this growth factor was co-delivered with TGF- β 1. Thus, these results highlight the necessity of investigations to study the effectiveness of growth factor delivery regimes *in situ* since *in vitro* findings do not always correlate to the wound healing environment.

The hydrogel delivery systems developed through this work will undoubtedly prove useful in further examining the role of IGF-1 and TGF- β 1 in chondrogenesis. As demonstrated through these investigations, the design flexibility and biocompatibility afforded by these and other tissue engineering scaffolds will aid in providing greater understanding of tissue repair and improving clinical treatments.

IX. LITERATURE CITED

1. Gillogly, S. D., Voight, M. & Blackburn, T. (1998) *J Orthop Sports Phys Ther* **28**, 241-51.
2. Hunziker, E. B. (1999) *Osteoarthritis Cartilage* **7**, 15-28.
3. LeBaron, R. G. & Athanasiou, K. A. (2000) *Biomaterials* **21**, 2575-87.
4. Stockwell, R. A. (1979) *Biology of Cartilage Cells* (Cambridge University Press, New York).
5. Rosier, R. N. & O'Keefe, R. J. (1998) *AAOS Instructional Course Lectures* **47**, 469-475.
6. Anfield, M. (1983) *The Chondrocyte - the Living Element of Articular Cartilage* (Hans Huber Publishers, Bern).
7. Silver, F. H. & Glasgold, A. I. (1995) *Otolaryngol Clin North Am* **28**, 847-64.
8. Wirth, C. J. & Rudert, M. (1996) *Arthroscopy* **12**, 300-8.
9. Demoor-Fossard, M., Galera, P., Santra, M., Iozzo, R. V., Pujol, J. P. & Redini, F. (2001) *J Biol Chem* **276**, 36983-92.
10. Seyedin, S. M., Rosen, D. M. & Segarini, P. R. (1988) *Pathol Immunopathol Res* **7**, 38-42.
11. Xie, D., Hui, F. & Homandberg, G. A. (1993) *Arch Biochem Biophys* **307**, 110-8.
12. Nguyen, Q., Murphy, G., Hughes, C. E., Mort, J. S. & Roughley, P. J. (1993) *Biochem J* **295** (Pt 2), 595-8.
13. Clark, I. M. & Murphy, G. (1999) in *Dynamics of Bone and Cartilage Metabolism*, eds. Seibel, M. J., Robins, S. P. & Bilezikian, J. P. (Academic Press, New York), pp. 137-150.
14. Martel-Pelletier, J., McCollum, R., Fujimoto, N., Obata, K., Cloutier, J. M. & Pelletier, J. P. (1994) *Lab Invest* **70**, 807-815.
15. Pimentel, E. (1994) *Handbook of Growth Factors: General Basic Aspects, Vol. 1* (CRC Press, Boca Raton, FL).
16. Nimni, M. E. (1997) *Biomaterials* **18**, 1201-25.
17. Martin, J. A. & Buckwalter, J. A. (2000) *Biorheology* **37**, 129-40.
18. Hauselmann, H. J. (1997) *Curr Opin Rheumatol* **9**, 241-50.

19. Pimentel, E. (1994) *Handbook of Growth Factors: Peptide Growth Factors, Vol. 2* (CRC Press, Boca Raton, FL).
20. Sporn, M. B., Roberts, A. B., Wakefield, L. M. & Assoian, R. K. (1986) *Science* **233**, 532-4.
21. Border, W. A. & Noble, N. A. (1994) *N Engl J Med* **331**, 1286-92.
22. Olofsson, A., Miyazono, K., Kanzaki, T., Colosetti, P., Engstrom, U. & Heldin, C. H. (1992) *J Biol Chem* **267**, 19482-8.
23. Seyedin, S. M., Segarini, P. R., Rosen, D. M., Thompson, A. Y., Bentz, H. & Graycar, J. (1987) *J Biol Chem* **262**, 1946-9.
24. Seyedin, S. M., Thompson, A. Y., Bentz, H., Rosen, D. M., McPherson, J. M., Conti, A., Siegel, N. R., Galluppi, G. R. & Piez, K. A. (1986) *J Biol Chem* **261**, 5693-5.
25. Flaumenhaft, R., Abe, M., Sato, Y., Miyazono, K., Harpel, J., Heldin, C. H. & Rifkin, D. B. (1993) *J Cell Biol* **120**, 995-1002.
26. Pedrozo, H. A., Schwartz, Z., Gomez, R., Ornoy, A., Xin-Sheng, W., Dallas, S. L., Bonewald, L. F., Dean, D. D. & Boyan, B. D. (1998) *J Cell Physiol* **177**, 343-54.
27. Ringe, J., Kaps, C., Schmitt, B., Buscher, K., Bartel, J., Smolian, H., Schultz, O., Burmester, G. R., Haupl, T. & Sittinger, M. (2002) *Cell Tissue Research* **307**, 321-327.
28. Iwasaki, M., Nakata, K., Nakahara, H., Nakase, T., Kimura, T., Kimata, K., Caplan, A. I. & Ono, K. (1993) *Endocrinology* **132**, 1603-8.
29. Majumdar, M. K., Banks, V., Peluso, D. P. & Morris, E. A. (2000) *J Cell Physiol* **185**, 98-106.
30. Joyce, M. E., Roberts, A. B., Sporn, M. B. & Bolander, M. E. (1990) *J Cell Biol* **110**, 2195-207.
31. Cassiede, P., Dennis, J. E., Ma, F. & Caplan, A. I. (1996) *J Bone Miner Res* **11**, 1264-73.
32. Morales, T. I. (1991) *Arch Biochem Biophys* **286**, 99-106.
33. Morales, T. I. (1997) *Arch Biochem Biophys* **343**, 164-72.
34. Venn, G., Lauder, R. M., Hardingham, T. E. & Muir, H. (1990) *Biochem Soc Trans* **18**, 973-4.
35. van Beuningen, H. M., van der Kraan, P. M., Arntz, O. J. & van den Berg, W. B. (1994) *Lab Invest* **71**, 279-90.

36. Rosier, R. N., O'Keefe, R. J., Crabb, I. D. & Puzas, J. E. (1989) *Connect Tissue Res* **20**, 295-301.
37. Vivien, D., Galera, P., Lebrun, E., Loyau, G. & Pujol, J. P. (1990) *J Cell Physiol* **143**, 534-45.
38. Xu, C., Oyajobi, B. O., Frazer, A., Kozaci, L. D., Russell, R. G. & Hollander, A. P. (1996) *Endocrinology* **137**, 3557-65.
39. Hui, W., Rowan, A. D. & Cawston, T. (2000) *Cytokine* **12**, 765-9.
40. Lum, Z. P., Hakala, B. E., Mort, J. S. & Recklies, A. D. (1996) *J Cell Physiol* **166**, 351-9.
41. Hulth, A., Johnell, O., Miyazono, K., Lindberg, L., Heinegard, D. & Heldin, C. H. (1996) *J Orthop Res* **14**, 547-53.
42. van Beuningen, H. M., Glansbeek, H. L., van der Kraan, P. M. & van den Berg, W. B. (1998) *Osteoarthritis Cartilage* **6**, 306-17.
43. Uchino, M., Izumi, T., Tominaga, T., Wakita, R., Minehara, H., Sekiguchi, M. & Itoman, M. (2000) *Clin Orthop*, 119-25.
44. Crabb, I. D., O'Keefe, R. J., Puzas, J. E. & Rosier, R. N. (1990) *J Bone Miner Res* **5**, 1105-12.
45. Inoue, H., Kato, Y., Iwamoto, M., Hiraki, Y., Sakuda, M. & Suzuki, F. (1989) *J Cell Physiol* **138**, 329-37.
46. Elford, P. R. & Lamberts, S. W. (1990) *Endocrinology* **127**, 1635-9.
47. Luyten, F. P., Chen, P., Paralkar, V. & Reddi, A. H. (1994) *Exp Cell Res* **210**, 224-9.
48. Kaps, C., Bramlage, C., Smolian, H., Haisch, A., Ungethum, U., Burmester, G. R., Sittering, M., Gross, G. & Haupl, T. (2002) *Arthritis Rheum* **46**, 149-62.
49. Sekiya, I., Colter, D. C. & Prockop, D. J. (2001) *Biochem Biophys Res Commun* **284**, 411-8.
50. Loredó, G. A., MacDonald, M. H. & Benton, H. P. (1996) *Am J Vet Res* **57**, 554-9.
51. Glansbeek, H. L., van Beuningen, H. M., Vitters, E. L., Morris, E. A., van der Kraan, P. M. & van den Berg, W. B. (1997) *Arthritis Rheum* **40**, 1020-8.
52. Luyten, F. P., Hascall, V. C., Nissley, S. P., Morales, T. I. & Reddi, A. H. (1988) *Arch Biochem Biophys* **267**, 416-25.

53. Gooch, K. J., Blunk, T., Courter, D. L., Sieminski, A. L., Bursac, P. M., Vunjak-Novakovic, G. & Freed, L. E. (2001) *Biochem Biophys Res Commun* **286**, 909-15.
54. Fukumoto, T., Sanyal, A., Fitzsimmons, J. & O'Driscoll, S. (2000) *Transactions of the Orthopaedic Research Society* **25**, 1056.
55. Hunziker, E. B., Wagner, J. & Zapf, J. (1994) *J Clin Invest* **93**, 1078-1086.
56. O'Keefe, R. J., Crabb, I. D., Puzas, J. E. & Rosier, R. N. (1994) *J Orthop Res* **12**, 299-310.
57. Loeser, R. F. (2000) *Biorheology* **37**, 109-16.
58. Martin, J. A. & Buckwalter, J. A. (1998) *J Orthop Res* **16**, 752-7.
59. Conover, C. A., Clarkson, J. T. & Bale, L. K. (1996) *Endocrinology* **137**, 2286-92.
60. Hunziker, E. B. & Rosenberg, L. C. (1996) *J Bone Joint Surg Am* **78**, 721-33.
61. Elisseeff, J., McIntosh, W., Fu, K., Blunk, B. T. & Langer, R. (2001) *J Orthop Res* **19**, 1098-104.
62. Cuevas, P., Burgos, J. & Baird, A. (1988) *Biochem Biophys Res Commun* **156**, 611-8.
63. Shida, J., Jingushi, S., Izumi, T., Iwaki, A. & Sugioka, Y. (1996) *J Orthop Res* **14**, 265-72.
64. Fosang, A. J., Tyler, J. A. & Hardingham, T. E. (1991) *Matrix* **11**, 17-24.
65. Hui, W., Rowan, A. D. & Cawston, T. (2001) *Cytokine* **16**, 31-5.
66. Guerne, P. A., Carson, D. A. & Lotz, M. (1990) *J Immunol* **144**, 499-505.
67. Shingu, M., Miyauchi, S., Nagai, Y., Yasutake, C. & Horie, K. (1995) *Br J Rheumatol* **34**, 101-6.
68. Tamura, T., Nakanishi, T., Kimura, Y., Hattori, T., Sasaki, K., Norimatsu, H., Takahashi, K. & Takigawa, M. (1996) *Endocrinology* **137**, 3729-37.
69. Gerber, H. P., Vu, T. H., Ryan, A. M., Kowalski, J., Werb, Z. & Ferrara, N. (1999) *Nat Med* **5**, 623-8.
70. Pfander, D., Kortje, D., Zimmermann, R., Weseloh, G., Kirsch, T., Gesslein, M., Cramer, T. & Swoboda, B. (2001) *Ann Rheum Dis* **60**, 1070-3.
71. Borden, P., Solymar, D., Sucharczuk, A., Lindman, B., Cannon, P. & Heller, R. A. (1996) *J Biol Chem* **271**, 23577-81.

72. Vincent, T., Hermansson, M., Bolton, M., Wait, R. & Saklatvala, J. (2002) *Proc Natl Acad Sci USA* **99**, 8259-64.
73. Olee, T., Hashimoto, S., Quach, J. & Lotz, M. (1999) *J Immunol* **162**, 1096-100.
74. Cai, L., Yin, J. P., Starovasnik, M. A., Hogue, D. A., Hillan, K. J., Mort, J. S. & Filvaroff, E. H. (2001) *Cytokine* **16**, 10-21.
75. Sasaki, K., Hattori, T., Fujisawa, T., Takahashi, K., Inoue, H. & Takigawa, M. (1998) *J Biochem (Tokyo)* **123**, 431-9.
76. Froger-Gaillard, B., Charrier, A. M., Thenet, S., Ronot, X. & Adolphe, M. (1989) *Exp Cell Res* **183**, 388-98.
77. Bradham, D. M. & Horton, W. E., Jr. (1998) *Clin Orthop*, 239-49.
78. Posever, J., Phillips, F. M. & Pottenger, L. A. (1995) *J Orthop Res* **13**, 832-7.
79. Sah, R. L., Chen, A. C., Grodzinsky, A. J. & Trippel, S. B. (1994) *Arch Biochem Biophys* **308**, 137-47.
80. Jakob, M., Demarteau, O., Schafer, D., Hintermann, B., Dick, W., Heberer, M. & Martin, I. (2001) *J Cell Biochem* **81**, 368-77.
81. Wilbrink, B., Nietfeld, J. J., den Otter, W., van Roy, J. L., Bijlsma, J. W. & Huber-Bruning, O. (1991) *Br J Rheumatol* **30**, 265-71.
82. Pimentel, E. (1994) *Handbook of Growth Factors: Hematopoietic Growth Factors and Cytokines, Vol. 3* (CRC Press, Boca Raton, FL).
83. Moos, V., J., S., V., H. & Muller, B. (2001) *Clinical Rheumatology* **20**, 353-358.
84. Patel, I. R., Attur, M. G., Patel, R. N., Stuchin, S. A., Abagyan, R. A., Abramson, S. B. & Amin, A. R. (1998) *J Immunol* **160**, 4570-9.
85. Jackson, D. W. & Simon, T. M. (1999) *Clin Orthop*, S31-45.
86. Coutts, R. D., Sah, R. L. & Amiel, D. (1997) *AAOS Instructional Course Lectures* **46**, 487-94.
87. Minas, T. (1999) *AAOS Instructional Course Lectures* **48**, 629-43.
88. Homandberg, G. A. & Hui, F. (1994) *Arch Biochem Biophys* **311**, 213-8.
89. Homandberg, G. A. & Hui, F. (1996) *Arch Biochem Biophys* **334**, 325-31.
90. Bullough, P. G., Jones, W. A. & Owen, R. (1997) (Mosby International, London).

91. Boyan, B. D., Lohmann, C. H., Romero, J. & Schwartz, Z. (1999) *Clin Plast Surg* **26**, 629-45, ix.
92. Brooks, P. M. & Day, R. O. (1991) *N Engl J Med* **324**, 1716-25.
93. van de Loo, F. A., Joosten, L. A., van Lent, P. L., Arntz, O. J. & van den Berg, W. B. (1995) *Arthritis Rheum* **38**, 164-72.
94. Hauselmann, H. J., Flechtenmacher, J., Michal, L., Thonar, E. J., Shinmei, M., Kuettner, K. E. & Aydelotte, M. B. (1996) *Arthritis Rheum* **39**, 478-88.
95. Champion, G. V., Lebsack, M. E., Lookabaugh, J., Gordon, G. & Catalano, M. (1996) *Arthritis Rheum* **39**, 1092-101.
96. Glansbeek, H. L., van Beuningen, H. M., Vitters, E. L., van der Kraan, P. M. & van den Berg, W. B. (1998) *Lab Invest* **78**, 133-42.
97. van den Berg, W. B., van der Kraan, P. M., Scharstuhl, A. & van Beuningen, H. M. (2001) *Clin Orthop* **391S**, S244-S250.
98. Martin, J. A., Scherb, M. B., Lembke, L. A. & Buckwalter, J. A. (2000) *Iowa Orthop J* **20**, 1-10.
99. Athanasiou, K. A., Schenck, R., Constantinides, V., Sylvia, V. L., Auldemorte, T. & Boyan, B. D. (1993) *Transactions of the Orthopaedic Research Society* **18**, 288.
100. Athanasiou, K. A., Korvick, D. & Schenck, R. (1997) *Tissue Engineering* **3**, 363-373.
101. Fujisato, T., Sajiki, T., Liu, Q. & Ikada, Y. (1996) *Biomaterials* **17**, 155-62.
102. Bragdon, B., Bertone, A. L., Hardy, J., Simmons, E. J. & Weisbrode, S. E. (2001) *J Invest Surg* **14**, 169-82.
103. Kim, M. R. & Park, T. G. (2002) *J Control Release* **80**, 69-77.
104. Sellers, R. S., Peluso, D. & Morris, E. A. (1997) *J Bone Joint Surg Am* **79**, 1452-63.
105. Hunziker, E. B., Driesang, I. M. & Saager, C. (2001) *Clin Orthop*, S182-9.
106. Lu, L., Stamatas, G. N. & Mikos, A. G. (2000) *J Biomed Mater Res* **50**, 440-51.
107. Boyan, B. D., Lohmann, C. H., Somers, A., Niederauer, G. G., Wozney, J. M., Dean, D. D., Carnes, D. L., Jr. & Schwartz, Z. (1999) *J Biomed Mater Res* **46**, 51-9.

108. Mattioli-Belmonte, M., Gigante, A., Muzzarelli, R. A., Politano, R., De Benedittis, A., Specchia, N., Buffa, A., Biagini, G. & Greco, F. (1999) *Med. Biol. Eng. Comp.* **37**, 130-134.
109. Horisawa, E., Hirota, T., Kawazoe, S., Yamada, J., Yamamoto, H., Takeuchi, H. & Kawashima, Y. (2002) *Pharm Res* **19**, 403-10.
110. Andrews, H. J., Plumpton, T. A., Harper, G. P. & Cawston, T. E. (1992) *Agents Actions* **37**, 147-54.
111. Wang, H., Convery, J. & Ryaby, J. T. (2002) *Transactions of the Orthopaedic Research Society* **27**, 234.
112. Karnaugh, R. D., Ryaby, J. T., Razzano, P., Crowther, R. A., Carney, D. H., Wu, D., Dines, D. M. & Grande, D. (2002) *Transactions of the Orthopaedic Research Society* **27**, 447.
113. Hedberg, E. L., Tang, A., Crowther, R. S., Carney, D. H. & Mikos, A. G. (2002) *J Control Release* **84**, 137-50.
114. Hunziker, E. B., Driesang, I. M. & Morris, E. A. (2001) *Clin Orthop*, S171-81.
115. Holland, T. A. & Mikos, A. G. (2003) *J Control Release* **86**, 1-14.
116. Temenoff, J. S. & Mikos, A. G. (2000) *Biomaterials* **21**, 2405-12.
117. Corkhill, P. H., Fitton, J. H. & Tighe, B. J. (1993) *J Biomater Sci Polym Ed* **4**, 615-30.
118. Temenoff, J. S. & Mikos, A. G. (2000) *Biomaterials* **21**, 431-40.
119. Fisher, J. P., Lalani, Z., Bossano, C. M., Brey, E. M., Demian, N., Johnston, C. M., Dean, D., Jansen, J. A., Wong, M. E. & Mikos, A. G. (2004) *J Biomed Mater Res* **68A**, 428-38.
120. Shin, H., Ruhe, P. Q., Mikos, A. G. & Jansen, J. A. (2003) *Biomaterials* **24**, 3201-3211.
121. Tabata, Y., Nagano, A. & Ikada, Y. (1999) *Tissue Eng* **5**, 127-138.
122. Tabata, Y., Hijikata, S., Muniruzzaman, M. & Ikada, Y. (1999) *J Biomater Sci Polym Ed* **10**, 79-94.
123. Hong, L., Tabata, Y., Miyamoto, S., Yamada, K., Aoyama, I., Tamura, M., Hashimoto, N. & Ikada, Y. (2000) *Tissue Eng* **6**, 331-40.
124. Yamamoto, M., I., Y. & Tabata, Y. (2001) *J. Biomater. Sci. Polymer Edn.* **12**, 77-88.

125. Jo, S., Shin, H., Shung, A. K., Fisher, J. P. & Mikos, A. G. (2001) *Macromolecules* **34**, 2839-2844.
126. Jabbari, E., Behraves, E. & Mikos, A. G. (2002) *Abstr. AIChE Meeting Abstract* **189h**.
127. Temenoff, J. S., Athanasiou, K. A., LeBaron, R. G. & Mikos, A. G. (2002) *J Biomed Mater Res* **59**, 429-37.
128. Peppas, N. A. & Barr-Howell, B. D. (1986) in *Hydrogels in medicine and pharmacy*, ed. Peppas, N. (CRC Press, Boca Raton, FL), pp. 27-56.
129. Peppas, N. A. & Merrill, E. W. (1977) *J Appl Polym Sci* **21**, 1763-1770.
130. Billmeyer, F. W. (1984) *Textbook of polymer science* (Wiley-Interscience, New York).
131. Taylor, J. R. (1982) *An introduction to error analysis*. (University Science Books, Mill Valley, CA).
132. Neter, J., Wasserman, W. & Kutner, M. H. (1985) *Applied linear statistical models* (Richard D. Irwin, Inc., Homewood, IL).
133. Fisher, J. P., Vehof, J. W. M., Dean, D., van der Waerden, J. P., Holland, T. A., Mikos, A. G. & Jansen, J. A. (2002) *J Biomed Mater Res* **59**, 547-556.
134. Holland, T. A., Tabata, Y. & Mikos, A. G. (2003) *J Control Release* **91**, 299-313.
135. Hollinger, J. O. & Leong, K. (1996) *Biomaterials* **17**, 187-94.
136. Yoshihara, Y., Nakamura, H., Obata, K., Yamada, H., Hayakawa, T., Fujikawa, K. & Okada, Y. (2000) *Ann Rheum Dis* **59**, 455-61.
137. Haralson, M. & Hassell, J. (1995) *Extracellular matrix: a practical approach* (IRL Press at Oxford University Press).
138. Solchaga, L. A., Dennis, J. E., Goldberg, V. M. & Caplan, A. I. (1999) *J Orthop Res* **17**, 205-13.
139. Bryant, S. J. & Anseth, K. S. (2003) *J Biomed Mater Res* **64A**, 70-79.
140. Bolen, J., Helmick, C., Sacks, J., Langmaid, G. & Division of Adult and Community Health of National Center for Chronic Disease Prevention and Health Promotion CDC (2002) *Morbidity and Mortality Weekly Report* **51**, 948-950.
141. McNeil, J., Binette, J., Bureau of the Census, Economics and Statistics Administration of US Department of Commerce, Disability and Health Branch, Division of Birth Defects, Child Development, Disability and Health of National Center for Environmental Health, Health Care and Aging Studies Branch &

Division of Adult and Community Health of National Center for Chronic Disease Prevention and Health Promotion CDC (2001) *Morbidity and Mortality Weekly Report* **50**, 120-125.

142. McPherson, J. M. & Tubo, R. (2000) in *Principles of Tissue Engineering*, eds. Lanza, R. P., Langer, R. & Vacanti, J. P. (Academic Press, San Diego), pp. 697-709.
143. Vangsness, C. T., Jr., Kurzweil, P. R. & Lieberman, J. R. (2004) *Am J Orthop* **33**, 29-34.
144. Driesang, I. M. & Hunziker, E. B. (2000) *J Orthop Res* **18**, 909-11.
145. Holland, T. A., Tabata, Y. & Mikos, A. G. (2005) *J Control Release* **101**, 111-25.
146. Holland, T. A., Tessmar, J. K., Tabata, Y. & Mikos, A. G. (2004) *J Control Release* **94**, 101-14.
147. Temenoff, J. S., Park, H., Jabbari, E., Conway, D. E., Sheffield, T. L., Ambrose, C. G. & Mikos, A. G. (2004) *Biomacromolecules* **5**, 5-10.
148. Temenoff, J. S., Park, H., Jabbari, E., Sheffield, T. L., LeBaron, R. G., Ambrose, C. G. & Mikos, A. G. (2004) *J Biomed Mater Res A* **70**, 235-44.
149. Gao, J., Dennis, J. E., Solchaga, L. A., Awadallah, A. S., Goldberg, V. M. & Caplan, A. I. (2001) *Tissue Eng* **7**, 363-71.
150. Solchaga, L. A., Yoo, J. U., Lundberg, M., Dennis, J. E., Huibregtse, B. A., Goldberg, V. M. & Caplan, A. I. (2000) *J Orthop Res* **18**, 773-80.
151. Solchaga, L. A., Gao, J., Dennis, J. E., Awadallah, A., Lundberg, M., Caplan, A. I. & Goldberg, V. M. (2002) *Tissue Eng* **8**, 333-47.
152. Sheehan, D. C. & Hrapchak, B. B. (1987) *Theory and practice of histotechnology* (Battelle Press, Columbus).
153. O'Driscoll, S. W., Keeley, F. W. & Salter, R. B. (1986) *J Bone Joint Surg Am* **68**, 1017-1035.
154. O'Driscoll, S. W., Keeley, F. W. & Salter, R. B. (1988) *J Bone Joint Surg Am* **70**, 595-606.
155. Buma, P., Pieper, J. S., van Tienen, T., van Susante, J. L., van der Kraan, P. M., Veerkamp, J. H., van den Berg, W. B., Veth, R. P. & van Kuppevelt, T. H. (2003) *Biomaterials* **24**, 3255-63.
156. Carranza-Bencano, A., Garcia-Paino, L., Armas Padron, J. R. & Cayuela Dominguez, A. (2000) *Osteoarthritis Cartilage* **8**, 351-8.

157. Agresti, A. (1984) *Analysis of ordinal categorical data* (John Wiley & Sons, Inc, New York).
158. Center for Disease Control and Prevention & www.cdc.gov/health/ (2003).
159. Fukumoto, T., Sperling, J. W., Sanyal, A., Fitzsimmons, J. S., Reinholz, G. G., Conover, C. A. & O'Driscoll, S. W. (2003) *Osteoarthritis Cartilage* **11**, 55-64.
160. Center for Disease Control and Prevention (2005) *National Center for Chronic Disease Prevention and Health Promotion* http://www.cdc.gov/arthritis/data_statistics/national_data_nhis.htm#future.
161. Darling, E. M. & Athanasiou, K. A. (2003) *Ann Biomed Eng* **31**, 1114-24.
162. Veilleux, N. & Spector, M. (2005) *Osteoarthritis Cartilage* **13**, 278-86.
163. Yaeger, P. C., Masi, T. L., de Ortiz, J. L., Binette, F., Tubo, R. & McPherson, J. M. (1997) *Exp Cell Res* **237**, 318-25.
164. Wu, L. N., Genge, B. R., Ishikawa, Y. & Wuthier, R. E. (1992) *J Cell Biochem* **49**, 181-98.
165. Chopra, R. & Anastasiades, T. (1998) *J Rheumatol* **25**, 1578-84.
166. Worster, A. A., Brower-Toland, B. D., Fortier, L. A., Bent, S. J., Williams, J. & Nixon, A. J. (2001) *J Orthop Res* **19**, 738-49.
167. Verschure, P. J., Joosten, L. A., van der Kraan, P. M. & Van den Berg, W. B. (1994) *Ann Rheum Dis* **53**, 455-60.
168. Darling, E. M. & Athanasiou, K. A. (2005) *J Orthop Res* **23**, 425-32.
169. Simmons, C. A., Alsberg, E., Hsiong, S., Kim, W. J. & Mooney, D. J. (2004) *Bone* **35**, 562-9.
170. Schmidmaier, G., Wildemann, B., Ostapowicz, D., Kandziora, F., Stange, R., Haas, N. P. & Raschke, M. (2004) *J Orthop Res* **22**, 514-9.
171. Richardson, T. P., Peters, M. C., Ennett, A. B. & Mooney, D. J. (2001) *Nat Biotechnol* **19**, 1029-34.
172. Holland, T. A., Bodde, E. W., Baggett, L. S., Tabata, Y., Mikos, A. G. & Jansen, J. A. (2005) *J Biomed Mater Res A*.
173. Park, H., Temenoff, J. S., Holland, T. A., Tabata, Y. & Mikos, A. G. (2005) *Biomaterials* **26**, 7095-103.
174. Beck, L. S., Deguzman, L., Lee, W. P., Xu, Y., McFatridge, L. A., Gillett, N. A. & Amento, E. P. (1991) *J Bone Miner Res* **6**, 1257-65.

175. Ferguson, D., Davis, W. L., Urist, M. R., Hurt, W. C. & Allen, E. P. (1987) *Clin Orthop*, 251-8.
176. Mori, M., Isobe, M., Yamazaki, Y., Ishihara, K. & Nakabayashi, N. (2000) *J Biomed Mater Res* **50**, 191-8.
177. Lucas, P. A., Laurencin, C., Syftestad, G. T., Domb, A., Goldberg, V. M., Caplan, A. I. & Langer, R. (1990) *J Biomed Mater Res* **24**, 901-11.
178. Winn, S. R., Schmitt, J. M., Buck, D., Hu, Y., Grainger, D. & Hollinger, J. O. (1999) *J Biomed Mater Res* **45**, 414-21.
179. Andriano, K. P., Tabata, Y., Ikada, Y. & Heller, J. (1999) *J Biomed Mater Res* **48**, 602-12.
180. van Beuningen, H. M., Glansbeek, H. L., van der Kraan, P. M. & van den Berg, W. B. (2000) *Osteoarthritis Cartilage* **8**, 25-33.
181. Bakker, A. C., van de Loo, F. A., van Beuningen, H. M., Sime, P., van Lent, P. L., van der Kraan, P. M., Richards, C. D. & van den Berg, W. B. (2001) *Osteoarthritis Cartilage* **9**, 128-36.
182. Mierisch, C. M., Cohen, S. B., Jordan, L. C., Robertson, P. G., Balian, G. & Diduch, D. R. (2002) *Arthroscopy* **18**, 892-900.
183. Wakitani, S., Goto, T., Pineda, S. J., Young, R. G., Mansour, J. M., Caplan, A. I. & Goldberg, V. M. (1994) *J Bone Joint Surg Am* **76**, 579-92.
184. Hunziker, E. B. & Driesang, I. M. (2003) *Osteoarthritis Cartilage* **11**, 320-7.
185. Solchaga, L. A., Temenoff, J. S., Gao, J., Mikos, A. G., Caplan, A. I. & Goldberg, V. M. (2005) *Osteoarthritis Cartilage* **13**, 297-309.
186. Tew, S., Redman, S., Kwan, A., Walker, E., Khan, I., Dowthwaite, G., Thomson, B. & Archer, C. (2001) *Clinical Orthopaedics & Related Research* **391**, S142-S152.

X. APPENDIX: BIODEGRADABLE POLYMERIC SCAFFOLDS, IMPROVEMENTS IN BONE TISSUE ENGINEERING THROUGH CONTROLLED DRUG DELIVERY[†]

Abstract

Recent advances in biology, medicine, and engineering have led to the discovery of new therapeutic agents and novel materials for the repair of large bone defects caused by trauma, congenital defects, or bone tumors. These repair strategies often utilize degradable polymeric scaffolds for the controlled, localized delivery of bioactive molecules to stimulate bone ingrowth as the scaffold degrades. Polymer composition, hydrophobicity, crystallinity, and degradability will affect the rate of drug release from these scaffolds, as well as the rate of tissue ingrowth. Accordingly, this chapter examines the wide range of synthetic, degradable polymers utilized for osteogenic drug delivery. Additionally, the therapeutic proteins involved in bone formation and in the stimulation of osteoblasts, osteoclasts, and progenitor cells are reviewed to direct attention to the many critical issues influencing effective scaffold design for bone repair.

Abbreviations

bFGF, basic fibroblastic growth factor; BMP, bone morphogenetic protein; BSA, bovine serum albumin; CMC, carboxymethylcellulose; IGF-1, insulin-like growth factor-1; OPF, oligo(poly(ethylene glycol) fumarate); PCCP-SA, poly(carboxyphenoxy propane-sebacic acid); PCL, poly(ϵ -caprolactone); PDGF, platelet derived growth factor; PEG, poly(ethylene glycol); PGA, poly(glycolic acid); PLGA, poly(lactic-*co*-glycolic acid); PLLA, poly(L-lactic acid); PMMA, poly(methyl methacrylate); PPF, poly(propylene fumarate); PPF-DA, poly(propylene fumarate)-diacrylate; rh, recombinant; ST-NH-PEG_x-PLA_y, *N*-succinimidyl tartrate monoamine poly(ethylene glycol)-poly(D,L-lactic acid); TGF- β 1, transforming growth factor- β 1; VEGF, vascular endothelial growth factor.

[†] This chapter was published as the book chapter: TA Holland and AG Mikos, "Biodegradable Polymeric Scaffolds, Improvements in Bone Tissue Engineering through Controlled Drug Delivery," in *Advances in Biochemical Engineering/Biotechnology*, K Lee and DL Kaplan, Eds., Springer Verlag, New York (2005).

Introduction

The field of tissue engineering continues to revolutionize modern medicine by designing novel materials to restore tissue function. For the repair of large tissue defects, scientific efforts have demonstrated the utility of implanting tissue scaffolds, or solid substrates, to which cells can attach, allowing the in-growth of new tissue (1). Although the presence of a tissue scaffold is necessary in wound and tissue repair, repeated research has demonstrated that scaffolds alone often fail to provide a sufficient template to guide tissue regeneration (2-7). Consequently, tissue engineering strategies must utilize biomaterials specifically designed to immobilize bioactive ligands, support cell transplantation, or deliver therapeutic molecules in order to achieve complete tissue repair (8-18). While each of these approaches have been used to enhance healing in a number of clinical applications, bone defects are excellent candidates for local drug delivery strategies, since these defects often have access to the cells which growth factors target. Accordingly, the following discussion examines novel, degradable, polymeric scaffolds developed to locally deliver regulatory molecules for bone repair. A brief overview of the degenerative conditions affecting bone tissue, the cellular processes involved in bone formation and remodeling, and the regulatory molecules guiding these events is first provided so that readers clearly understand the physiological and biological challenges in bone tissue engineering. Subsequently, recent advances in drug delivery for bone repair are reviewed with an emphasis on polymeric scaffold design and the parameters affecting drug release.

Degenerative Bone Disorders

Trauma, congenital defects, and bone metastases frequently result in large bone deficiencies in both load bearing and non-load bearing skeletal sites. Additionally, a

number of other degenerative bone conditions are also in need of improved clinical therapies. Specifically, osteoporosis, Paget's disease, and rheumatoid arthritis lead to significant bone deterioration due to the excessive proliferation and resorptive activity of osteoclasts (19). Although hormone replacement therapies may help to inhibit bone resorption, oral ingestion of these pleiotrophic agents has also been associated with an increased incidence of cancer and thromboembolic events (19, 20). Furthermore, these treatment options, and the use of non-degradable bone cements to fill osseous voids, fail to stimulate osteoblasts to synthesize new bone. Although, poly(methyl methacrylate) (PMMA), a clinically used bone cement, has also been explored as a local delivery vehicle for chemotherapeutics, hormones, and antibiotics, observed release rates are generally too slow since this polymer is non-degradable (21-23). Additionally, PMMA requires elevated curing temperatures (60°C) which may engender further osteonecrosis (24, 25). Accordingly, improved clinical strategies and materials for localized delivery of therapeutic molecules to bone defects are imperative.

Bone Formation

Bone tissue provides our bodies with an internal mechanical support system, while ensuring calcium homeostasis and housing the biological elements required for hematopoiesis, the process by which blood and immune cells are renewed (26). This important tissue is formed from two distinct pathways. Intramembraneous bone formation, in which mesenchymal progenitor cells differentiate directly into osteoblasts, or bone forming cells, leads to the development of the periosteal surfaces of the long bones, parts of the mandible and clavicle, and many cranial bones. Alternatively, the long bones and vertebrae are formed through endochondral bone formation in which

mesenchymal progenitor cells differentiate first into chondrocytes. These cells deposit a cartilaginous template which is later mineralized and replaced by bone (26).

Upon fracture, bone is repaired by a process which recapitulates many of the events of both intramembraneous and endochondral bone formation (26). Initially, after injury, a hematoma fills the defect site and may act as a source of signaling molecules to recruit reparative cells. An inflammatory response ensues as fibroblasts and macrophages replace this clot with an external callus, a fibrovascular tissue rich in collagen fibers. Within 7-10 days, intramembraneous bone, or hard callus, formation near the defect edges begins as osteoprogenitor cells of the periosteum differentiate into osteoblasts. Simultaneously, endochondral bone formation proceeds as additional progenitor cells differentiate into chondrocytes, which replace the external callus with cartilage. Finally, this cartilaginous, soft callus is mineralized and remodeled by the combined actions of both osteoclasts and osteoblasts (25, 26).

Bone Remodeling by Osteoclasts and Osteoblasts

Although bone remodeling follows fracture, this dynamic tissue is continually undergoing remodeling to maintain mechanical integrity and to respond to the body's changing demands (26, 27). Remodeling results from the balance of two key processes, osteolysis, bone resorption by osteoclasts, and osteogenesis, bone formation by osteoblasts. Osteoclasts mature from macrophage precursor cells, and like many cells of the immune system, release numerous enzymes into the surrounding tissue. Osteolysis begins as the cell membrane of osteoclasts polarizes to secrete hydrochloric acid for dissolution of bone's inorganic, mineral component. Then, lysosomal protease and cathepsin K are mobilized to degrade the remaining organic component, mainly type I

collagen fibers (27). Osteoclast apoptosis marks the end of the resorptive phase of remodeling, and pre-osteoblastic cells are chemotactically recruited and differentiated into mature osteoblasts through numerous mitogens and growth factors. These cells fill the site with new bone matrix, which is completely mineralized within approximately 2 weeks (26, 28).

Regulatory Molecules

A host of bioactive proteins interact with the cell receptors on osteoblasts, osteoclasts, and progenitor cells to direct both new bone formation and bone remodeling. Specifically, these polypeptides may act as differentiation factors to guide progenitor cells toward a particular lineage or as progression factors to stimulate cell proliferation and extracellular matrix production (29-31). However, many of these molecules function as both morphogens and growth factors (9). In most cases, these soluble factors are synthesized and secreted by cells as precursor molecules which must be activated by binding to extracellular matrix components or by proteolytic cleavage (9, 29).

Bone morphogenetic protein-2 (BMP-2) is perhaps the most widely investigated agent in the field of bone tissue engineering. This molecule belongs to a group of proteins isolated from the inorganic component of bone by Marshall Urist, after researchers discovered that decalcified bone matrix could induce bone formation (32). Advances in biochemistry led to the purification of at least 15 distinct molecules from this heterogeneous protein mixture, including BMP-2, BMP-4, BMP-7 (osteogenic protein-1), BMP-8 (osteogenic protein-2), and BMP-3 (osteogenin) (30). These molecules mainly function as differentiation factors, guiding mesenchymal stem cells toward chondrogenic or osteoblastic lineage, and are osteoinductive agents capable of inducing bone formation

ectopically (29, 30, 32, 33). In fact, clinical trials are currently investigating the use of both BMP-2 and BMP-7 for bone repair (32).

BMPs actually belong to a broader, superfamily of proteins, known as the transforming growth factor- β (TGF- β) family, and can share up to 50% sequence homology with TGF- β 1 (29). While the BMPs are osteoinductive agents, TGF- β 1 appears to function as an osteoconductive agent, capable of inducing bone formation only in the vicinity of bone (29, 30). Since this molecule is synthesized by osteoblasts and stored in bone matrix, bone serves as the body's largest reservoir of TGF- β 1 (34). This multifunctional protein has been shown to stimulate mesenchymal stem cell differentiation, enhance osteoblast proliferation, and inhibit osteoclast function (2, 26, 34). However, at high doses, this pleiotrophic agent is associated with inflammation, fibrosis, and scarring (35).

Additional signaling molecules involved in both bone repair and remodeling include basic fibroblastic growth factor (bFGF), platelet derived growth factor (PDGF), and insulin-like growth factor-1 (IGF-1). Like TGF- β 1, bFGF has been shown to modulate the functions of a number of cell types, such as, osteoblasts, chondrocytes, fibroblasts, endothelial cells, and smooth muscle cells (26). However, bFGF may be useful in bone tissue engineering since this protein can stimulate chondrocyte and osteoblast proliferation and enhance osteogenesis and angiogenesis (29, 30). Like bFGF, PDGF and IGF-1 also encourage osteoblast expansion (26, 36). Additionally, PDGF has been shown to act as a chemotractant and mitogen for mesenchymal progenitor cells (29, 31). Both PDGF and IGF-1 stimulate the synthesis of collagen I and osteopontin, important organic components of the bone matrix (37).

Critical Issues in Drug Delivery System Design

Regardless of the bioactive protein or drug employed in delivery systems for tissue repair, engineers must ensure that these agents are released to the surrounding tissue within a therapeutic time frame and dosage. Thus, the resulting release profile should be optimized for each agent and clinical application. Since most morphogens and growth factors are relatively large proteins with precise three-dimensional conformations, care must be taken to ensure that processing conditions used to fabricate drug delivery implants do not adversely affect the activity and half life of these agents. In particular, harsh loading conditions which promote protein aggregation or denaturation should be avoided (9, 38).

Since drug delivery systems for bone repair also serve as tissue scaffolds, these implants must conform to the design criteria used in the selection of all tissue engineering scaffolds. In addition to supporting cell adhesion, scaffolds should be biocompatible to prevent prolonged inflammation, as well as biodegradable to minimize the necessity of surgery (30, 39). Ideally, scaffold materials should be metabolized by the body into acceptable degradation products at a rate which coincides with the rate of tissue ingrowth. Furthermore, drug-releasing scaffolds for bone repair must provide suitable mechanical support at the defect site and sufficient porosity to facilitate nutrient transport and cell infiltration (25). Finally, implant materials should be chosen to allow for ease in sterilizing and processing scaffolds with a shape and volume identical to the tissue defect (40).

A wide variety of natural materials have been used for the controlled delivery of osteogenic agents, including glycoasminoglycans, fibrin, alginate, gelatin, and collagen (41-47). Initially, demineralized bone matrix, obtained from the cortical bone of various

animal sources, was widely investigated in bone repair, since this mixture of collagenous proteins is a natural carrier of BMPs (48, 49). However, these materials often fail to possess the mechanical properties and resorption rates necessary for load bearing applications (50). Alternatively, the physical and chemical parameters of polymeric devices can be easily and reproducibly tailored for a given application (24, 40). Furthermore, implantation of delivery scaffolds based on synthetic polymers circumvents concerns regarding immunogenic reactions and disease transmission from materials derived from allogenic or xenogenic tissues. The following discussion examines many biodegradable, polymeric, drug delivery systems for bone tissue repair. As illustrated by in vitro and in vivo research, polymer composition, hydrophobicity, crystallinity, and degradability, as well as the method of drug loading, are among the many properties affecting drug release and tissue formation.

Polymeric Scaffolds for Bone Drug Delivery

Perhaps one of the most influential material parameters dictating drug release centers on carrier degradability. In general biodegradable polymers possess hydrolytically unstable linkages in their backbone, such as ester, ether-ester, anhydride, or amide functional groups (40, 51, 52). Often scientists classify the mechanism by which hydrolysis proceeds as either bulk degradation or surface erosion. In the case of bulk degradation, the rate at which water penetrates an implant exceeds the rate at which the polymer is converted into water soluble fragments, resulting in material deterioration throughout the device. Surface erosion refers to the opposing situation, when water penetration occurs more slowly than the rate of polymer solubilization, allowing bulk integrity to be maintained as surfaces exposed to water erode (40, 53, 54).

Systems which undergo bulk degradation often display first order, diffusion controlled release kinetics and may be too hydrophilic for drugs that are highly unstable in an aqueous environment. Release from surface-eroding polymers typically proceeds at zero order rates controlled by the rate of surface degradation. Accordingly, these materials tend to be more hydrophobic and may better preserve the activity of molecules within the polymer matrix (55, 56). Polyesters, polyether-esters, and polyester-amides are generally classified as bulk-degrading polymers, while polyanhydrides and polyorthoesters degrade primarily by surface erosion (7, 40, 55, 56). However, engineers should be aware that changes to the microarchitecture and surface properties of drug release systems, stemming from mechanical loading, fibrosis, or vascularization of implants may alter both polymer degradation and the release and activity of incorporated proteins (9, 30). Additionally, since many drug delivery scaffolds are fabricated from two or more polymers, hydrolysis often proceeds through both bulk and surface degradation.

Poly(lactic acid)

The most widely investigated polymeric drug carriers have arise from a group of degradable, aliphatic polyesters approved by the FDA for use in other clinical applications, including surgical sutures, pins, clips, and staples (9, 54, 55). Early drug delivery research sought to extend the use of these polymers for the sustained, local release of antibiotics as an alternative to treating post-operative osteomyelitis by lengthy oral or intravenous drug regimes (57-59). For instance, the polyester poly(lactic acid) was explored as a coating for implants releasing gentamicin and allowed for sustained release of this antibiotic at the minimum, inhibitory concentration toward the bacteria

Staphylococcus aureus for approximately 4 weeks (60). Given these successes, engineers have extended the use of these polyesters for the design of more complicated systems for tissue regeneration.

The structure of poly(lactic acid) is shown in Table 1 along with numerous polymers investigated as carriers of therapeutic molecules for bone repair. Poly(lactic acid) is formed by ring opening polymerization of lactide, the dimerization product of lactic acid. Two optical isomers of lactic acid exist, corresponding to L-lactide or D-lactide. Poly(L-lactic acid) (PLLA), formed from the naturally occurring isomer, is a semicrystalline polymer with a relatively high melting point (178°C) and glass transition temperature (65°C). Accordingly, these properties impart high tensile strength and extended degradation times (3-5 years) to PLLA scaffolds. Poly(D,L-lactic acid), polymerized from a blend of D-lactide and L-lactide, is amorphous, and thus, possesses considerably lower melting point (60°C), tensile strength, and degradation times (12-16 months) than PLLA (40, 55). However, since the degradation of PLLA yields the naturally occurring stereoisomer of lactic acid, a normal intermediate of carbohydrate metabolism, this form of poly(lactic acid) is generally preferred (54, 55).

Early growth factor release systems based on PLLA and other polyesters utilized simple adsorptive techniques to surface coat polymeric particulates (61, 62). Non-uniform particulates were obtained by such means as the shredding of solid polymer rods. Often the protein of interest was dissolved in a solution containing additional agents, such as collagen, serum, chitosan, or carboxymethylcellulose (CMC), to promote sorption to the polymer. However, these particulates were not able to function as true tissue scaffolds due to their lack of mechanical support. In fact, to maintain particles at a defect

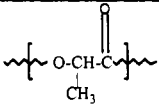
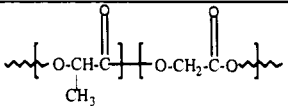
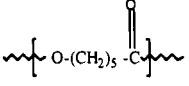
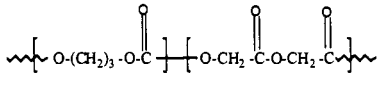
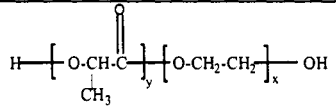
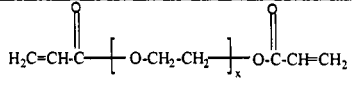
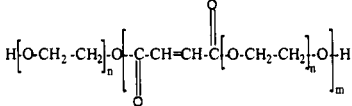
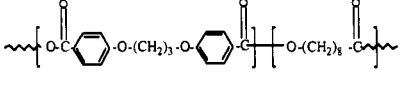
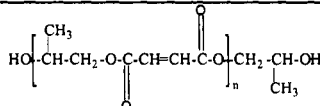
site, gelatin or collagen capsules were sometimes employed, making it difficult to clearly assess device efficiency and to correlate in vivo and in vitro behavior. Such delivery systems were primarily investigated in non-loading bearing models and often displayed inadequate bone regeneration.

Despite their limitations, these early release systems assisted in elucidating valuable information regarding various biological-material interactions. For instance, systematic investigations with polymeric particulates helped to optimize the PLLA molecular weight range appropriate for bone implants (68). Specifically, PLLA particulates (100 mg) of various molecular weights were wetted with 4 mg semipurified BMP and then implanted in the dorsal muscles of mice. No bone formation was visible after three weeks with particulates of high molecular weight (greater than 3,300 Da), since the slow degradation rate of these polymers restricted tissue ingrowth. Tissue necrosis was observed with particulates of extremely low molecular weight (160 Da), due to the high acidity and rapid degradation of these formulations. However, an intermediate PLLA molecular weight (650 Da) resulted in limited bone formation (68). Additional studies compared bone regeneration from polymeric based systems to the previous standard carriers, collagen or demineralized bone, and demonstrated that PLLA and other polyesters did not adversely affect the activity of released growth factors (50, 62).

With the development of more advanced scaffold fabrication techniques, such as solvent casting, gas foaming, and emulsion freeze drying, PLLA was formulated into three-dimensional scaffolds for drug delivery to loading bearing defects (38). For instance, 50 μ g recombinant BMP-2 (rhBMP-2) was reconstituted in a collagen solution and then adsorbed to the surface of prefabricated PLLA disks before implantation in

critical size rat calvarial defects. After 4 weeks, defects treated with these simple delivery systems demonstrated enhanced bone formation by radiomorphometric and histomorphometric analysis when compared to PLLA disks seeded with osteoprogenitor cells and unloaded PLLA controls (6).

Table A- 1: Biodegradable Polymers Utilized in Osteogenic Drug Delivery

Polymer	Chemical Structure	Bone Engineering Research
Poly(lactic acid)		(6, 57, 58, 60, 66-68)
Poly(lactic-co-glycolic acid)		(61-65, 69, 70)
Poly(ε-caprolactone)		(77-79)
Polyglyconate		(40)
Poly(lactic acid)-poly(ethylene glycol)		(10, 80-86)
Poly(ethylene glycol) diacrylate		(87)
Oligo(poly(ethylene glycol) fumarate)		(16, 18, 88-92)
Poly(carboxyphenoxy propane-sebacic acid)		(5, 93-97)
Poly(propylene fumarate)		(98-106)

However, more precise control over protein release kinetics, and thus, substantially lower, yet still therapeutic, drug loadings, were often achieved by

incorporating the desired protein directly into the polymer network (66, 67). For example, using an air-drying phase inversion process, PLLA was mixed with 200 ng PDGF and fabricated into porous membranes. In vitro release experiments demonstrated sustained PDGF release over the course of 28 days. Release rates could be increased through dual loading of both PDGF and bovine serum albumin (BSA) into these matrices. Furthermore, bony formation within critical size rat calvarial defects was achieved using these delivery systems within approximately 2 weeks post-implantation, demonstrating maintenance of protein activity with this scaffold fabrication technique (66).

Poly(lactic-co-glycolic acid) Copolymers

Additional efforts to achieve further control over protein release led to the copolymerization of lactide and glycolide to form poly(lactic-co-glycolic acid) (PLGA). Pure poly(glycolic acid) (PGA) was used to develop DEXON®, first commercially available, synthetic, absorbable suture (55). Like PLLA, PGA is formed by ring opening polymerization of a cyclic dimer and results in a semicrystalline network (40). However, copolymerization of lactide and with glycolide disrupts the crystallinity of these monomers, leading to an amorphous network with a rate of degradation and protein release dictated by the monomer ratio (54). PLGA with a lactide to glycolide ratio of 7:3 is commercially used to produce surgical staples marketed as Lactomer™ (55). Solvent casting/porogen leaching techniques have been utilized to fabricate porous PLGA foams which support osteoblast and mesenchymal stem cell attachment and proliferation (69, 70, 107).

To deliver therapeutic agents from PLGA-based materials, a number of scaffold processing techniques have been employed. Emulsion freezing drying methods have been

used to fabricate and model release of active rhBMP-2 from scaffolds of various pore sizes (71, 108). Innovative methods for encapsulating proteins within PLGA microspheres have been also developed (4, 109). The most popular of these methods, a double-emulsion-solvent-extraction technique, has been shown successfully entrap rhBMP-2, TGF- β 1, and IGF-1 within polymeric microparticles without significant loss in protein activity (72, 74, 75). Protein release kinetics from PLGA microparticles can be controlled by altering the loading of additional components, including poly(ethylene glycol) (PEG), BSA, and gelatin (73, 75).

Utilizing these and other processing techniques for the fabrication of both PLGA microparticles and scaffolds, researchers now have the ability to create composite materials with precise release profiles (76, 98). For instance, delivery of multiple growth factors at specific rates is now possible. Slow release of PDGF (approximately 0.1 pmol/day) and fast release of vascular endothelial growth factor (VEGF) (1.7 pmol/day) was achieved using a novel scaffold design. PDGF was first encapsulated with PLGA microparticles, while VEGF was mixed PLGA particulates. The microparticles and particulates were then combined and processed into porous foams using a gas foaming technique. After 4 weeks post-implantation in the hind limbs of mice, these dual release systems demonstrated enhanced vasculature when compared to systems releasing only PDGF or VEGF (76). More importantly, similar polymeric devices will provide researchers with a tool to assess how various growth factors interact in tissue repair. Additionally, these systems can be utilized to optimize the therapeutic release profiles of particular proteins in bone healing.

Other Polyesters

Unfortunately, the mechanical properties of scaffolds based on PLGA are well below the mechanical properties of human trabecular bone (107). Thus, researchers have investigated several other polyesters for bone engineering applications. For instance, porous scaffolds fabricated by solvent casting/porogen leaching and based on the polyester poly(ϵ -caprolactone) (PCL) demonstrated significantly higher tensile strength and Young's modulus than PLGA scaffolds (77). However, like PLLA, PCL is a semicrystalline polymer with a degradation time of approximately 2 years (40). To speed degradation, copolymers of ϵ -caprolactone and DL-lactide have been synthesized. However, when implanted in femoral defects in rats, this material still remained after 1 year and appeared to retard bone formation when compared to untreated defects (79). Other researchers have taken advantage of the lengthy degradation time of highly crystalline polymers to protect bone grafts from displacement and rapid resorption (78, 110). However, their slow degradation has limited the extension of these materials to drug delivery.

Following a similar strategy to tailor both polymer strength and degradability to tissue engineering applications, additional research groups have synthesized PGA-based copolymers. In particular, polyglyconate, a copolymer of glycolide and trimethylene carbonate, is utilized in surgical sutures, tacks, and screws. Copolymers with a 2:1 glycolide to trimethylene carbonate ratio demonstrate increased flexibility and faster degradation times (7 months) than pure PGA (40). Similar trends are reported when glycolide is polymerized with both trimethylene carbonate and/or p-dioxanone (40, 111). Yet, like lactide based copolymers, these materials have not been widely used in drug delivery.

Poly(lactic acid)-Poly(ethylene glycol) Block Copolymers

One group of copolymers which has been investigated as a protein carrier is the family of poly(D,L-lactic acid)_y-poly(ethylene glycol)_x (PLA_y-PEG_x) block copolymers. These copolymers consist of altering segments of PLA and PEG, whose respective molecular weights *y* and *x* are dictated by the polymerization reaction. The hydrophilic nature of the repeating PEG unit helps to neutralize the acidity of low molecular weight PLA segments, while modulating the degradation rate (83). When loaded with rhBMP-2, block copolymers with a 7:3 PLA to PEG ratio demonstrate promising bone formation. More specifically, 10 µg rhBMP-2 was incorporated into PLA₆₅₀₀PEG₃₀₀₀ devices, and then surgically implanted into the back muscles of mice. After approximately 3 weeks, only 21% of the polymer remained, and bone formation with osseous trabeculae was apparent. However, BMP-2 release from implants with a higher PLA to PEG ratio did not result in osteoinduction due to the extensive amount of polymer remaining (94-98%) after 3 weeks (84). The optimal total block copolymer molecular weight for BMP-releasing implants with a PLA to PEG ratio of 7:3 was found to be 6400 Da, allowing for complete in vivo degradation by 3 weeks (86).

Additional research demonstrated that the degradation rate of these block copolymers could be further tailored by introducing a random linkage of p-dioxane. Furthermore, these materials, when loaded with 0.5-10 µg rhBMP-2, were able to illicit bone formation intramuscularly in rats (85). Accordingly, these studies demonstrate that as the material properties of a delivery system are improved, the minimal effective dosage of a particular drug or growth factor is often substantially reduced. However, further experimental investigations are necessary to understand the interplay between in vivo material degradation, protein release kinetics, and tissue formation.

While such investigations are ongoing, a novel means of immobilizing proteins within scaffolds was developed by modifying these copolymers. Specifically, N-succinimidyl tartrate monoamine poly(ethylene glycol)-poly(D,L-lactic acid) (ST-NH-PEGx-PLAy), an amine reactive polymer, was synthesized using innovative chemical techniques (112). The amine group of this polymer was shown to facilitate covalent attachment of model proteins in both solution (insulin and somatostatin) and solid phase (trypsin). Similar results were found with a novel, thiol reactive polymer, synthesized by attaching N-succinimidyl 3-maleinimido propionate to monoamine poly(ethylene glycol)-poly(D,L-lactic acid) (112). Although the bioactivity of the attached proteins has not yet been confirmed in this system, in vitro and in vivo studies with similar protein tethering methods suggest that these methods should not alter protein activity (113, 114).

Taking this technology even further, an inventive means of fabricating scaffolds with interconnected pore networks was developed through incorporation of lipid microparticles during ST-NH-PEGx-PLAy precipitation into n-hexane. This method avoids an aqueous environment, preserving the amine group from hydrolysis, and thus, permitting the covalent attachment of proteins. Upon polymer precipitation into 3-dimensional structures, lipid microparticles are subsequently extracted by melting to yield porous scaffolds (82). Such creative techniques will undoubtedly revolutionize tissue engineering, allowing for the creation of truly biomimetic structures.

Additional Poly(ethylene glycol)-Based Materials

Towards the goal of minimizing implantation surgeries, researchers have also been developing novel, injectable polymers from the delivery of bioactive molecules. Many of these polymers have a repeating PEG unit within their backbone, since the

hydrophilicity of PEG often imparts water solubility. Upon thermal or photo-initiated reactions, these polymers are converted from their soluble state into crosslinked hydrogels. For instance, macromers of PEG with acrylated end groups have been photo-crosslinked into hydrogels and utilized for protein delivery (87). Likewise, macromers of PLA-PEG-PLA with acrylated end groups have been examined as osteogenic protein or cell delivery vehicles (10, 80, 81). However, these systems have mainly been studied in vitro or in subcutaneous implantations.

Another PEG-based macromer, oligo(poly(ethylene glycol) fumarate) (OPF) has been extensively examined in vitro (16, 18, 90) and utilized in vivo for the repair of both bone and soft tissue defects by modification with bioactive peptides (88). The ester linkage in the backbone of this macromer facilitates hydrolytic degradation, while the double bond facilitates crosslinking through thermal initiation. Thus, OPF can be crosslinked into degradable hydrogels at physiological temperatures (89). Furthermore, TGF- β 1 release from OPF hydrogels can be tailored by altering the swelling ratio and mesh size of these networks (92). However, since all of these PEG-based materials form water absorbent gels, their utility will be limited to soft tissue defects and non-load bearing bone defects. Additionally, this characteristic prevents their use as a carrier for drugs which are highly unstable in an aqueous environment.

Polyanhydrides

Alternative carriers for hydrolytically unstable molecules are often based upon more hydrophobic polymers like polyanhydrides. These polymers are synthesized by melt polycondensation. Typically, a diacid monomer is reacted with excess acetic anhydride, yielding an anhydride oligomer, which can then be polymerized under

vacuum (56). Homopolyanhydrides of aliphatic or aromatic diacid monomers generally possess some degree of crystallinity. As discussed previously, copolymers show a decrease in crystallinity due to the presence of other units in the polymer chain, and the degree of monomer hydrophobicity will dictate the polymer's degradation time (55, 56).

The most widely investigated polyanhydride is a copolymer of sebacic acid and 1,3-bis(p-carboxyphenoxy)-propane, known as poly(carboxyphenoxy propane-sebacic acid) (PCCP-SA) (40, 55). Copolymers with high sebacic acid contents demonstrate relatively short degradation times due to the relative hydrophilicity of this monomer (93, 95). Drug release from PCCP-SA and other surface eroding polymers has been shown to directly coincide with the rate of degradation (36, 51, 55, 56). Like polyesters, early polyanhydride release systems were examined for the localized delivery of antibiotics to treat osteomyelitis (96). However, PCCP-SA and other polyanhydrides have been successfully fabricated into microparticles and scaffolds for the controlled delivery of a number of different bioactive molecules.

For instance, a hot melt microencapsulation procedure was developed to entrap a model drug (insulin) within PCPP-SA microparticles (94). The biological activity of insulin released from these microparticles was later verified. In particular, insulin-incorporated microspheres injected into diabetic rats resulted in normoglycemia for a period of approximately 5 days (93). Scaffolds have also been fabricated for the controlled delivery of active proteins. Using compression molding, a mixture of osteogenic proteins and polymer was fabricated into polyanhydride scaffolds based on several different macromers (5). Protein release from these systems was shown to induce osteogenesis intramuscularly in mice. However, osteoinduction did not result in animals

receiving an injection of the same drug dosage, due to protein solubility, and thus, distribution within the body (5).

In similarity to the challenges facing polyester-based systems, considerable work is necessary to enhance the performance of polyanhydride scaffolds so that these materials provide the appropriate mechanical properties to ensure tissue repair. Accordingly, researchers are investigating the use of dimethacrylated anhydride monomers which can be crosslinked into networks with improved mechanical properties. In particular, dimethacrylated sebacic acid and 1,3-bis(p-carboxyphenoxy) hexane were photo-crosslinked into networks with respective compressive strengths of 34 ± 4 MPa and 39 ± 11 MPa. While these values are comparable to the compressive strength of trabecular bone (5-10 MPa), further improvement is necessary to reach the strength of cortical bone (130-220 MPa) (97).

Poly(propylene fumarate)

A material that has been shown to form networks with compressive strength on the order of cortical bone is the linear unsaturated polyester, poly(propylene fumarate) (PPF) (105). The double bond in the backbone of PPF allows this viscous polymer to be crosslinked into solid structures via thermal or photo-initiation (74, 103). By altering the molecular weight, adding poly(propylene fumarate)-diacrylate (PPF-DA), and varying the crosslinking reaction, the compressive strength of PPF-based networks can be tailored within the range of 31 ± 13 to 129 ± 17 MPa (105). Furthermore, PPF scaffolds with an interconnected pore network can be easily fabricated by incorporating a porogen during the crosslinking reaction (101).

These scaffolds have been shown to be both biodegradable and biocompatible in vivo (102). Their use as delivery vehicles has also been explored. Preliminary work investigating the repair of rabbit cranial defects demonstrated significant bone formation when defects were treated with PPF scaffolds to which rhTGF- β 1 was adsorbed (106). More sophisticated systems for the controlled delivery of osteogenic agents have also been developed using PPF. In particular, microparticles encapsulating the therapeutic peptide TP508 have successfully been integrated into both the pores and polymer network of PPF scaffolds for the sustained release of this molecule (98). These systems were then implanted into critical size rabbit femoral defects to evaluate how the kinetics of TP508 release affect bone repair. Complete bone regeneration was observed when TP508-loaded microparticles were incorporated into the pores of these scaffolds, indicating that a burst release of this molecule promotes bone formation. However, slow release of TP508 from microparticles within the polymer network demonstrated considerably less bone formation (99). Thus, scaffolds based on this novel polymer not only impart improved mechanical properties, but also provide a means of controlled protein delivery to systematically evaluate the therapeutic time course of individual proteins.

Future Directions

As illustrated in the preceding discussion, researchers have developed many novel materials for the delivery of osteogenic agents. While initial release systems focused on the use of simple aliphatic polyesters, the shortcomings of these materials have led researchers to synthesize various polyester copolymers, as well as alternative polymers like PCPP-SA and PPF. Still other researchers have developed injectable polymers to

minimize the necessity of surgery (8, 84, 89, 115, 116). Meanwhile, scientists outside the arena of polymer chemistry have also significantly contributed to the field of bone tissue engineering.

For instance, biologists have not only isolated a number of therapeutic proteins for bone repair, but have also investigated the affinity of these agents to extracellular matrix components (42, 45, 117-119). Accordingly, new composite systems are now incorporating some of these components into synthetic polymeric scaffolds to allow growth factor release to be catalyzed by natural processes (91). Additionally, mechanical engineers have shown that hydroxyapatite and β -tricalcium phosphate can be incorporated into synthetic polymeric scaffolds to improve the mechanical properties of these networks (77, 104, 111, 120). Scientists in the field of nanoscience are also contributing to the field of tissue engineering, demonstrating that nanoreinforcement of polymers may assist in building stronger scaffolds (121, 122). Methods for encapsulating proteins within nanoparticles have also arisen (123-125). Finally, advances in computer-aided design have led to the fabrication of scaffolds of precise three-dimensional shape and volume (1, 100). Accordingly, researchers now have the material and processing tools to build more effective polymeric scaffolds for drug delivery. However, to develop highly efficient release systems, engineers must now work closely with biologists to study how the kinetics of protein release from these systems affects bone repair.

Conclusions

A host of bioactive proteins have been isolated from bone tissue and shown to influence the cellular and molecular events involved in both bone formation and remodeling. Likewise, numerous degradable polymers have been developed as carriers of

these molecules. These polymers include the early polyesters, such as PLLA and PLGA, as well as a later generation of injectable materials based on PEG, and more hydrophobic materials, such as PPCP-SA and PPF. By altering the molecular weight, monomer composition, and crosslinking method, scientists can tailor the crystallinity, hydrophilicity, and degradability of these polymers. In combination with innovative processing methods, this ability allows engineers to design scaffolds and microparticles with specific drug release kinetics. In order to reduce the minimum effective drug loading within these systems, engineers, biologists, and physicians must now work together to assess how the time course of protein release affects tissue repair. By optimizing interplay between both the material and bioactive components of these drug delivery systems, the field of tissue engineering will undoubtedly revolutionize the treatment for bone degenerative disorders.

Appendix References

1. Hutmacher, D. W. (2000) *Biomaterials* 21, 2529-43.
2. Beck, L. S., Deguzman, L., Lee, W. P., Xu, Y., McFatridge, L. A., Gillett, N. A. & Amento, E. P. (1991) *J Bone Miner Res* 6, 1257-65.
3. Ferguson, D., Davis, W. L., Urist, M. R., Hurt, W. C. & Allen, E. P. (1987) *Clin Orthop*, 251-8.
4. Mori, M., Isobe, M., Yamazaki, Y., Ishihara, K. & Nakabayashi, N. (2000) *J Biomed Mater Res* 50, 191-8.
5. Lucas, P. A., Laurencin, C., Syftestad, G. T., Domb, A., Goldberg, V. M., Caplan, A. I. & Langer, R. (1990) *J Biomed Mater Res* 24, 901-11.
6. Winn, S. R., Schmitt, J. M., Buck, D., Hu, Y., Grainger, D. & Hollinger, J. O. (1999) *J Biomed Mater Res* 45, 414-21.
7. Andriano, K. P., Tabata, Y., Ikada, Y. & Heller, J. (1999) *J Biomed Mater Res* 48, 602-12.

8. Elisseeff, J., Anseth, K., Sims, D., McIntosh, W., Randolph, M. & Langer, R. (1999) *Proc Natl Acad Sci U S A* 96, 3104-7.
9. Babensee, J. E., McIntire, L. V. & Mikos, A. G. (2000) *Pharm Res* 17, 497-504.
10. Anseth, K. S., Metters, A. T., Bryant, S. J., Martens, P. J., Elisseeff, J. H. & Bowman, C. N. (2002) *J Control Release* 78, 199-209.
11. Payne, R. G., McGonigle, J. S., Yaszemski, M. J., Yasko, A. W. & Mikos, A. G. (2002) *Biomaterials* 23, 4381-7.
12. Payne, R. G., McGonigle, J. S., Yaszemski, M. J., Yasko, A. W. & Mikos, A. G. (2002) *Biomaterials* 23, 4373-80.
13. Payne, R. G., Yaszemski, M. J., Yasko, A. W. & Mikos, A. G. (2002) *Biomaterials* 23, 4359-71.
14. Ito, Y., Inoue, M., Liu, S. Q. & Imanishi, Y. (1993) *J Biomed Mater Res* 27, 901-7.
15. Liu, S. Q., Ito, Y. & Imanishi, Y. (1993) *J Biomed Mater Res* 27, 909-15.
16. Shin, H., Jo, S. & Mikos, A. G. (2002) *J Biomed Mater Res* 61, 169-79.
17. Shin, H., Jo, S. & Mikos, A. G. (2003) *Biomaterials* 24, 4353-4364.
18. Shin, H., Zygourakis, K., Farach-Carson, M. C., Yaszemski, M. J. & Mikos, A. G. (2004) *Biomaterials* 25, 895-906.
19. Rodan, G. A. & Martin, T. J. (2000) *Science* 289, 1508-14.
20. Wang, J., Chow, D., Heiati, H. & Shen, W. C. (2003) *J Control Release* 88, 369-80.
21. Mestiri, M., Benoit, J. P., Hernigou, P., Devissaguet, J. P. & Puisieux, F. (1995) *J Control Release* 33, 107-113.
22. Downes, S. (1995) in *Encyclopedic handbook of biomaterials and bioengineering, part a: materials.*, eds. Wise, D. L., Trantolo, D. J., Altobelli, D. E., Yaszemski, M. J., Gresser, J. D. & Schwartz, E. R. (Marcel Dekker, Inc., New York), Vol. 2, pp. 1135-1149.
23. Seligson, D. & Henry, S. L. (1993) *Clin Orthop* 295, 2-118.

24. Thomson, R. C., Ishaug, S. L., Mikos, A. G. & Langer, R. (1995) in *Molecular biology and biotechnology, a comprehensive desk reference*, ed. Meyers, R. A. (VCH Publishers, Inc., New York), pp. 717-724.
25. Burg, K. J., Porter, S. & Kellam, J. F. (2000) *Biomaterials* 21, 2347-59.
26. Gittens, S. A. & Uludag, H. (2001) *Journal of Drug Targeting* 9, 407-429.
27. Teitelbaum, S. L. (2000) *Science* 289, 1504-8.
28. Ducky, P., Schinke, T. & Karsenty, G. (2000) *Science* 289, 1501-4.
29. Nimni, M. E. (1997) *Biomaterials* 18, 1201-25.
30. Lee, S. J. (2000) *Yonsei Med J* 41, 704-19.
31. Kim, H. D. & Valentini, R. F. (1997) *Biomaterials* 18, 1175-84.
32. Wozney, J. M. (2002) *Spine* 27, S2-S8.
33. Solchaga, L. A., Cassiede, P. & Caplan, A. I. (1998) *Acta Orthop Scand* 69, 426-32.
34. Bonewald, L. F. & Mundy, G. R. (1990) *Clin Orthop*, 261-76.
35. Border, W. A. & Noble, N. A. (1994) *N Engl J Med* 331, 1286-92.
36. Busch, O., Solheim, E., Bang, G. & Tornes, K. (1996) *Int J Oral Maxillofac Implants* 11, 498-505.
37. Anusaksathien, O. & Giannobile, W. V. (2002) *Curr Pharm Biotechnol* 3, 129-39.
38. Thomson, R. C., Shung, A. K., Yaszemski, M. J. & Mikos, A. G. (2000) in *Principles of Tissue Engineering*, eds. Lanza, R. P., R., L. & Vacanti, J. (Academic Press, San Diego), pp. 251-262.
39. Ratner, B. D. (2002) *J Control Release* 78, 211-8.
40. Middleton, J. C. & Tipton, A. J. (2000) *Biomaterials* 21, 2335-46.
41. Bulpitt, P. & Aeschlimann, D. (1999) *J Biomed Mater Res* 47, 152-69.
42. DeBlois, C., Cote, M. F. & Doillon, C. J. (1994) *Biomaterials* 15, 665-72.
43. Yamamoto, M., Takahashi, J. & Tabata, Y. (2003) *Biomaterials* 24, 4375-4383.

44. Edelman, E. R., Mathiowitz, E., Langer, R. & Klagsbrun, M. (1991) *Biomaterials* 12, 619-26.
45. Sakiyama-Elbert, S. E. & Hubbell, J. A. (2000) *J Control Release* 65, 389-402.
46. Park, Y. J., Lee, Y. M., Lee, J. Y., Seol, Y. J., Chung, C. P. & Lee, S. J. (2000) *J Control Release* 67, 385-94.
47. Mattioli-Belmonte, M., Gigante, A., Muzzarelli, R. A., Politano, R., De Benedittis, A., Specchia, N., Buffa, A., Biagini, G. & Greco, F. (1999) *Med. Biol. Eng. Comp.* 37, 130-134.
48. Urist, M. R., Silverman, B. F., Buring, K., Dubuc, F. L. & Rosenberg, J. M. (1967) *Clin Orthop* 53, 243-83.
49. Urist, M. R. (1995) in *Encyclopedic handbook of biomaterials and bioengineering, part a: materials.*, eds. Wise, D. L., Trantolo, D. J., Altobelli, D. E., Yaszemski, M. J., Gresser, J. D. & Schwartz, E. R. (Marcel Dekker, Inc., New York), Vol. 2, pp. 1093-1133.
50. Gombotz, W. R., Pankey, S. C., Bouchard, L. S., Ranchalis, J. & Puolakkainen, P. (1993) *J Biomater Sci Polym Ed* 5, 49-63.
51. Appel, L. E., Balena, R., Cortese, M., Opas, E., Rodan, G., Seedor, G. & Zentner, G. M. (1993) *J Control Release* 26, 77-85.
52. Deschamps, A. A., Claase, M. B., Sleijster, W. J., de Bruijn, J. D., Grijpma, D. W. & Feijen, J. (2002) *J Control Release* 78, 175-86.
53. Gopferich, A. (1996) *Biomaterials* 17, 103-114.
54. Kohn, J. & Langer, R. (1996) in *Biomaterials science: an introduction to materials in medicine.*, eds. Ratner, B. D., Hoffman, A. S., Schoen, F. J. & Lemons, J. E. (Academic Press, New York), pp. 64-72.
55. Barrows, T. H. (1986) *Clinical Materials* 1, 233-257.
56. Domb, A. J., Amselem, S., Langer, R. & Maniar, M. (1994) in *Biomedical polymers, designed-to-degrade systems.*, ed. Shalaby, S. W. (Hanser Publishers, New York), pp. 69-96.
57. Schmidt, C., Wenz, R., Nies, B. & Moll, F. (1995) *J Control Release* 37, 83-94.
58. Soriano, I. & Evora, C. (2000) *J Control Release* 68, 121-34.
59. Ramchandani, M. & Robinson, D. (1998) *J Control Release* 54, 167-75.

60. Baro, M., Sanchez, E., Delgado, A., Perera, A. & Evora, C. (2002) *J Control Release* 83, 353-64.
61. Smith, J. L., Jin, L., Parsons, T., Turek, T., Ron, E., Philibrook, C. M., Kenley, R. A., Marden, L., Hollinger, J., Bostrom, M. P. G., Tomin, E. & Lane, J. M. (1995) *J Control Release* 36, 183-195.
62. Zellin, G. & Linde, A. (1997) *J Biomed Mater Res* 35, 181-90.
63. Isobe, M., Yamazaki, Y., Mori, M. & Amagasa, T. (1999) *J Oral Maxillofac Surg* 57, 695-8; discussion 699.
64. Mayer, M., Hollinger, J., Ron, E. & Wozney, J. (1996) *Plast Reconstr Surg* 98, 247-59.
65. Kirker-Head, C. A., Gerhart, T. N., Armstrong, R., Schelling, S. H. & Carmel, L. A. (1998) *Clin Orthop*, 205-17.
66. Park, Y. J., Ku, Y., Chung, C. P. & Lee, S. J. (1998) *J Control Release* 51, 201-11.
67. Lee, J. Y., Nam, S. H., Im, S. Y., Park, Y. J., Lee, Y. M., Seol, Y. J., Chung, C. P. & Lee, S. J. (2002) *J Control Release* 78, 187-97.
68. Miyamoto, S., Takaoka, K., Okada, T., Yoshikawa, H., Hashimoto, J., Suzuki, S. & Ono, K. (1992) *Clin Orthop*, 274-85.
69. Ishaug, S. L., Payne, R. G., Yaszemski, M. J., Aufdemorte, T. B., Bizios, R. & Mikos, A. G. (1996) *Biotechnol Bioeng* 50, 443-451.
70. Ishaug-Riley, S. L., Crane, G. M., Gurlek, A., Miller, M. J., Yasko, A. W., Yaszemski, M. J. & Mikos, A. G. (1997) *J Biomed Mater Res* 36, 1-8.
71. Whang, K., Goldstick, T. K. & Healy, K. E. (2000) *Biomaterials* 21, 2545-51.
72. Oldham, J. B., Lu, L., Zhu, X., Porter, B. D., Hefferan, T. E., Larson, D. R., Currier, B. L., Mikos, A. G. & Yaszemski, M. J. (2000) *J Biomech Eng* 122, 289-92.
73. Lu, L., Stamatias, G. N. & Mikos, A. G. (2000) *J Biomed Mater Res* 50, 440-51.
74. Peter, S. J., Lu, L., Kim, D. J., Stamatias, G. N., Miller, M. J., Yaszemski, M. J. & Mikos, A. G. (2000) *J Biomed Mater Res* 50, 452-62.
75. Meinel, L., Illi, O. E., Zapf, J., Malfanti, M., Peter Merkle, H. & Gander, B. (2001) *J Control Release* 70, 193-202.

76. Richardson, T. P., Peters, M. C., Ennett, A. B. & Mooney, D. J. (2001) *Nat Biotechnol* 19, 1029-34.
77. Marra, K. G., Szem, J. W., Kumta, P. N., DiMilla, P. A. & Weiss, L. E. (1999) *J Biomed Mater Res* 47, 324-35.
78. Kellomaki, M., Niiranen, H., Puumanen, K., Ashammakhi, N., Waris, T. & Tormala, P. (2000) *Biomaterials* 21, 2495-505.
79. Ekholm, M., Hietanen, J., Lindqvist, C., Rautavuori, J., Santavirta, S. & Suuronen, R. (1999) *Biomaterials* 20, 1257-62.
80. Burdick, J. A., Mason, M. N., Hinman, A. D., Thorne, K. & Anseth, K. S. (2002) *J Control Release* 83, 53-63.
81. Mason, M. N., Metters, A. T., Bowman, C. N. & Anseth, K. (2001) *Macromol* 34.
82. Hacker, M., Tessmar, J., Neubauer, M., Blaimer, A., Blunk, T., Gopferich, A. & Schulz, M. B. (2003) *Biomaterials* 24, 4459-4473.
83. Miyamoto, S., Takaoka, K., Okada, T., Yoshikawa, H., Hashimoto, J., Suzuki, S. & Ono, K. (1993) *Clin Orthop*, 333-43.
84. Saito, N., Okada, T., Horiuchi, H., Murakami, N., Takahashi, J., Nawata, M., Ota, H., Miyamoto, S., Nozaki, K. & Takaoka, K. (2001) *J Bone Joint Surg Am* 83-A Suppl 1, S92-8.
85. Saito, N., Okada, T., Horiuchi, H., Murakami, N., Takahashi, J., Nawata, M., Ota, H., Nozaki, K. & Takaoka, K. (2001) *Nat Biotechnol* 19, 332-5.
86. Saito, N., Okada, T., Horiuchi, H., Ota, H., Takahashi, J., Murakami, N., Nawata, M., Kojima, S., Nozaki, K. & Takaoka, K. (2003) *Bone* 32, 381-386.
87. West, J. L. & Hubbell, J. A. (1995) *React. Polym.* 25, 139-147.
88. Shin, H., Ruhe, P. Q., Mikos, A. G. & Jansen, J. A. (2003) *Biomaterials* 24, 3201-3211.
89. Temenoff, J. S., Athanasiou, K. A., LeBaron, R. G. & Mikos, A. G. (2002) *J Biomed Mater Res* 59, 429-37.
90. Jo, S., Shin, H., Shung, A. K., Fisher, J. P. & Mikos, A. G. (2001) *Macromolecules* 34, 2839-2844.
91. Holland, T. A., Tessmar, J. K., Tabata, Y. & Mikos, A. G. (2004) *J Control Release* 94, 101-14.

92. Holland, T. A., Tabata, Y. & Mikos, A. G. (2003) *J Control Release* 91, 299-313.
93. Mathiowitz, E. & Langer, R. (1987) *J Control Release* 5, 13-22.
94. Mathiowitz, E., Kline, D. & Langer, R. (1990) *Scanning Microsc* 4, 329-40.
95. Ron, E., Turek, T., Mathiowitz, E., Chasin, M., Hageman, M. & Langer, R. (1993) *Proc Natl Acad Sci U S A* 90, 4176-80.
96. Nelson, C. L., Hickmon, S. G. & Skinner, R. A. (1992) *Orthopaedic Research Society 38th Annual Meeting*, 431.
97. Anseth, K. S., Shastri, V. R. & Langer, R. (1999) *Nat Biotechnol* 17, 156-9.
98. Hedberg, E. L., Tang, A., Crowther, R. S., Carney, D. H. & Mikos, A. G. (2002) *J Control Release* 84, 137-50.
99. Hedberg, E., Kroese-Deutman, H., Lemoine, J., Shih, C., Crowther, R., Carney, D., Liebschner, M., Mikos, A. & Jansen, J. (2003) *Controlled Release Society 30th Annual Meeting Proceedings* 90.
100. Cooke, M. N., Fisher, J. P., Dean, D., Rimnac, C. & Mikos, A. G. (2003) *J Biomed Mater Res* 64B, 65-9.
101. Fisher, J. P., Holland, T. A., Dean, D., Engel, P. S. & Mikos, A. G. (2001) *J Biomater Sci Polym Ed* 12, 673-87.
102. Fisher, J. P., Vehof, J. W., Dean, D., van der Waerden, J. P., Holland, T. A., Mikos, A. G. & Jansen, J. A. (2002) *J Biomed Mater Res* 59, 547-56.
103. Fisher, J. P., Timmer, M. D., Holland, T. A., Dean, D., Engel, P. S. & Mikos, A. G. (2003) *Biomacromolecules* 4, 1327-1334.
104. Peter, S. J., Kim, P., Yasko, A. W., Yaszemski, M. J. & Mikos, A. G. (1999) *J Biomed Mater Res* 44, 314-21.
105. Timmer, M. D., Ambrose, C. G. & Mikos, A. G. (2003) *J Biomed Mater Res* 66A, 811-818.
106. Vehof, J. W., Fisher, J. P., Dean, D., van der Waerden, J. P., Spauwen, P. H., Mikos, A. G. & Jansen, J. A. (2002) *J Biomed Mater Res* 60, 241-51.
107. Peter, S. J., Miller, M. J., Yasko, A. W., Yaszemski, M. J. & Mikos, A. G. (1998) *J Biomed Mater Res* 43, 422-7.

108. Whang, K., Tsai, D. C., Nam, E. K., Aitken, M., Sprague, S. M., Patel, P. K. & Healy, K. E. (1998) *J Biomed Mater Res* 42, 491-9.
109. Wu, X. S. (1995) in *Encyclopedic handbook of biomaterials and bioengineering, part a: materials.*, eds. Wise, D. L., Trantolo, D. J., Altobelli, D. E., Yaszemski, M. J., Gresser, J. D. & Schwartz, E. R. (Marcel Dekker, Inc., New York), Vol. 2, pp. 1151-1199.
110. Jazayeri, M. A., Nichter, L. S., Zhou, Z. Y., Wellisz, T. & Cheung, D. T. (1994) *Journal of Craniofacial Surgery* 5, 172-178.
111. Bennett, S., Connolly, K., Lee, D. R., Jiang, Y., Buck, D., Hollinger, J. O. & Gruskin, E. A. (1996) *Bone* 19, 101S-107S.
112. Tessmar, J., Mikos, A. G. & Gopferich, A. (2003) *Biomaterials* 24, 4475-4486.
113. Gao, T. J., Kousinioris, N. A., Wozney, J. M., Winn, S. & Uludag, H. (2002) *Tissue Eng* 8, 429-40.
114. Uludag, H., Norrie, B., Kousinioris, N. & Gao, T. (2001) *Biotechnol Bioeng* 73, 510-21.
115. Uludag, H. & Fan, X. D. (2000) in *Drug delivery in the 21st century.*, eds. Park, K. & Msryn, R. (ACS Press, Washington, D.C.), pp. 253-262.
116. Hahn, M., Gornitz, E. & Dautzenberg, H. (1998) *Macromol* 31, 5616-5623.
117. Cordoba, F., Dong, S. S., Robinson, M., Strates, B. S. & Nimni, M. E. (1993) *Orthopaedic Research Society 39th Annual Meeting*, 102.
118. McGill, J. J., Strates, B. S. & McGuire, M. H. (1991) *Journal of Bone and Mineral Research* 6, 503.
119. Strates, B. S., Kilagblian, V., Nimni, M. E., McGuire, M. H. & Petty, R. W. (1992) *Orthopaedic Research Society 38th Annual Meeting*, 591.
120. Zhang, R. & Ma, P. X. (1999) *J Biomed Mater Res* 44, 446-55.
121. Vogelson, C., Koide, Y. & Barron, A. (2000) *Materials Research Society Symposium Proceedings* 581, 369-374.
122. Vogelson, C., Koide, Y., Alemany, L. & Barron, A. (2000) *Chemistry of Materials* 12, 795-904.
123. Illi, O. E. & Feldmann, C. P. (1998) *Eur J Pediatr Surg* 8, 251-5.

124. Barratt, G., Couarraze, G., Couvreur, P., Dubernet, C., Fattal, E., Gref, R., Labarre, D., Legrand, P., Ponchel, G. & Vauthier, C. (2002) in *Polymeric biomaterials.*, ed. Dumitriu, S. (Marcel Dekker, Inc., New York), pp. 753-781.
125. Gibaud, S., Rousseau, C., Weingarten, C., Favier, R., Douay, L., Andreux, J. P. & Couvreur, P. (1998) *J Control Release* 52, 131-9.